Vessel motion limits to guarantee operable pipe integrity

A motion limits study to improve workability

B. Metz

Technische Universiteit Delft

TU Delft Delft University of Technology

Challenge the future

Vessel motion limits to guarantee operable pipe integrity

A motion limits study to improve workability

by

B. Metz

in partial fulfillment of the requirements for the degree of

Master of Science
in Applied Physics

at the Delft University of Technology,
to be defended publicly on Friday April 13th, 2018 at 14:30.

Supervisor:	Prof. dr. ir. A. Metrikine	TU Delft
Thesis committee:	Ir. D.J.M Fallais,	TU Delft
	Dr. ir. K.N. van Dalen	TU Delft
	Ing. S. Meeuwissen,	Heerema Marine Contractors
	Ir. J. van Drunen	Heerema Marine Contractors

This thesis is confidential and cannot be made public until April 13, 2023.

TU Delft Delft University of Technology

Preface

Dear reader,

Thank you for taking the time to read this documentation of my graduation thesis. It has been a challenging research project due to the endless number of parameters that influence the outcome. However, the project was highly rewarding due to the better understanding of the phenomena afterwards. Many times new research questions came up when other were just answered. In the end all these steps were needed to accomplish the result.
In the beginning of this research it was not clear whether it would be possible to summarize all the parameters that effect the pipe bending moment into a few vessel motion limits. I am very pleased that I have been able to obtain accurate vessel motion limits for normal-lay installation and curious what Heerema is going to do with this work.
I would like to thank all members of my graduation committee, as without them this thesis would not have the same results. The daily guidance and feedback from Ing. Stefan Meeuwissen and Ir. J. Van Drunen at Heerema proved to be very helpful and were very much appreciated. Even trough hard times there were always suggestions to work on. Furthermore the analytical view and critical questions of Ir. D.J.M Fallais are greatly valued. He pushed me into the right direction of the accomplishment of this report. Finally I would like to thank Prof. Dr. Andrei Metrikine as the chairman of my committee, we didn't have daily contact but during the progress meetings his feedback was always helpful.
Last but definitely not least I would also like to thank my family, friends and girlfriend for their support and encouragements during this graduation project. In paralytically my family who made it possible to go to the university in the first place.

B. Metz
Leiden, April 2018

Abstract

Subsea pipelines are extensively used to transport oil and gas from offshore facilities to offshore terminals, pump stations or to the coast. As the installation of pipelines makes up a significant percentage of the total costs of a project, the workability of the installation vessel is of great value. The workability is dependent on the weather conditions and multiple operability limits. The operability limits guarantee the safety during offshore installation. A more accurate methodology of describing the operability limits will usually result in a higher workability. The operability limits in this work describe the limitations of the pipe integrity.

Traditionally, operability in offshore construction projects is defined in terms of operable weather conditions. The operability limit is based on critical sea states which can be compared with the actual sea conditions. The critical sea states are characterized using the significant wave height (H_s) and peak wave period (T_p) and given for multiple directions. The crew has to assess the actual sea state and compare it to prescribed limiting sea states. The human assessment of the actual sea state lead to inaccuracies which can lead to a loss of workability.

The sea states that are used to describe measurable operability limits are not the direct cause of the pipe integrity infringement. The vessel moves due to the waves and the vessel motions cause significant loads on the pipe during normal-lay operations. The simplification of sea states and the vessels RAO are two conservative steps that are not taken into account for operability limits based on vessel motion. The pipe integrity criteria (unity check) consist out of pipe bending moment, pipe tension and hydrostatic pressure. The focus of this work is the pipe bending moment because the dynamic part of the pipe bending moment is larger compared to the other loads. The objective of this thesis is to develop a methodology that determines the operable conditions based on vessel motion limits for pipe bending moment during normal-lay operations.

Previous work only achieved some basic operating criteria such as limiting the vessel roll to 2 degrees single amplitude in a 3-hour time window to determine the workability. Since the pipe bending moment at the overbend is not only dependent on a single degree of freedom vessel motion, a new methodology needs to be developed. An accurate vessel motion limit can predict the maximum pipe bending moment. This can only be achieved with highly correlated vessel motions and pipe bending moments at the points of interest. A delay between vessel motions and pipe bending response have a negative effect on this relation and must be corrected if present.

This thesis applies a model based approach to determine the relation between the vessel motions and pipe bending moment. The points of interest are roller box 3 in the Hang-off module of the D.C.V. Aegir and the sagbend where the pipe radius is minimum. This research concluded that a frequency dependent delay is present between the vessel and the sagbend bending moment. This delay shows a clear relation with the wave frequencies at sea. A methodology is presented to correct the pipe bending moment signal towards the governing vessel motion.

The vessel motion limits that are obtained for the overbend pipe bending moment are presented in figure 1). The figure shows a 2DOF vessel motion limit (black dashed line) which is based on the lateral and transversal rotations at FC1. The vessel motion limit represents the pipe bending moment limit of 2000 kNm.

Before evaluating the correlations, the pipe bending moment signal at the sagbend is corrected in the frequency domain towards the vessel motions. This resulted in the sagbend pipe bending moment showing a clear dependency on the axial acceleration and a large improvement in correlation.

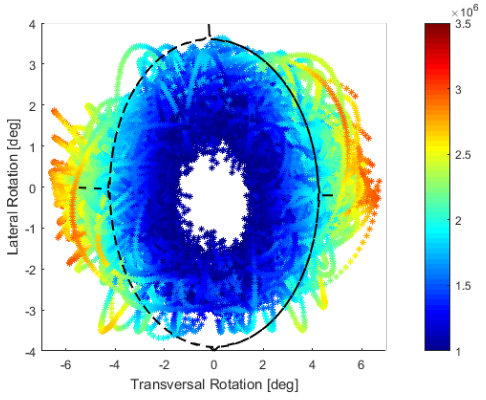

Figure 1: 2DOF Vessel motion limit with pipe BM at RB3 in the color axis

The relation between the vessel motions and pipe bending moment responses are described by a curve fitting equation with a probability of p90. This p90 curve fit is able to accurately predict the pipe bending moment due to the high correlation between the limit and the modeled BM data. This achievement makes it possible to determine reliable vessel motion limits for normal-lay.
An accurate vessel motion limit saves engineering hours and prevents conservative decisions during operations, especially when the operability limits are low during e.g. during installation of structures. The presented methodology can already be implemented in the current workability calculations as well as on deck of the vessel.

Acronyms

AI	Artificial Intelligence
BM	Bending Moment
COG	Centre of Gravity
DAF	Dynamic Amplification Factor
DNV	Det Norske Veritas
DOF	Degree of freedom
DP	Dynamic Positioning
EoM	Equation of Motion
FC(1,2,3)	Friction Clamp (number of Friction Clamp in question)
FEM	Finite Element Method
HMC	Heerema Marine Contractors
HOC	Hang-off Clamp
HOM	Hang-off Module
ILS	In-line structure
LB	Lower boundary
OB	Overbend
OD	Outer Diameter
UC	Unity check
RAO	Response Amplitude Operator
RB(1,2,3)	Roller box (number of Roller box in question)
SB	Sagbend
TA	Tower Angle
TDP	Touchdown point
UB	Upper boundary
WD	Water Depth
WT	Wall Thickness

Sign conventions

Wave direction

The wave direction in this thesis are referred to as the wave heading with respect to the lay-direction of DCV Aegir. A visualization of the wave heading conventions is depicted in figure 2. Head waves are propagating in the 0 degrees direction and beam waves from 90 degrees.

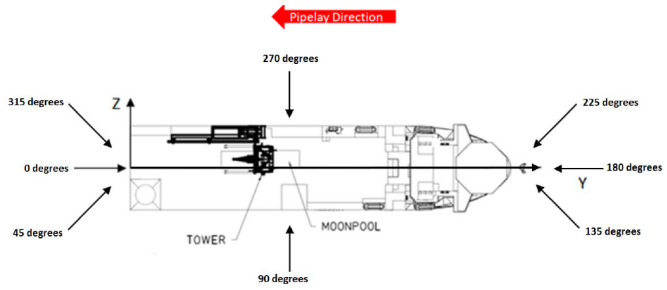

Figure 2: Wave directions with respect to DCV Aegir

Flexcom axis system

Due to the extensive use of Flexcom for this research the sign convention and axis system of this software is governing, see figure 3. Unless specifically stated otherwise the axis system of the Flexcom software shown in figure 3b is used in this thesis.

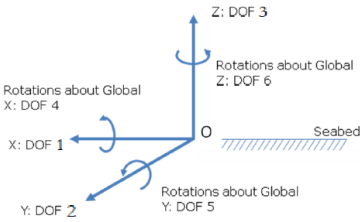

(a) Conventional axis system

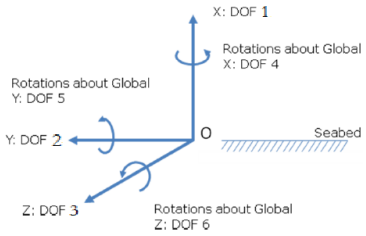

(b) Flexcom Axis system

Figure 3: Different axis systems used

Bending moment direction

In an academic world, most of the time the bending moment is positive if it tends to bend a beam element section concave facing upward with respect to the local axis. A positive bending moment about the local z axis will put the upper surface of the beam (positive y) into compression and the lower surface into tension. Note that the local x axis for the element points from the first node to the second. See figure 4.

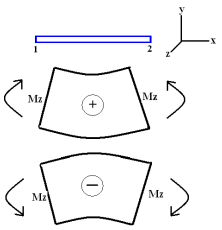

Figure 4: Bending Moment Sign Convention

Contents

1

Introduction

1.1. Background

Subsea pipelines are extensively used to transport oil and gas from offshore facilities to offshore terminals, pump stations or to the coast. Oftentimes these pipelines cover hundreds of kilometers, whilst installed at continuously increasing depths (currently up to 2900 meters). These pipelines range in diameter from 7.5 cm to over 1.5 m and are typically installed by pipe lay vessels.

To support cost calculations and to guarantee the safety during the offshore execution, weather conditions are incorporated in workability predictions for the pipe lay vessel. In literature different definitions of the term 'workability' can be found. In this thesis report the term is workability is defined as "the percentage of time that on operation or process can statically be expected to work satisfactory under the conditions to be expected at the given location [1]".

As the installation of pipelines makes up a significant percentage of the total costs of the project, the installation vessel workability is of great value. The workability is dependent on the weather conditions and the project operability limits, thus a more accurate methodology of describing the operability limits will usually result in a higher workability. Operability is the ability to keep equipment, a system or a whole industrial installation in reliable functioning conditions, according to pre– defined operational requirements [2]. The operability limits are based on limitations of pipe integrity, equipment limits and deck handling (workable conditions for the vessel crew).

Traditionally, operability limits in offshore execution are characterized by operable weather conditions. Therefore the pipe integrity limitations are transformed to measurable and limiting weather conditions, so called critical sea states. The weather conditions are typically forecasted by waves buoys. With this information project engineers determine the critical sea states for offshore execution. The operability limits based on sea states generally result in a range of possible pipe integrity responses. This range of possible pipe bending moments causes an inaccuracy in the limit that describes the actual pipe bending moment limit. This is because the waves are not direct cause of pipe integrity infringement, which is not the case for vessel motions.

The vessel motions cause direct loading on the free hanging pipe which emerges from the J-lay tower. The vessel motions can provide the ultimate loading on the pipe that can halt the operation. If a direct relation between vessel motions and pipe integrity can be found, operability can be defined based on vessel motions. With the installation of dynamic positioning (DP) systems, many pipe lay vessels are now equipped with Motion Recording Units (MRU). Vessels with a MRU system can measure real-time vessel positions during offshore execution.

Increasing the operability limits is interesting for marine contractors that perform offshore executions. The world leading marine contractor Heerema Marine Contractors (HMC) is deeply involved in the pipe lay industry. Heerema's latest deep-water construction vessel is called the D.C.V. Aegir and its characteristics are used in this research. The D.C.V. Aegir is equipped with a J- and R-lay tower which allow the installation of pipelines up to a water depth of 3500m.

1.2. Motivation

As the activity of offshore pipe laying is extreme costly, increasing the workability leads to significant cost reduction. Increasing the accuracy of operability limits which ensures that the pipe integrity limits are not exceeded, result in an increase of the workability. The aim of this thesis is to define more accurate and better measurable operability limits that are based on vessel motions. Especially in harsh environmental conditions, in which the vessel motions are close to or beyond the limits of a safe installation process, accurate operability limits are valuable.

Heerema Marine Contractors calculates the vessel operability using a methodology based on the significant wave hight (H_s) and peak wave period (T_p). An overview of the methodology to determine the workability based on critical sea states is shown in figure 1.1. The first step in this methodology is to gather the project dependent data: consisting of the metocean data, the equipment limits and the clients requirements. A representative simplification of the metocean data, expressed as several combinations of significant wave heights, wave peak periods and wave directions, is used as the input for a static and dynamic analysis to calculate the operability limits for every step of the installation process. In this analysis the sea states determine whether the pipe integrity capacity or equipment limits are exceeded. If so, the H_s and T_p limits are lowered until the unity check (UC) is below one. The unity check contains a number of criteria, among which the hydrostatic pressure, pipe tension and bending moment in the catenary. This analysis is repeated until the calculated workability is acceptable.

The operability limits, based on sea states, are provided for certain headings. In general they are conservatively combined together. This means that for some headings the critical sea state would not exceeded the pipe integrity criteria but is not accepted to be operable.

Figure 1.2 shows the three steps from sea states to pipe integrity responses in the pipe. This first step is not included in the operability limits based on vessel motions, which provides the opportunity of a more accurate definition of the pipe responses and consequently less conservative operability limits.

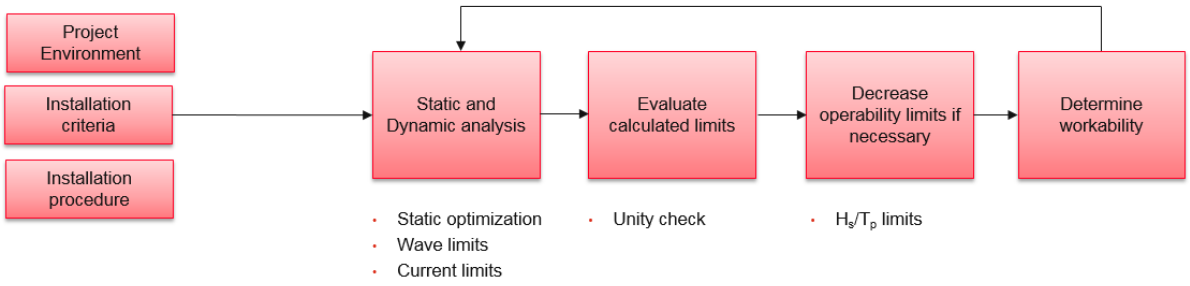

Figure 1.1: Overview methodology to determine workability based on H_s/T_p limits

Figure 1.2: Representative sea states to pipe responses

The crew on site has to compare the critical sea states with forecasted sea states, which occasionally differ from each other. These H_s/T_p limits are mostly determined for three or four headings. When this is the case, the team needs to decide whether it is safe to work based on their experience. This uncertainty leads to a lower workability, as the superintendent needs to introduce a margin of error to guarantee safety during operation. This leads to a conservative decision. Figure 1.3 shows an overview for operability limits based on sea states and vessel motions. By transforming the forcasted sea states to vessel motions, the operability limits and weather forecasts are based on vessel motions which prevents a loss of workability to due conservative decision making. Besides the increase in workability this methodology is also more user friendly.

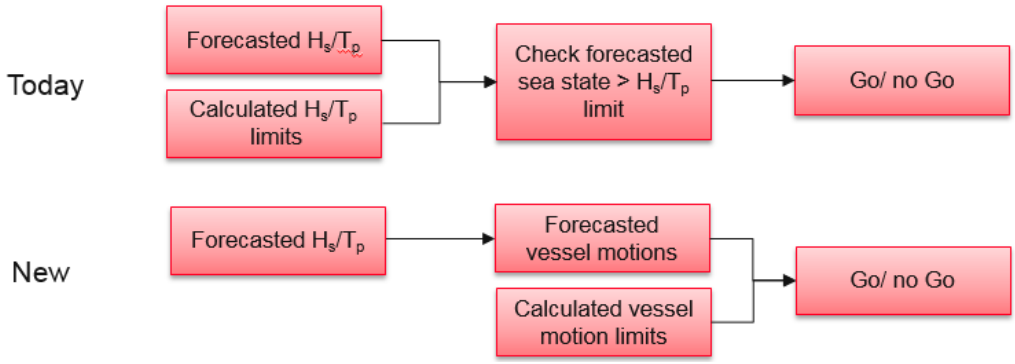

Figure 1.3: Overview current and proposed methodology during offshore execution

Another advantage of a methodology based on a direct relation between vessel motions and pipe responses is the optimization of the equipment settings and the vessel position. The obtained relation can be used to determine which vessel motions result in a significant pipe bending moment response. This knowledge can be used to adjust the vessel to an optimal position, which leads to lower pipe integrity response. The hang-off module (HOM) is the equipment on the vessel that holds the pipe string. The settings of this equipment have a direct influence on the pipe integrity responses and can therefore also be optimized by applying the knowledge gained trough this approach.

1.3. Previous work acknowledgement

This section reviews the research that is available on the topic of operability limits based on vessel motions. In the past, some simple basic operating criteria such as limiting the vessel roll to 2 degrees single amplitude in a 3-hour time window, have been used to determine the workability. Although there are some examples of the application of unidirectional vessel motions limits, so far no complete methodology to transform multiple motions into limiting vessel motions has been established. To achieve the highest possible operability to ensure the highest percentage of workability, these vessel motions limits need to be the as close as possible to the criteria response limit of the equipment or pipe.

Legras and Wang [3] posed that the use of real-time measurements of vessel motions improve the determination of limiting criteria in offshore crane operations. They state that by using MRU data instead of office based hydrodynamic software, more accurate RAOs (Response Amplitude Operator) can be generated for the lifted object. In their research, Legras and Wang only apply a single degree of freedom.

Valen [**?**] investigated the operational limits further using Det Norske Veritas (DNV) Recommended Practices [4]. The DNV GL is an international accredited registrar and classification society for multiple industries among which the oil and gas industry.

Valen states that performing time domain simulations based on real-time data can increase operational limits but are still limited by inaccuracies in the added mass and damping of the lifted equipment as well as external factors, such as scheduling, extreme forecasts and/or equipment malfunctions.

Clauss [**?**] concludes that " a real-time pipe stress analysis based on measured vessel motions during pipe laying process seems to be a feasible application". The real time MRU data is used to improve the determination of limiting criteria in offshore operations.

These three independent researches are all positive about potential of the development of operability limits based on vessel motions limits.

1.4. Objective

The motions of the pipe lay vessel are imposed on the pipe which emerges from the vessel in the J-lay tower. These imposed vessel motions cause different types of loads in the pipe, of which bending moment has been found to be critical in most cases [5]. This pipe bending moment will be used as the criterion for this work. Therefore, the objective of this thesis is formulates as follows as:

" To develop a methodology that determines the operable conditions based on vessel motion limits for pipe bending moment during normal lay operations. "

Beside the pipe bending moment, axial compressive and tensile waves contribute to the internal loading. A requirement of the methodology is to be generic and applicable for different types of pipe lay integrity. The vessel motions limits for the other type of internal loading are a recommended research.

1.5. Problem description

During offshore execution, the vessel motions can result in a critical response of the pipe bending moment. The current methodology, based on sea sates, results in a spreading of pipe bending moments. This inaccuracy leads to non optimal operability limits and conservative decision making. This thesis describes a new methodology that transforms the pipe bending moment limits into the measurable operability limits based on vessel motions. An accurate relation between vessel motions and pipe bending moment is able to predict the maximum bending moment in the pipe accurately.
The optimal operability limits can be determined for strong correlated vessel motions and pipe bending moment. A delay between vessel motions and pipe bending moment decreases the correlation between both signals. It is expected that a delay is present between the vessel motions and pipe bending moment response. When the delay (in time) or phase lag (in radians) is zero, the peaks of both signals are aligned and the most optimal vessel motion limits can be determined.
Besides vessel motions, other phenomena like the impact of waves on the pipe, can decrease the correlation between vessel motions and pipe bending moment. This is because the impact of waves can result in an increase of pipe bending moment which are not caused by vessel motions. This problem needs to be investigated and addressed to achieve optimal operability limits.
The pipe bending moment can be affected by combinations of multiple degrees of freedom (DOF) vessel motions, therefore part of the new methodology is to integrate multiple DOF vessel motions into the operability limits.

1.6. Problem approach

In this thesis a model based approach is applied to determine the relation between vessel motions and pipe bending moment. Flexcom, an advanced computational technique that uses an industry-proven finite element formulation, is used as modeling software. The approach to address the problems formulated in the previous section is divided in three sections.

Characteristic pipe responses for normal-lay operations
Due to the complex system and great number of parameters that are involved in this research, the first step is to gain insight into the pipe bending moment responses due to 1DOF vessel motions. The approach and objectives of this 1DOF investigation are described as follows:

- Single degree of freedom vessel motions are applied to determine the magnitude of the pipe bending moment response. This provides insight in which DOF vessel motions are influencing the pipe bending moment at the points of interest.
- Multiple vessel motion frequencies are applied to determine whether the pipe bending moment is dependent on the vessel motion frequency. This investigation provides insight whether the displacement, velocity or acceleration are the governing motion and whether the pipe bending moment is dependent on the vessel motion frequency.
- An unidirectional motion in the form of a step function is applied to determine the delay between the vessel motions and the pipe bending moment.

The physical transformation of vessel motions to pipe bending moment is investigated to understand the expected phase lag phenomena. An analytical approach is applied to determine the vessel motion frequency dependency on this phase lag. To support the analytical approach a model based approach is performed as well. The analytical approach can be used to verify the results of the model.
Since the vessel moves in all 6DOF vessel motions during offshore activities, another investigation is performed to investigate the systems behavior for irregular vessel motions.
The final steps to understand the characteristic pipe responses due to vessel motions are:

- Analytical approach to determine whether the phase lag is dependent on the frequency of vessel motions. This approach provides insight in the phase lag velocity per motion frequency.
- Model based approach to determine the delay/phase lag per 1DOF vessel motion frequency.
- Irregular waves are used as an input to gain insight in the systems behavior due to irregular vessel motions.

Delayed responses
The research that is described in the previous section determines whether an expected phase lag between vessel motions and pipe bending moment responses is present at the points of interest. This delay is relevant because it decreases the correlation between governing vessel motions and pipe bending moments which results in non-optimal vessel motions limits.
To determine the optimal vessel motions limits it is investigated how the sagbend bending moment responses can be aligned to the initial vessel motion. This investigation aligns a delayed bending moment response for an initial 1DOF vessel motions and determines whether the correlation improves. This step is not performed in earlier research and is part of the methodology to be developed.

Determine vessel motions limits
The last part of the problem approach is to investigate how the vessel motion limits can be determined for multiple degree of freedom vessel motions. Section 1.3 describes that this is only done for single degree of freedom vessel motions. Since pipe bending moments can be caused by combinations of DOF vessel motions, the vessel motions limits should be described in a form that is able to describe multiple DOF vessel motions. Due to the complex system it is not expected that the vessel motions limits are perfectly accurate. Therefore a probability of failure is determined for the obtained vessel motions limits.
When the vessel motions limits are obtained for multiple DOF vessel motions, the last step is to describe how these vessel motions limits can be implemented in the today's offshore execution methodology. As described in the objective, part of the methodology is to describe the implementation of the developed vessel motions limits into the calculation of the workability and the implementation on deck of the vessel.

1.7. Report outline

This report consist of six chapters that will contribute to the research of this thesis. The chapter are organized chronologically by the topics mentioned in the problem approach.

- Chapter 1. Introduction
  This chapter contains the motivation and the objective of this research. To explain how this objective will be achieved, a problem description and approach are included.
- Chapter 2. Literature Study
  This study aims to gain knowledge in academic approaches and/or equations. Part of this research is a literature study into measurements to quantify the correlation between signals. A background study in the Flexcom software and how the pipe bending moment is determined.
- Chapter 3. Characteristic pipe responses for normal-lay operations
  Here the research that gives insight into the behavior of pipelay integrity responses due to vessel motions is reported.

- Chapter 4. Align signals by shifting phase lag
  This chapter aligns the time domain signals for a known phase lag. It gives an overview of the steps that need to be taken and the outcome of this method.
- Chapter 5. Methodology to determine vessel motions limits for pipe bending moment
  This chapter contains the methodology that determines the vessel motions limits for pipe bending moment at the points of interest.
- Chapter 6. Verification and sensitivity analysis
  This chapter contains a verification of the relations between vessel motions and pipe bending moment. Also a sensitivity study is performed to reflect upon the sensitivity of the assumptions that are made.
- Chapter 7. Conclusions and recommendations
  This chapter summarizes the conclusions of this research and provides a list of recommended research topics.
- Chapter 8. Discussion
  In this chapter the outcomes of this research are discussed and placed in the context of the today's knowledge of the current offshore industry.

2

Literature study

This chapter contains information about the subjects that are required to understand before reading this thesis. In section 2.1 the correlation coefficient is explained, where in section 2.2 background information is given about pipe integrity criteria. The third section contains background about the model based approach of this thesis. In the last section contains background about the vessel dynamics.

2.1. Pearson correlation coefficient

A correlation between sets of data is a measure of how well they are related. The most common measure of correlation is statistics in the Pearson Correlation. It shows the linear relationship between two sets of data. Pearson's correlation coefficient is the covariance of the two variables divided by the product of their standard deviation (see equation 2.1).

$$\rho(X,Y) = \frac{\mathrm{Cov}(X,Y)}{\sqrt{\sigma(X)\sigma(Y)}} \tag{2.1}$$

where:

Cov = is the covariance
$\sigma(X)$ = is the standard deviation of X
$\sigma(Y)$ = is the standard deviation of Y

$$Cov(X,Y) = E\left[X - \mu_X)(Y - \mu_Y)\right] \tag{2.2}$$

where:

μ_X = is the mean of X
E = is the expected value

The expected value of a random variable, is the long-run average value of repetitions of the experiment it represents. The Pearson correlation is not able to tell the difference between dependent variables and independent variables. [6].Therefore, as a researcher, you have to be aware of the data that is used to determine the correlation.

2.2. Pipe integrity criteria

2.2.1. Bending stress and moment

The shape of the catenary for a J-lay configuration results in a static pipe tension and pipe bending moment. More information about the J-lay installation method is presented in section 3.1. It is expected that the dynamic behavior of the vessel results in a larger dynamic amplification factor for pipe bending moment than for pipe tension. Therefore the focus of this thesis is to determine the vessel motion limit for pipe bending moment at the point(s) of interest.

The bending stress in the pipe is dependent on the pipe bending moment. The bending stress in an element cross section is defined by equation 2.3, referenced to figure 2.1. The according axis system is presented in figure 3.8.

$$\sigma(\theta) = \frac{M_y D_0}{2I_{yy}} sin\theta + \frac{M_z D_0}{2I_{zz}} cos\theta \tag{2.3}$$

where:

$\sigma_b(\theta)$ = is the bending stress for an angle θ as defined in Figure 2.1.
M_y, M_z = are the bending moments about the local y- and z-axes, respectively.
I_{yy}, I_{zz} = are the second moment of area about the local y- and z-axes, respectively.
D_0 = is the effective outer diameter

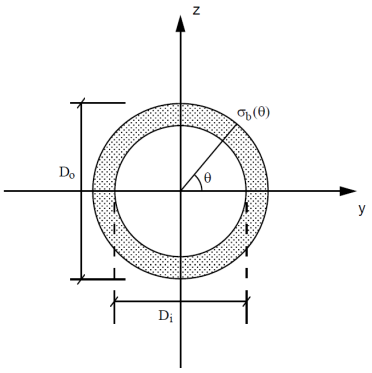

Figure 2.1: Bending Stress calculation

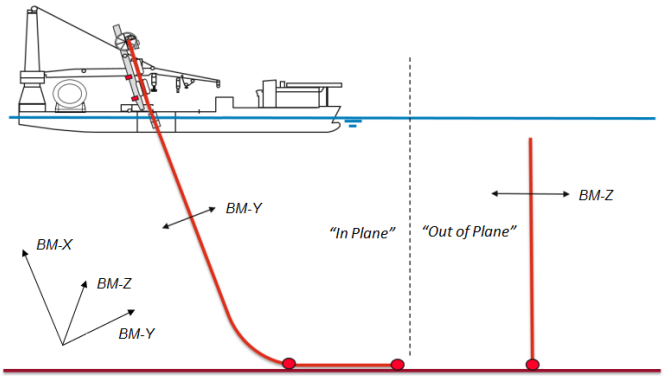

Figure 2.2: Bending moment axis system

2.2.2. Submarine Pipeline systems

The sagbend region will govern the wall thickness design for the pipeline in many cases. This is due to the active bending, low tension and external pressure on the pipeline. The overbend is controlled by the the top tension, bending due to vessel motions, tower angle and to a lesser extent the flexural rigidity of the pipeline.
In order to guarantee safety during installation procedures the international classification society Det Norske Veritas Germanischer Lloyd (DNV GL) investigated this behavior and dedicated a section to it in their service document Offshore Standard: Submarine Pipeline Systems (Ref.[7]). The general practice within the industry is to use the Load and Resistance Factor Design (LRFD) format. This design format is based on a limit state and partial safety factor methodology. The consequences of the failure define the load and resistance factors on the safety class. Section 5.607 of DNV-OS-F101 applies for the sagbend region. This section gives the design criterion for pipe members subjected to bending moment, effective axial force and external overpressure. For the equations of these parameters, see the DNV reference.

$$\left\{\gamma_m * \gamma_{SC} * \frac{|M_{Sd}|}{\alpha_c * M_p(t_2)} + \left\{\frac{\gamma_m * \gamma_{SC} * S_{Sd}}{\alpha_c * S_P(t_2)}\right\}^2\right\}^2 + \left(\gamma_m * \gamma_{SC} * \frac{p_e - p_{min}}{p_c(t_2)}\right)^2 \leq 1 \tag{2.4}$$

$15 \leq \frac{D}{t_2} \leq 45$, $P_i < P_e |S_{Sd}|/S_p < 0.4$

where:

M_{Sd} = is the design moment
S_{Sd} = is the design effective axial force
P_i = is the internal pressure
P_{min} = is the minimum internal pressure
P_e = is the external pressure
P_c = is the characteristic collapse pressure
P_b = is the burst pressure
γ_m = is the material resistance factor
γ_{SC} = is the safety class resistance factor
γ_C = is the condition load effect factor
S_p, M_P = denote the plastic capacities for a pipe.

2.3. Flexcom software

Flexcom uses the Finite Element Method (FEM) as a numerical method for solving engineering problems. The software packages is used for the analysis of a wide range of compliant and rigid offshore structures [**?**]. It is used within HMC to analyze the installation of pipelines and risers both statically and dynamically. For the calculations of hydrodynamic forces in Flexcom the Morison equation is used. In Flexcom both the drag and inertia/added mass components of the Morison equation acting on the pipeline are based on the drag diameter (Dd), instead of the inertia and added terms being based on the displaced volume. The algorithms used within Flexcom for the discretization of the finite element equations of motion in time are the Hilber-Hughes-Taylor integration and the Generalised-α method. Flexcom only uses Euler beam elements and specials elements like springs, hinges or flex joints. An Euler beam can only encounter small deflections because the cross section are can not change in shape. This means that mainly the elastic effects are modeled.

2.4. Vessel dynamics

Vessel motions are an important part of modeling the vessel dynamics. Vessel motions are caused by pressure difference around the hull coming from the waves. The vessel motions can be determined when the interaction between the waves and the vessel is known. This interaction can be determined by the potential flow theory and CFD-calculations, which are computationally expensive. Instead of these calculations, Flexcom applies a predefined Response Amplitude Operator (RAO) to calculate the motions of the vessel. These RAO's can be used to determine the response spectrum for an encountered wave spectrum. The equation that describes the transfer function of the motion and the wave spectrum is presented in equation 2.5 [8]. The vessels that have MRU systems on board are able to measure the vessel motions during operation. Earlier researches [9] verified the Flexcom software by comparing it with measured vessel motions.

$$S_{vessel} = S_{wave} * RAO^2 \tag{2.5}$$

The principle of this transformation of waves to responses is presented in Figure 2.3. The irregular wave signal $\zeta(t)$ is the sum of a large number of regular wave components. Each of these waves have an amplitude, frequency and a random phase shift. The wave energy spectrum ($S_\zeta(\omega)$) represents the energy of the waves within a bin of frequencies. Each of these regular wave components can be transferred to a regular response (e.g. motion) components by a multiplication of the transfer function. The response spectrum $S_{motion}(\omega)$ can be calculated by adding up all the regular response components. [8]

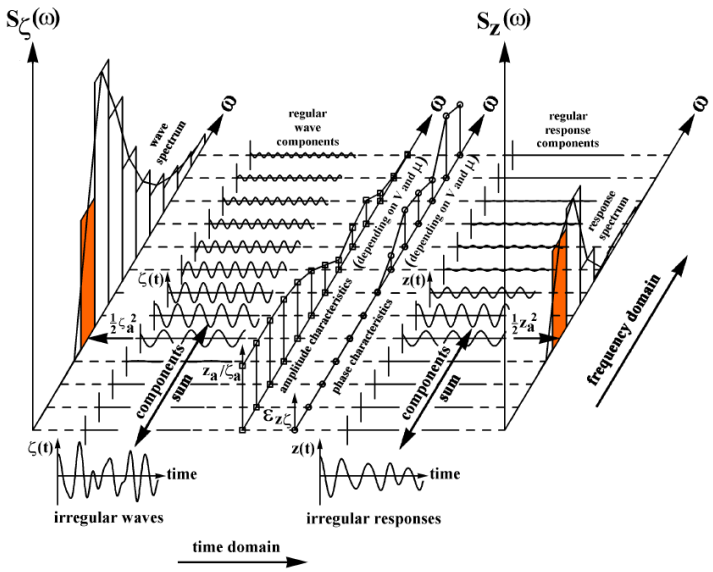

Figure 2.3: Principle of Transfers of Waves into Responses [8]

3

Characteristic pipe responses for normal-lay operations

To achieve accurate operability limits based on vessel motions it is necessary to transform the pipe bending moment limits to equivalent vessel motion limits. The endeavored operability limits are therefore based on the relation between vessel motions and the pipe bending moment at the points of interest.

This relation consists out of a factor in amplitude and a phase difference between both signals. A model based analysis is performed separately for each degree of freedom of the vessel. This gives insights in the relation between vessel motions and pipe bending moment. The frequency dependent vessel motions may affect the maximum bending moment that occurs and is investigated in this chapter. Special attention is given to the influence of each degree of freedom on the pipe bending moment as well as on the delay between the imposed motion and the resulting bending moment at critical locations in the pipe. The delay is the time between a vessel motion and the according pipe bending moment response for a given location.

The last part of this chapter contains an analysis based on 6DOF vessel motions to determine the effect of generic vessel motions on the pipe bending moment.

3.1. J-Lay installation method

In deeper water (certainly from 1000 meters and deeper) pipelines of large diameter are often laid with the J-lay method. A sketch is given in figure 3.1, the pipeline leaves the pipe-lay vessel under an angle of 60 to 90 degrees with the horizontal. The definitions of the acronyms that are used in this figure are shown in table 3.1. The installation method owes its name to the shape of the suspended pipeline, known as the catenary, which resembles the letter "J". For this installation method, prefabricated pipe segments are fed into the tower, where they are welded to the suspended pipeline. The pipe can be suspended from collars (heavy J-lay mode) or friction clamps (light J-lay mode).

The module below the tower of the Aegir from where the pipe is suspended is called the Hang-off module (HOM). The HOM contains three roller boxes and three friction clamps during light J-lay operations. The settings of these roller boxes and friction clamps are project dependent and will be discussed later on.

During installation the dynamic positioning (DP) ensures that the vessel is kept at the position within the watch circle. The watch circle is a maximum allowable offset of the vessel, whilst maintaining the integrity of the pipeline and keeping loads on the vessel equipment within capacity limits. The shape of the watch circle differs per project, it increases with the depth of the project and it is not always symmetric because the transversal limits can be lower than the lateral limits.

Table 3.1: Basic pipe laying definitions [10] and [5]

Type of Acronym	Definition
Nominal Position	Typically, the vessel position where the departure angle of the pipe equals the pipe-lay tower angle giving little or no bending in the pipe and no loads on the roller boxes
Vessel offset	This is offset between the actual vessel location and the nominal position
Hang-off Module	The module on the tower where the pipe is suspended
Overbend	The region where the pipe bends at the Hang-off Module (HOM)
Tower Angle	This is the angle between the tower and the horizontal
Lay back	The horizontal distance between firing line at 90 deg and the touchdown point (TDP)
Sagbend	The region where the pipe bends from the strait suspended section till the pipe on the seabed
Anchorage point	Final point of the pipe for the model (boundary condition).
Watch Circle	This is a maximum allowable offset of the vessel, whilst maintaining the integrity of the pipeline and keeping loads on the vessel equipment within capacity limits

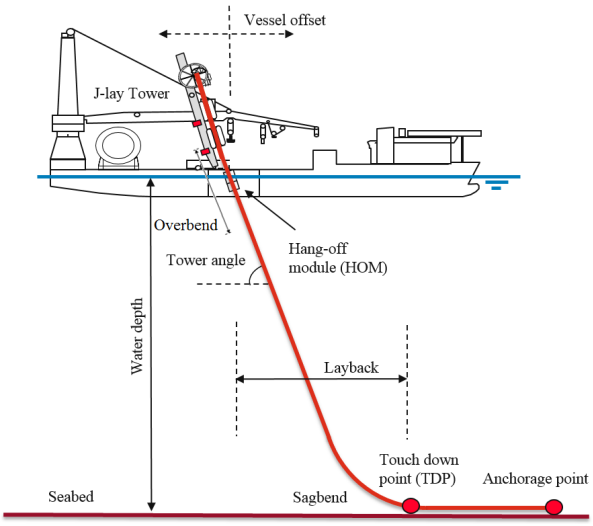

Figure 3.1: Basic J-lay Definitions

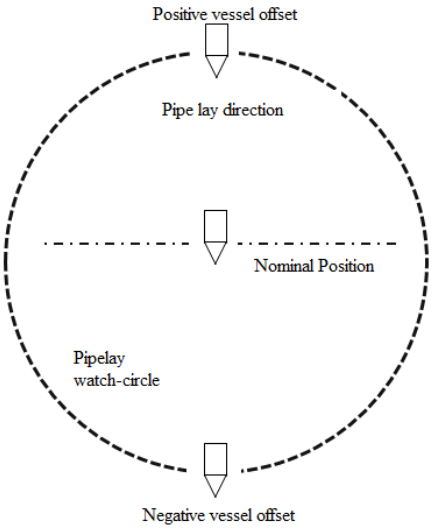

Figure 3.2: Top view watch circle

3.2. Model characteristics

The relation between vessel motions and pipe bending moments is dependent on the project data. The Aegir that is used in this research is a deepwater construction vessel and therefore typical deep water project characteristics are applied in this research. These project characteristics represents a J-lay installation of a 22 inch pipe in 1400m deep water. Additional project characteristics presented in table 3.2 are common values in the work portfolio of Heerema.

A model corresponding to the project characteristics is implement in Flexcom. The Flexcom model consists out of a pipe line and the modeled Hang-off table of the Aegir, where the pipe is attached to the vessel. The vessels centre of gravity (COG) is modeled and a RAO (Response Amplitude Operator) is implemented to calculate the according vessel motions due to waves for example.

The discretized model consists out of a typical number of nodes and elements over the length of the pipe. Due to the complexity of the overbend small spacing is used. In the straight section of the pipe and the catenary to the seabed larger node spacing is applied with a typical length of 4m. The static model is in nominal position, this means that when no loading is applied, the bending moment in the pipe at the HOM of the D.C.V. Aegir is relatively low.

Table 3.2: Deep water project characteristics

Property	Unit	22" Flowline
Method of installation	[-]	Light J-lay
Condition	[-]	Empty at nominal position
Water depth	[m]	1400
TA	[deg]	81.86
Draft	[m]	10.5
Pipe OD	[inch]	22
Pipe WT	[inch]	1.37

Table 3.3: Hydrodynamic properties model

Hydrodynamic properties	Unit	Value
Normal drag coefficient	[-]	0.8
Tangential drag coefficient	[-]	0
Normal inertia coefficient	[-]	2
Tangential added mass coefficient	[-]	0

Boundary conditions and settings HOM

The light J-lay model contains multiple boundary conditions. The first boundary condition is 350 meters away from the touchdown point at the seabed. This anchor point is translation fixed in all directions.

The HOM of the Aegir is a complex system which consist out of roller boxes and friction clamps, see for the location figure 3.1. Figure 3.3 shows a schematic drawing of the hang-off module where figure 3.4 shows the modeled HOM in Flexcom. At friction clamp 1 (FC1) the pipe is fully constraint to the vessel. A motion that is applied at FC1 automatically results in the same motion of the complete HOM. The distance between FC1 and roller box 3 (RB3) is around 7.1m. When rotations are applied at FC1 this arm and rotations will also cause translations at RB3 .

Roller boxes 1,2,3 and friction clamp 2,3 are modeled as springs and are all engaged. This means that the clamps and roller boxes are attached to the pipe. These roller boxes and friction clamps are modeled as an in-plane and out of plane springs. The end of the springs are modeled with boundary conditions which are constraint in all translation directions. The lowest two roller boxes are modeled as two non-linear springs acting perpendicular to the pipe. The characteristics of these springs can be found in appendix A.

The settings of the HOM, such as the distance between the pipe and the roller boxes, have effect on the bending moment distribution in the HOM during installation. Typically, the maximum pipe bending moment in the HOM occurs at RB3, this is due to the settings of the HOM and to prevent that a significant pipe bending moment occurs at FC1 where it is attached to the vessel.

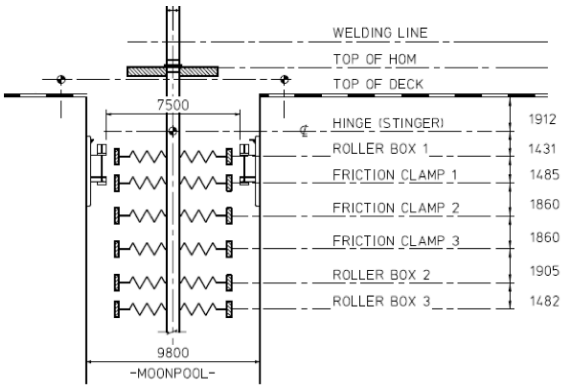

Figure 3.3: Schematic image Hang off Module (HOM)

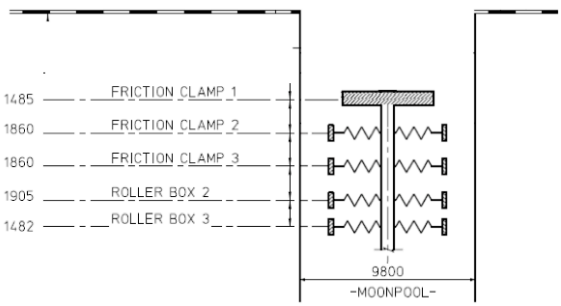

Figure 3.4: Modeled Hang off Module (HOM)

3.3. Origin of catenary loads

During offshore execution multiple effects may result in bending moment in the pipe. Therefore it is required to verify that the pipe bending moments are mainly caused by the vessel motions and that other influences have a significantly smaller effect.

Hereby a few examples of effects that can result in pipe bending moment. At first, vessel motions can cause bending moment in the pipe because the vessel is attached to the pipe. Secondly, wave loads near the surface can result in a pipe bending moment. Third, water result in hydrostatic pressure on a pipe. In this thesis, damage or collision are not taken into account.

To analyze the effect of waves two types of input are modeled. The first input are combinations of irregular beam and head waves. It is expected that larger wave heights result in a larger effect in pipe bending moment and therefore used as input values in the model. The vessel motions at the COG are extracted and used as an input for the second simulation. The vessel motions are equal to the first simulation but no further wave input is implemented. The difference in pipe bending moment between both simulations is equal to the contribution of wave loads in the splash zone at the overbend.

Multiple input combinations are simulated, Table 3.4 gives the H_s and T_P values of the Jonswap waves that are applied. Figures 3.5 and 3.6 show the overbend bending moment at RB3 with and without the effect of wave slamming. The impact of this wave loading on the total bending moment at RB3 is around 5%, this effect can go up to 10% for larger waves. More information about this study can be found in the appendix A.

Since only two combinations are simulated, the precise contribution can not be concluded. Due to the low values of the effect wave loading it is assumed that the dynamic bending moment responses in the pipe are caused by vessel motions and the influence of wave loading is not taken into account.

Table 3.4: Input irregular waves

Case	**Direction [deg]**	H_s **[m]**	T_p **[s]**
Case 1	0	5.42	16
	90	2.09	16
Case 2	0	8.68	10
	90	2.1	16

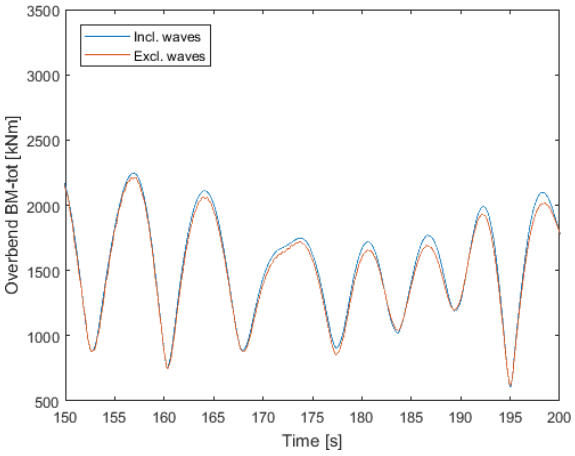

Figure 3.5: Influence wave slamming case 1 at RB3

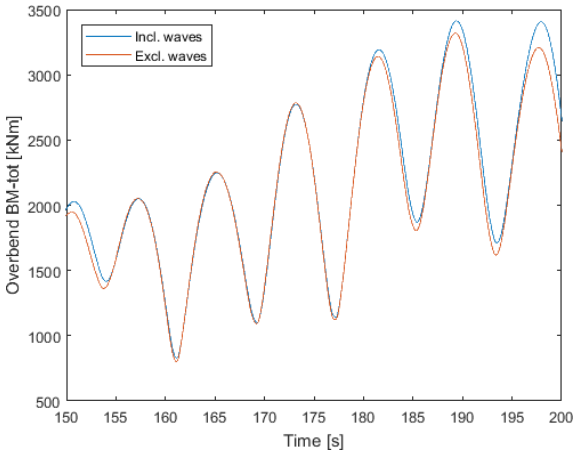

Figure 3.6: Influence wave slamming case 2 at RB3

The hydrostatic pressure of the water column increases over the length of the pipe. The point of interest at the overbend (at RB3) is located above the water level and therefore the roller box encounters no hydrostatic pressure. For the pipe at the sagbend the hydrostatic pressure is not neglected, however, the pressure is assumed to be constant during offshore execution due to small wave energy dissipation over the water depth. Dynamic pipe bending moment responses are therefore assumed not be affected by the hydrostatic pressure.

3.4. Effect of 1DOF motions on pipe bending moment

The pipe bending moment at the overbend (at RB3) and the sagbend (minimum pipe radius) due to due to an imposed motion at FC1 are investigated . The analysis will be performed for each degree of freedom separately to assess the effect of each DOF vessel motion on the pipe bending moment. FC1 is chosen because it is fixed to the vessel. The vessels COG is not recommended because it can differ per project (position crane, location of heavy equipment, etc.). In the end, if the vessel motion limits are known for FC1, these can be converted to all other locations of the vessel. The objectives of this investigation are:

- To determine the magnitude of the bending moment responses for each single DOF motion. This determines the governing motions for the pipe bending moment at the point of interest. It provides insight which DOF motions are influencing the pipe bending moment at the points of interest.
- To determine if the pipe bending moment has a frequency dependency for each DOF motion. If this is the case, the investigation is expanded to determine whether the displacement, velocity or acceleration has the highest contribution to the pipe bending moment.
- To determine the delay in time between the vessel motions and the pipe bending moment. The delay decreases the correlation between vessel motions and result in a less accurate relation between vessel motions and bending moment.

This section is divided in three different types of motions applied at FC1: axial translations, lateral & transversal translations and rotational motions. The pipe departure angle determines the angle between the local and global axis. The local axis is in length of the pipe, in plane of the system. The local and global axis orientations are presented in figures 3.7 respectively 3.8. Since the objective is to develop a methodology that is generic, the motions are applied in the local axis because these motions are applicable for all tower angles. Hereby an overview of the applied motions at FC1:

- Axial (longitudinal) translations.
- Lateral and transversal translations.
- Rotational motions.

As explained in the previous section, the gap between the roller boxes and the pipe are set identical. For the overbend, the lowest roller box, RB3, is taken as the point of interest as it is typically the governing location. For the sagbend, the location where the pipe radius is minimum is taken as the point of interest for the same reason. To understand the pipe bending moment responses due to vessel motions two types of motions are applied:

- A motion in the form of a step function, this motion contains a very rapid change in position. This provides insight in the delay between vessel motions and pipe bending moment responses. However, this step function is not representing actual vessel motions. A rapid change in motion can occur during collisions but are not taken into account in this scope of work.
- A motion in the form of a continuous sinusoidal function with a frequency of 0.5 and 0.75 radians per second, respectively a period of 12.56 and 8.37 seconds. This provides insight in the magnitude of the pipe bending moment response for the applied motions and whether the pipe response is different for two motion frequencies.

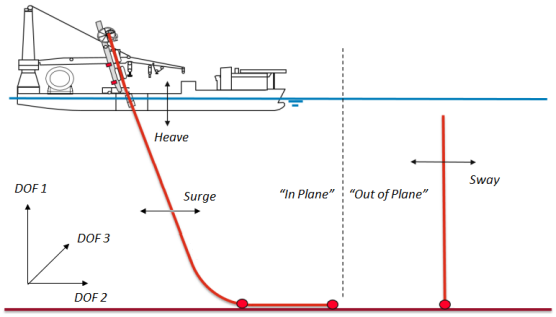

Figure 3.7: Overview J-lay project in global axis

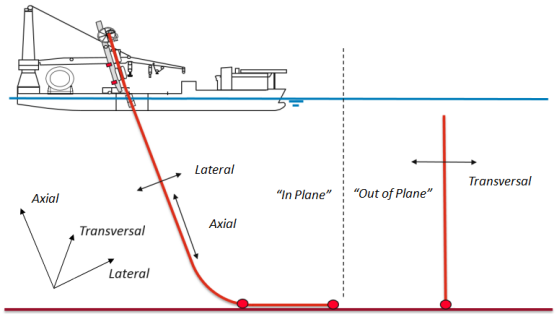

Figure 3.8: Overview J-lay project in local axis

Multiple pipe bending moment locations are used to investigate these effects and they are presented in figure 3.9. Node 10103 (presented as a green cross) represents the sagbend bending moment where the pipe radius is minimum (in the static model).

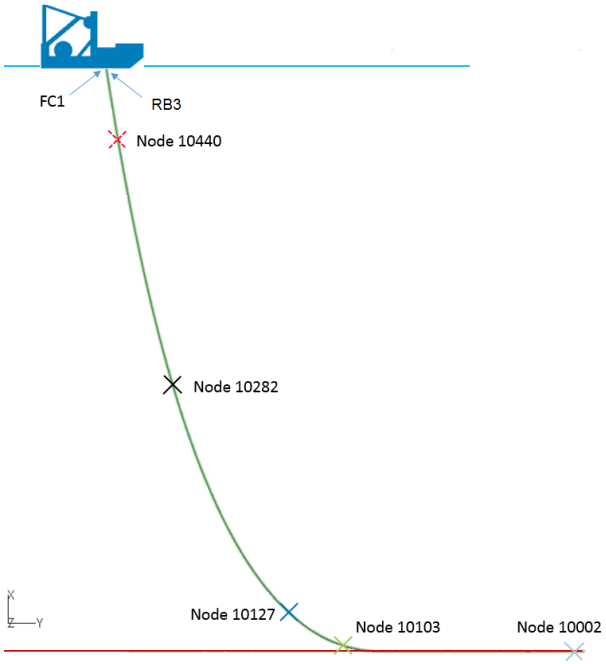

Figure 3.9: Response locations over the length of the pipe

3.4.1. Axial translations

First, the model is in a static equilibrium, no motions or loads are applied. Secondly, after 125 seconds, an axial displacement of 1 meter is applied at FC1. This is followed by the pipe bending moment responses according to the pipe locations of the previous section.

The axial displacement results in a very low bending moment at RB3. This is because the pipe at RB3 encounters no bending due to the applied motion.

The axial displacement results only in a response in plane, this also means that the BM-Y direction is zero and BM-Z is equal to BM-total. The bending moment axis system is shown earlier in section 2.2.

The applied motion and the bending moment responses over the length of the pipe are presented in figure 3.10. The left axis shows the axial displacement and the right axis the pipe bending moment. It can be observed that the static pipe bending moment at the green cross (at the sagbend minimum radius) is higher than the blue and black response locations. The shape of the catenary results in a larger pipe bending moment for a lower pipe radius.

The pipe bending moment at Node 10103 (green) shows a peak in the bending moment shortly after the displacement is applied. Node 10282 (black) and Node 10127 (blue), between the sagbend and

overbend, show larger delays, which suggests an increasing delay from the seabed towards the vessel. This phenomena is investigated later on in this chapter.

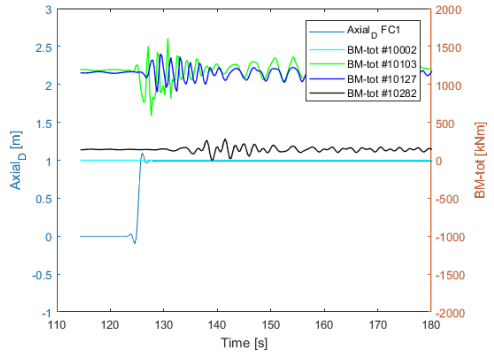

Figure 3.10: Effect axial step motion on pipe BM-tot over the catenary

The two motions in the form a continuous sinusoidal function resulted in a different maximum pipe bending moment. Therefore the investigation is expanded to 20 simulations where each simulation contains a single DOF sinusoidal motion which varies in axial amplitude -and frequency. The maximum sagbend bending moment that occurs is used to compare the dependency of amplitude and frequency. The results are presented in figure 3.11. The x-axis represent the axial frequency of the input, the y-axis the axial amplitude and the z-axis the maximum pipe bending moment that occurs. The purple transparent square around 520 kNm represent the static value of the pipe bending moment, this is caused by the shape of the catenary. All motions are applied at FC1 and the sagbend bending moment is measured where the pipe radius is minimum.
It can be observed that the pipe bending moment is non linear dependent on the amplitude and frequency. It is expected that this non linearity is caused by the damping of the system. It can be concluded that a larger axial amplitude and frequency result in a larger maximum pipe bending moment.

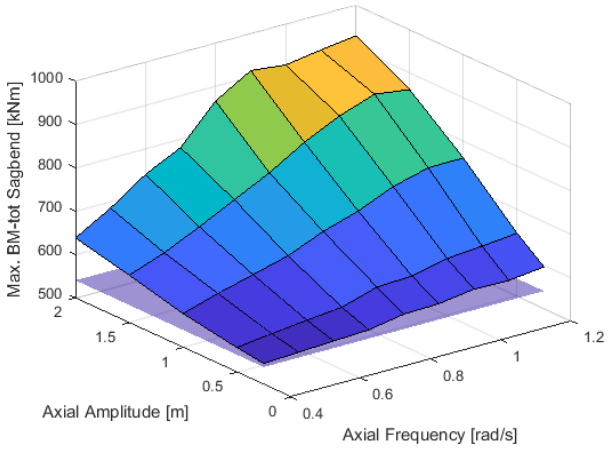

Figure 3.11: Sagbend BM dependency of axial amplitude -and frequency

3.4.2. Lateral and transversal translations

In this section the influence of transverse and lateral imposed motions on the pipe bending moment are discussed. The effects of lateral translations are explained extensively and the effects of transversal translations are discussed at the end of the section. These type of translations at FC1 occur mainly due to the vessel offset. Due to the tower angle the lateral and transverse motions of the pipe are also caused by heave and roll motions of the vessel.
The imposed motions are equal to the motions of the previous section. Since the previous section already concluded that the maximum pipe bending moment is dependent on the motion frequency, in this section only the sinusoidal motion with a period of 0.75 [rad/s] is applied .

The figures in this section present the lateral displacements on the left axis and the pipe bending moments on the right axis. The applied motion in form of a step function presented in figure 3.12 shows an instantaneous peak for RB3 in bending moment due to the fast impact (high acceleration) and a small difference in the static values (before and after).

Figure 3.13 shows the responses in bending moment along the pipe. The maximum pipe bending moments occurs first at node 10440 (red dashed line) followed by the black, blue and finally green bending moment responses. This suggests an increasing delay between the pipe bending moments and the imposed motion from the vessel towards the seabed.

In figures 3.14 and 3.15 a motion is applied in the form of a continuous sinusoidal function. Figure 3.14 shows that the imposed motion and the pipe bending moment at RB3 are in phase or they have a phase difference of 180 degrees. The bending moment axis are defined in section 2.2 and the axis for the imposed motions at the beginning of this chapter. For the applied axis systems, a negative lateral motion result in a positive BM-Z response. Therefore the imposed motions are in phase with the pipe bending moment response at RB3.

The effect of the sinusoidal motion on the sagbend bending moment is presented in figure 3.15. The same phenomena occurs as for the imposed step function, the sagbend bending moment is out of phase with the applied motions. The lateral motion also shows a significant lower maximum pipe bending moment compared to the imposed axial motions.

The effects by imposed transversal translations are comparable with lateral translations. The transversal translations result in a pipe BM-Y response due to the change axis of the imposed motion. The overbend pipe bending moment response is also almost instantaneous with the imposed motion. The sagbend pipe bending moment response is also delayed and the magnitude is significantly lower compared to the lateral translations. This is because for deep water projects 1m of transversal translations has a small effect on the shape of the catenary compared to the lateral translation.

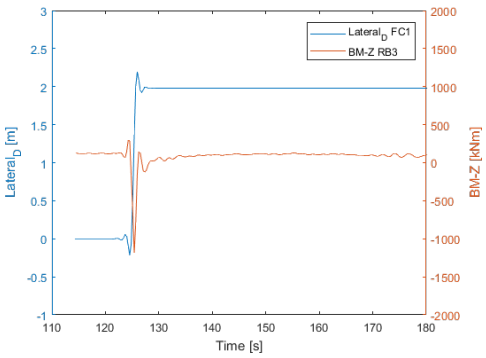

Figure 3.12: Effect lateral step motion on pipe BM-Z at RB3

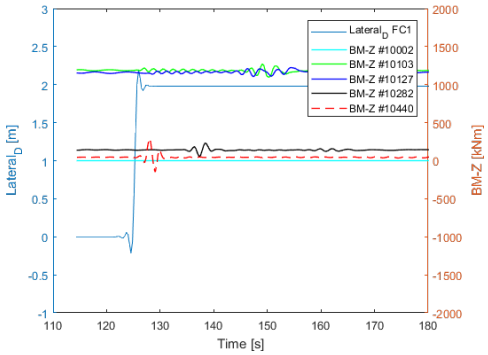

Figure 3.13: Effect lateral step motion on pipe BM-Z over the catenary

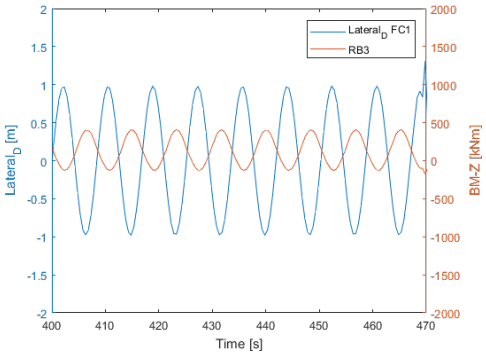

Figure 3.14: Effect lateral sinusoidal motion on pipe BM-Z at the RB3

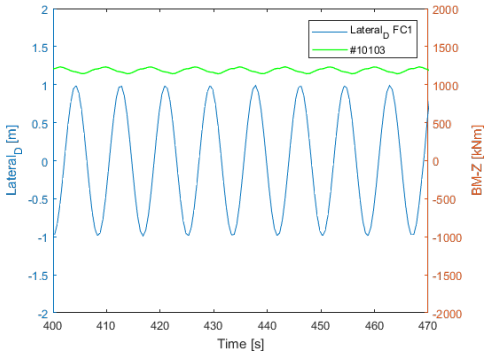

Figure 3.15: Effect lateral sinusoidal motion on pipe BM-tot at the sagbend

3.4.3. Rotational motions

The three rotations in local axis are called called the transversal, lateral and axial rotations, see figures 3.16, 3.17 and 3.18. Each type of rotation is investigated to gain insight in the effect of the pipe bending moments responses due to rotational motions at FC1. Part of this insight is the delay between the imposed motions and the pipe bending moment responses as well as the magnitude of the maximum bending moment that occurs. The transversal rotations are discussed extensively and the effects of lateral and axial rotations are discussed at the end of the section.

Vessel rotations at FC1 result in a rotation of the complete HOM. During these vessel rotations all roller boxes and frictions clamps rotate as well. The length between FC1 and RB3 is 7.1m. An imposed rotational motion therefore causes also translations (heave, surge and sway). The magnitude of these rotations is dependent on the tower angle (TA), since the length between FC1 and RB3 is constant. For example, for a TA of 81.86 degrees, 3 degrees of transversal rotation result in .06m axial displacement.

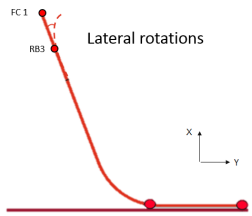

Figure 3.16: In plane: Lateral rotations

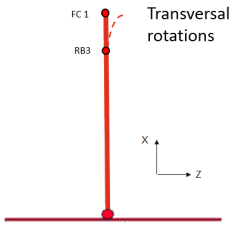

Figure 3.17: Out of plane: Transversal rotations

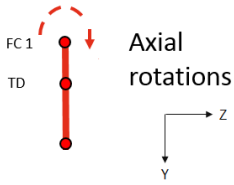

Figure 3.18: Top view: Axial rotations

The effect of the transversal rotation in the form of a step function on the pipe bending moment at RB3 is shown in figure 3.19. The left y-axis shows the applied rotation and the right y-axis represents the pipe bending moment. Also a transversal rotation at FC1 results in an almost instantaneous response at RB3.

In figure 3.20 the same transversal rotation is applied but show the pipe bending moment response at the sagbend where the pipe radius is minimum. The delay between the imposed motion and the sagbend bending moment is around 25 seconds. The amplitude of the bending moment response is rather small compared to the bending moment response due to axial motion. To further investigate this delay more pipe bending moment responses are shown in figure 3.21. Two phenomenas occur in this figure and are explained.

At first, the peak of the pipe bending moments response occurs first at the node 10440 (red dashed line) followed by the black, blue and green responses. This suggest that the response in bending moment starts at the overbend and develops towards the seabed for rotational motions at FC1.

Secondly, a relatively low magnitude response shortly after the initial step input occurs at node 10103 (green) and 10127 (blue) compared to the maximum bending moment peak of these responses. This phenomena occurs due to the axial displacement that occurs during rotations of the vessel. In section 3.4.1 axial motions are applied and show a pipe bending moment response shortly after the initial step motion.

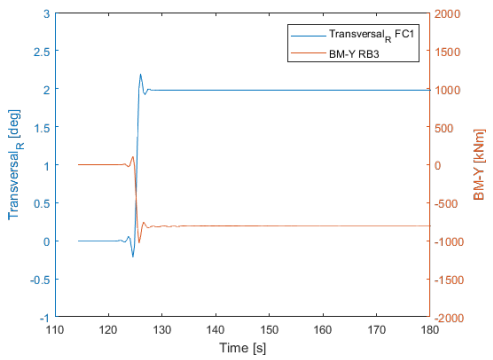

Figure 3.19: Effect lateral step rotation on pipe BM at RB3

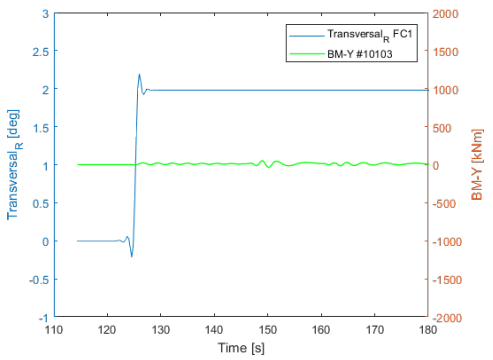

Figure 3.20: Effect lateral step rotation on pipe BM at the sagbend

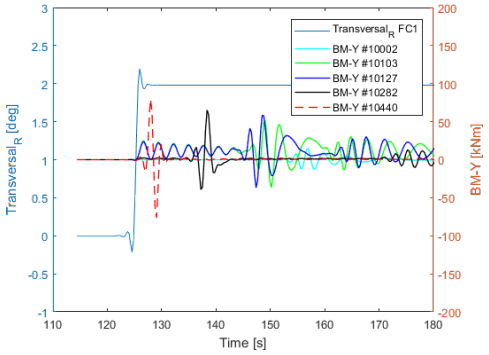

Figure 3.21: Effect lateral step rotation on pipe BM over the catenary

Transverse motions in the form of a sinusoidal are applied to determine the overbend pipe bending moment dependency of out of plane rotations. First a single DOF sinusoidal motion is presented in figures 3.22 and 3.23. From figure 3.22 it can be seen that for this case the imposed rotations have a significant effect on the bending moment at RB3. From figure 3.23 it can be observed that the imposed motion has a very low impact on the sagbend pipe bending moment.
An investigation is performed to investigate the dependency of amplitude and frequency of the imposed motion on the pipe bending moment response at RB3. Multiple simulations are performed where each simulations applies a single DOF sinusoidal motion and each simulation varies in amplitude and frequency. The results are presented in figure 3.24. It can be seen that the maximum pipe bending moment is significantly affected by the amplitude of the transversal rotation compared to the frequency.

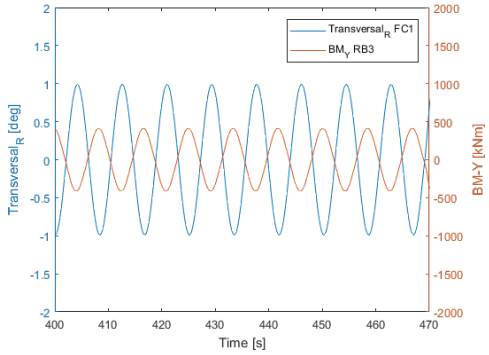

Figure 3.22: Effect transverse sinusoidal rotation on pipe BM-Y at RB3

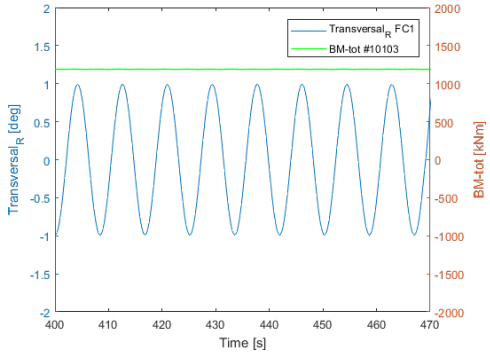

Figure 3.23: Effect transverse sinusoidal rotation on pipe BM-tot at the sagbend

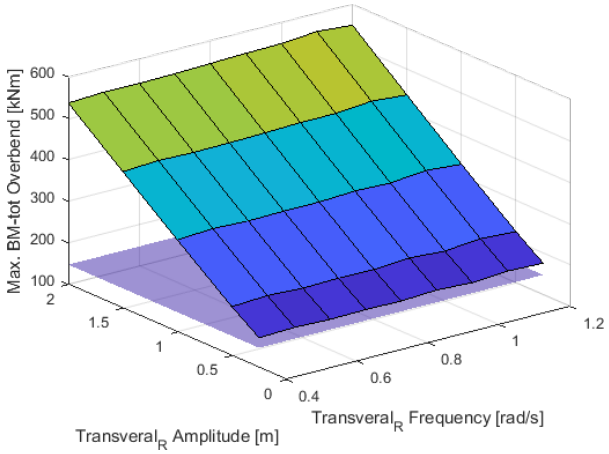

Figure 3.24: Overbend BM dependency of transversal$_R$ amplitude -and frequency

The effects by lateral rotations were comparable with the effects due to transverse rotations. The delay at the overbend is close to zero for all rotations. The lateral rotations also cause a delayed pipe bending moment response at the sagbend. An imposed axial rotation causes torque in the pipe. The torque causes stress in the pipe and no pipe bending moment. However, the pipe is not perfectly straight between FC1 and RB3. This results in secondary effects such as translations. As mentioned in the previous section, translations at FC1 cause a pipe bending moment response at RB3.

3.5. Physical explanation pipe bending moment delay at the sagbend

Sections 3.4.1, 3.4.2 and 3.4.3 demonstrated the existence of the delay between imposed motions and sagbend pipe bending moments. An investigation is preformed to gain insight in when the maximum bending moment occurs for an unidirectional motion at FC1. It is expected that the insight in the transformation from vessel motions to sagbend bending moment can help to predict the delay accurately. Section 3.4.1 showed that the maximum sagbend bending moment occurs shortly after the imposed axial motion. This phenomena is described in section 3.5.1. Section 3.4.3 showed that the maximum sagbend bending moment occurs around around 25 seconds after the applied motions. This phenomena is described in section 3.5.2.

3.5.1. Delay due to axial translations

The applied axial translation in section 3.4.1 was in the form of a sinusoidal and resulted in maximum sagbend bending moment shortly after the applied motion at FC1. The first step of this investigation is to determine the forces in the catenary close to the location of excitation. Since the bending moments close to the friction clamp appeared to be relatively low, the tension is also investigated.

Tensile wave

It is expected that the axial motion causes a change in the pipe tension. Therefore the tension forces are investigated over the length of the pipe. The pipe output locations are presented in figure 3.25. Figure 3.26 demonstrates the pipe tensions due to an imposed sinusoidal motion at FC1. Tension is shown on the left axis and on the right axis the imposed axial acceleration is shown. The black dashed line represents the axial acceleration and the colored lines represent the tension at different locations of the pipe. The figure shows that the maximum tension occurs at RB3 and that the tension is aligned/in phase with the imposed axial acceleration. This phenomena will be discussed later in this chapter. It can also be seen that the peaks of the tensions responses towards the seabed occur later in time than the tension peaks at RB3. This phenomena is called the phase shift. It also indicates that a tensile wave propagates from the vessel towards the seabed.

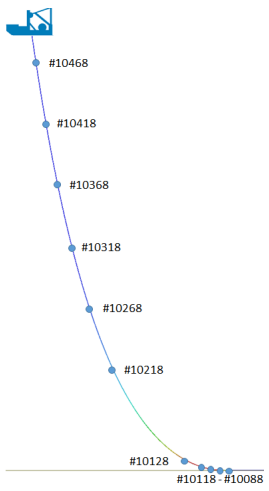

Figure 3.25: Output locations

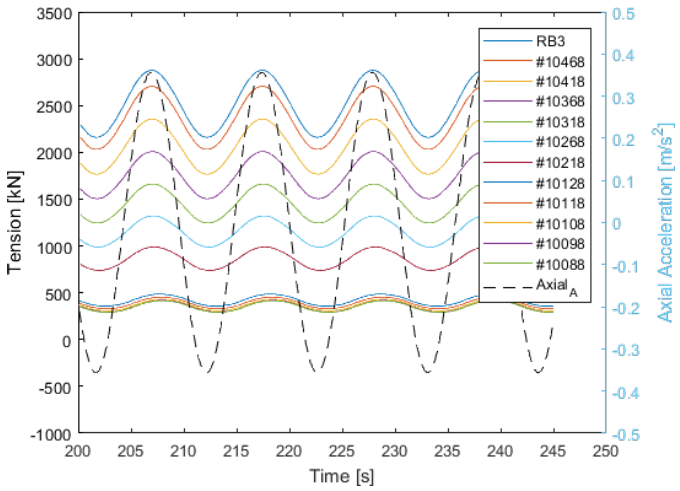

Figure 3.26: Tension and imposed motion over the length of the pipe

Effect of tensile wave at the seabed

The effect of the tensile wave at the seabed are investigated to gain insight in the behavior of the system. Special attention is given to the pipe responses at the touchdown point (TD), where the

pipe catenary is in contact with the seabed. Figure 3.27 demonstrates the tension and the vertical displacement of this node. It can be seen that when the tensile wave reach the seabed, the pipe is lifted from the seabed shortly after. A delay is present between the tension peak and the vertical displacement peak at the TD point. It is expected that the tensile wave propagates further along the pipe and the reaction in vertical displacement decreases towards the model boundary conditions at the seabed.

The relation between the axial displacement at FC1 and the vertical displacement of the pipe is determined by the shape of the catenary. For example, the pipe locations that have a large vertical direction component will have an axial displacement close to amplitude of the applied axial motion and the pipe locations near the seabed will experience a small vertical displacement. This explains that for an imposed axial motion of 1 meter the vertical displacement at the seabed is only 0.04 m.

The vertical displacement of the pipe at the static touchdown point causes a change in the catenary shape. Therefore the pipe bending moment increases shortly after this vertical displacement. Figure 3.28 demonstrates the pipe bending moment and the vertical displacement of the pipe at Node 10088. This figure suggests that the an imposed axial motion at FC1 results in a fast propagating tensile wave towards the seabed. This wave lifts the pipe from the seabed and results in a reflecting pipe bending moment wave towards the vessel. Further investigation is required to confirm the propagating pipe bending moment wave.

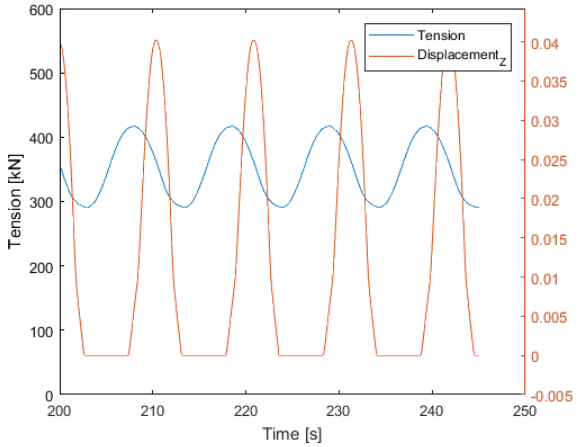

Figure 3.27: Tension and vertical displacement at Node 10088

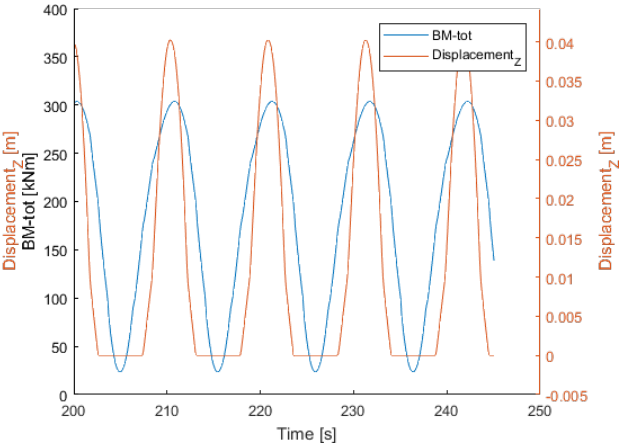

Figure 3.28: BM-tot and vertical displacement at Node 10088

Pipe bending moment wave

This section investigates the pipe bending moment responses near the seabed to confirm that the pipe bending moment propagates from the seabed towards the vessel. This phenomena is demonstrated in figure 3.29. The left axis presents the pipe bending moment total and the right axis presents the imposed axial acceleration. Larger node numbers are located higher up in the catenary as can be seen in figure 3.30. It can be seen that the phase shift between the initial motion and the pipe bending moment increases towards the vessel.

The delay at the point of interest is dependent on the phase velocity. The phase velocity between the TD point and the sagbend minimum pipe radius can be calculated by the difference in time between a zero crossing of the bending moment at the TD and the sagbend bending moment.

The phase velocity is assumed to be constant to approximate the phase velocity between the TD point and the sagbend minimum radius. The time between the two zero crossings is 8.9 seconds (obtained from figure 3.29) and the pipe length is around 60 meters. This gives a phase velocity of 6.7 m/s for an input frequency of 0.6 rad/s. The phase velocity per input frequency is investigated in section 3.6.

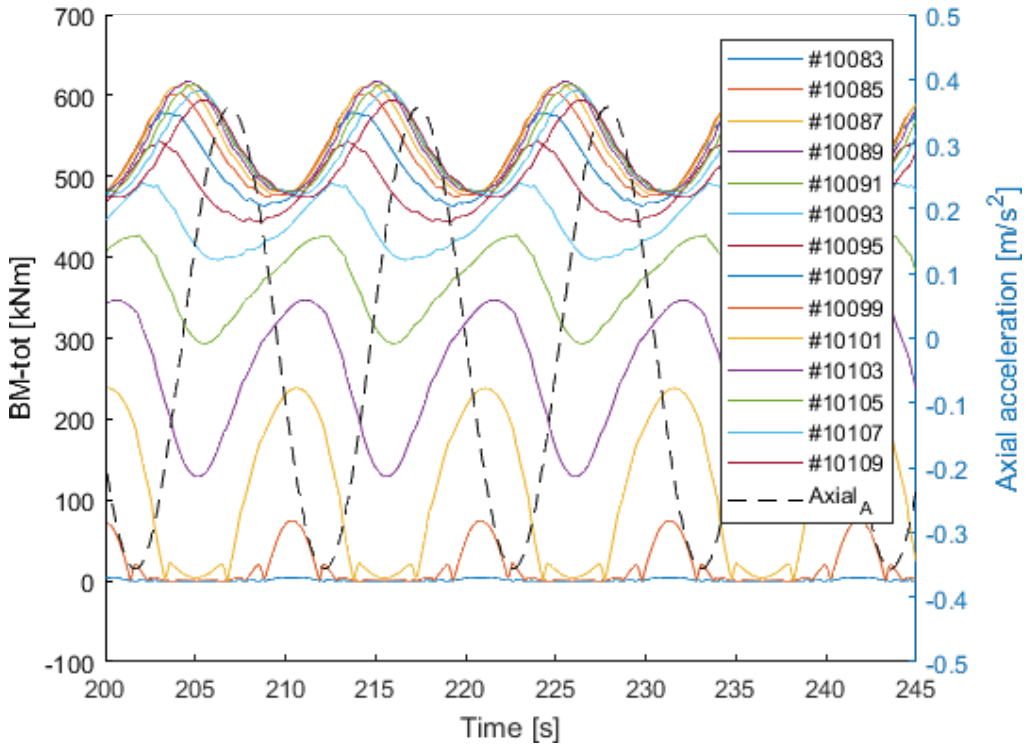

Figure 3.29: BM-tot and imposed motion over the length of the pipe

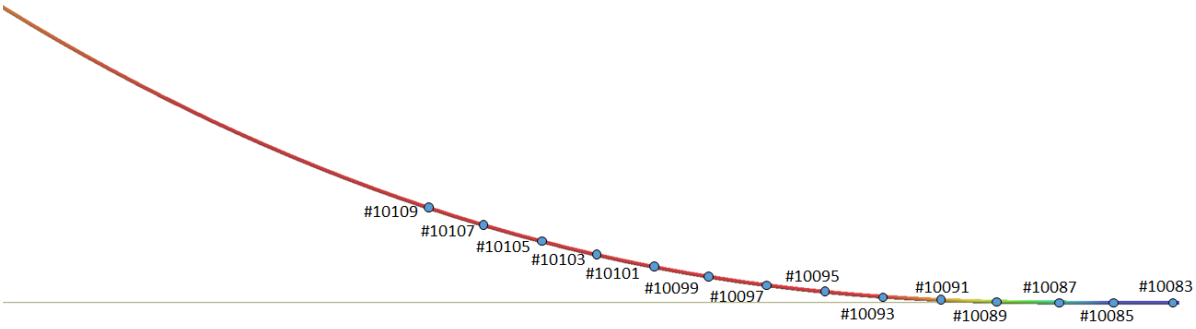

Figure 3.30: BM-tot response locations

Overview response delay

The previous three subsections concluded that an axial motion at friction clamp 1 results in pipe responses in tension, displacement and pipe bending moment.

The obtained results from these sections suggests that the delay between the sagbend bending moment and the imposed motions is a summation of the duration that the tensile wave propagates from the vessel towards the seabed, the duration between the tensile wave reaching the seabed and the vertical displacement of the pipe and finally the duration that the bending moment wave propagates from the seabed towards the point of interest. An overview of the transformation of an applied axial translation to a response in the sagbend bending moment is indicated in four steps in figure 3.31.

This means that the delay is dependent on the location of interest and the propagation velocity of the tensile and bending moment wave. The propagation velocity is dependent on the input frequency and the pipe characteristics such as pipe stiffness.

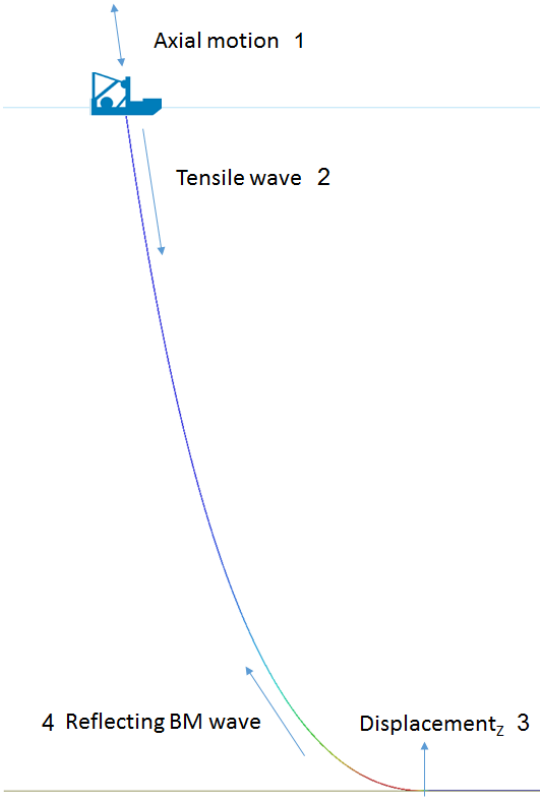

Figure 3.31: Pipe responses due to axial motion

Mass dominated system

This section describes a preformed investigation to determine whether the tension at RB3 is also in phase with the axial acceleration for frequency ranges that occur at sea. The frequency characteristics of a system consists out of amplitude and phase characteristics. The amplitude characteristics are also referred to as Response Amplitude Operator. An example of the calculation of a RAO is presented in Appendix B.

As explained in the Appendix, the behavior of the RAO can be separated in three ranges of frequencies, also presented in figure 3.32. The boundaries of the ranges are determined by the natural frequency of the system. Input frequencies significantly lower than the natural frequency result in motions that are dominated by the spring terms. Input frequencies close to the natural frequency are dominated by the damping terms and input frequencies significantly higher than the natural frequency are dominated by the mass terms. The natural frequency is difficult to determine for a complex system. However, more simulations can be performed to determine whether other input frequencies also result in a mass dominated system.

The natural frequency is dependent on the ratio between the mass, damping and stiffness of the system and the applied frequency of the motion, see Appendix B. The imposed axial motion in figure 3.26 is a sinusoidal function with a period of 0.6 rad/s. This frequency resulted in a tension that is in phase with axial acceleration at FC1. The axial acceleration can be found in the mass terms of the equation of motion. Therefore it can be concluded that the system was dominated by the mass terms for applied frequency. This will also be the case of higher input frequencies.

Typical periods of wind waves are dependent per project locations. The ISO-19901-1 [11] gives indicative values for multiple seas. For example, the North sea spectral peak period (T_p) range between 6-16 seconds, 1.2 rad/s to 0.4 rad/s respectively.

Therefore it still needs to be determined whether the system is also dominated by the mass terms for frequencies lower than 0.6 rad/s. Figure 3.33 presents that the tension at FC1 is also in phase with the axial acceleration frequency of 0.4 rad/s. These observations indicates that for axial motions within a frequency range of 0.4-1.2 rad/s the system is dominated by the mass terms for this particular case.

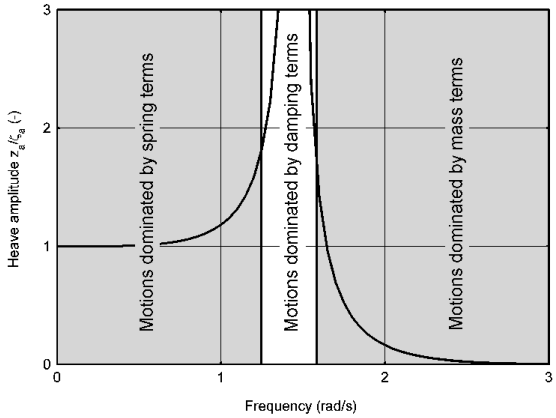

Figure 3.32: Frequency areas with respect to motional behavior [8]

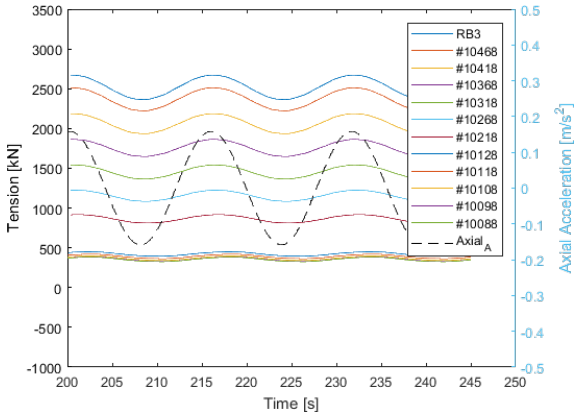

Figure 3.33: Tension and imposed motion over the length of the pipe

Irregular axial translations

The axial translations that are applied so far were regular motions. The waves that occur at sea are typically irregular and this will result in irregular axial motions. These irregular waves are modeled as a summation of multiple regular waves. Therefore the axial motion frequencies that occur due to irregular motion are within the range of the investigated regular motion frequencies. Since the system is dominated by the mass terms for regular motion frequencies this is also expected for irregular axial motion frequencies.

A vessel that moves irregular along the axial axis due to irregular waves will also experience irregular motions in other DOF. Therefore the effect of irregular waves in a free floating body will be investigated in section 3.7. This means that the vessel moves in all the degrees of freedom.

3.5.2. Delay due to rotational motions

In section 3.4.3 it is observed that a rotational motion at FC1 results in a delay of 25 seconds with the sagbend bending moment at the minimum pipe radius. In this thesis the effects of imposed rotational motions are not calculated with the Flexcom model. The Flexcom software applies a discretization of multiple Cantilever or Euler beams. To still gain understanding about the physical behavior for an imposed rotational motion, a clamped Cantilever beam is used as a simplification of the system. The stiffness modes and eigenfrequencies of this cantilever beam are presented in Appendix B.

A cantilever beam has three different modes of vibrations: Transverse, torsional and axial vibrations. The stiffness per modes for a cantilever beam are determined by equations 3.1. For the simplified model the same pipe characteristics as in table 6.1 are applied. The pipe length between the TD point and FC1 is used as the beam length. The according stiffness modes are $k_{Transverse}$=0.098 [N/m], $k_{Torsional}$=64375 [N/m] and k_{Axial}=$4.9 * 10^6$ [N/m] respectively. For projects with lower water depths the pipe will be automatically reduced in length and this reduces the governing effect of the length of the pipe. Therefore it is expected for a shallow water project the effect of other DOF vessel motions increases regarding the sagbend bending moment.

It can observed that the stiffness for transverse motions is divided by the third power of the beam length. Therefore the stiffness in transverse direction is significantly lower than for the axial motion. A low beam stiffness results in a low effect of the impose motion at the end of the beam. Based on this observation is it expected that the rotational motion at FC1 will have a significantly lower effect on the sagbend bending moment than the axial motion.

$$k_{Transverse} = \sqrt{\frac{3EI}{L^3}}, k_{Torsional} = \sqrt{\frac{GJ}{L}}, k_{Axial} = \sqrt{\frac{EA}{L}} \tag{3.1}$$

3.6. Phase shift dependency of vessel motions frequency

Section 3.5 describes that the sagbend bending moment phase shift is dependent on the imposed axial motion frequency and the location at the point of interest. To predict when the peaks of the sagbend

moment response occurs, it is necessary to understand the relation between the delay and the motion frequency.
In section 3.5.1 the phase shift is shown for the tensile and bending moment wave. The contribution of tensile wave to the delay is much lower than the pipe bending moment wave due to the large difference in the propagation velocities. An analytical approach is preformed to determine the delay caused by the bending moment wave in section 3.6.1.
The phase lag between the motions at FC1 is not only dependent on the bending moment wave. Therefore a model based approach is applied to determine the phase shift dependency on vessel motion frequency. Multiple input frequencies are used as input for the Flexcom model and the phase shift is calculated per frequency. This results of this investigation are shown in section 3.6.2. The outcome of these two sections are discussed in section 3.6.3.

3.6.1. Analytical approach

Section 3.5 describes that tensile and bending moments wave are propagating trough the pipe due to the imposed axial motion. The tensile and pipe bending moment wave have different propagation velocities due to the difference in pipe stiffnesses for the direction of the imposed motion. The pipe bending moment wave is propagating from the touchdown point towards the vessel. The duration from the TD point to the sagbend minimum pipe radius is the contribution of the pipe bending moment wave to the delay. To determine the delay (due to bending moment) per input motion frequency the delay is associated with the wave velocity or so called phase velocity.
An analytical approach is used to determine the phase velocity of the pipe bending moment wave from the TD point to the point of interest. The sagbend section is modeled as a simplified tensioned Cantilever beam. The pipe is cut-off at the sagbend minimum pipe radius and clamped at the touchdown point. In this simplified model no discretization is applied to determine the forces for each discretized part of the pipe. Therefore the pipe is now modeled as a straight beam to solve this model analytically. It is expected that this simplification is possible due to the small change in geometry for this part of the sagbend. The sagbend part of static Flexcom model is presented in figure 3.34 and the sagbend modeled as a Cantilever beam is presented in figure 3.35.
The equation of motion (EOM) of the tensioned and straight Cantilever beam is presented in equation 3.2 [12]. The pipe properties of table 6.1 are used as input. The pipe endures static tension to maintain the shape of the catenary. Therefore the average and static tension at the sagbend is used as an input in the EOM.
The applied motion is in the form of a sinusoidal and can be described as equation 3.3. The phase velocity is dependent on the wave frequency and the wave number, this relation is shown in equation 3.4. By substituting equations 3.3 and 3.4 into equation 3.2 and divide by $\omega_0 k^2$, equation 3.5 can be obtained. This equation is called the dispersion equation. With these equations it is possible to determine the relation between the pipe bending moment phase velocity per applied motion frequency. This relation can also be verified with the Flexcom results in section 3.5.1. The Flexcom data determined a phase velocity of 6.7 m/s for an input frequency of 0.6 rad/s. The analytical determined phase velocity, presented in figure 3.36, shows almost the same phase velocity for an equal input frequency.

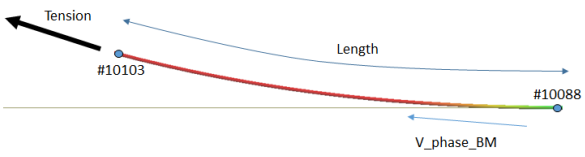

Figure 3.34: Catenary forces at the Sagbend

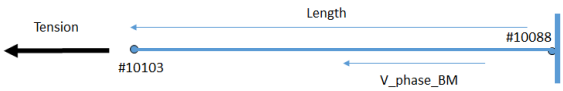

Figure 3.35: Sagbend modeled as Cantilever beam

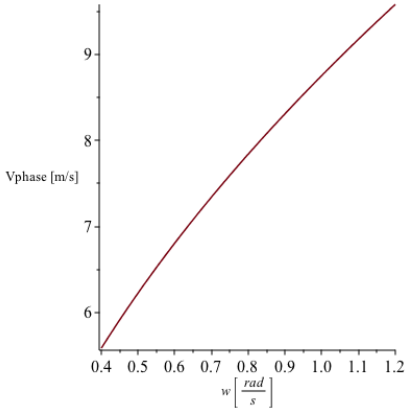

Figure 3.36: Phase velocity bending moment

$$EI\omega'''' - T\omega'' + M\ddot{\omega} = 0 \tag{3.2}$$

$$\omega = \omega_0 * e^{(i(\omega t - k*x))} \tag{3.3}$$

$$V_{ph} = \frac{\omega}{k} \tag{3.4}$$

$$EIk^2 + T - M * V_{ph}^2 = 0 \tag{3.5}$$

where:

M = Mass [kg]
E = Elastic Modules $[N/m^2]$
I = Area moment of inertia $[m^4]$
T = Tension [N]
ω = Frequency of the wave $[rad/s]$
ω_0 = Natural frequency of the wave $[rad/s]$
k = corresponding wave number $[m^{-1}]$
x = coordinate along the pipe [m]
V_{ph} = phase velocity [m/s]

3.6.2. Model based approach

A model based approach is preformed to determine the phase shift dependency of axial motions frequency. Table 3.5 shows the range of frequencies that are used as an input on the same model earlier in this chapter. These frequencies are within the frequency ranges that can occur at sea. These frequency are also close to some of the eigenmodes of the system to take these effects into account. The eigenmodes are presented in appendix A.4.

Table 3.5: Input frequencies

Input #	1	2	3	4	5	6	7	8	9
Sinusoidal period [rad/s]	0.4	0.5	0.6	0.7	0.8	0.9	1	1.1	1.2

The imposed axial motions at FC1 result in a pipe bending moment response that is not a sinusoidal response. These pipe bending moment responses are not all smooth and this results in problems to determine the delay. If the applied motion is a perfect sinusoidal and the response isn't, the delay is not constant for every moment in time.
This is mainly for the sagbend bending moments that are located close to the touchdown point, see figure 3.29. The sagbend pipe bending moment at the point of interest resembles closely a sinusoidal behavior. To determine a constant delay for all the nodes in the sagbend all the pipe bending moment outputs are fitted by a sinusoidal function. Due to the sinusoidal shape the delay between the imposed motion and sagbend bending moment is constant. The effect of this fitting is discussed in appendix C.3.
In line with the delay definition described in section 3.5.1, the delay is calculated for pipe locations from the touchdown point towards the vessel. The delay in time can be transformed to a phase shift in radians.
For example, an input frequency of 0.4 rad/s result in a delay of 10 seconds. The period of the input frequency is equal to $2\pi/0.4 = 15.7[s]$. The phase shift is then calculated by $10/15 * 2 * \pi = 1.3\pi$.
In figure 3.37 the phase shift, in radians, is demonstrated over the length of the pipe per input frequency. The blue dots are showing the location of the sagbend minimum pipe radius. Since the same model is used for all input frequencies, the distance to the TD point is equal for all blue dots. The error of the sinusoidal fitting increases from the sagbend mimimum pipe radius towards the TD point due to non-sinusoidal behavior of the pipe bending moment at these locations. Therefore the phase lag between the TD and the blue dots presented in the figure are less reliable. To improve the calculation

of the phase lag between these locations it is recommended to include the analytical approach. The maximum sagbend bending moment occurs around the sagbend minimum pipe radius and therefore this investigation is not preformed in this thesis.

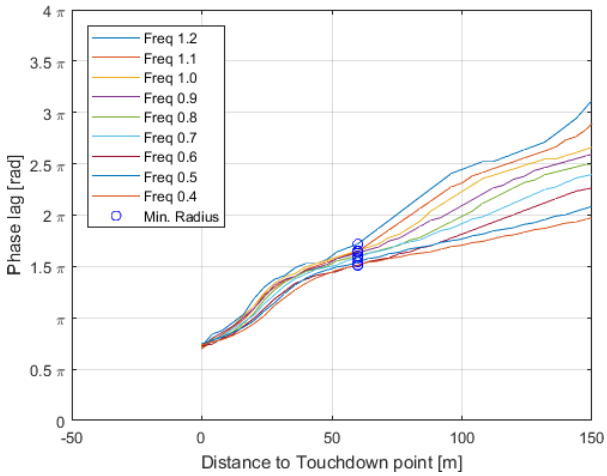

Figure 3.37: Phase shift between axial acceleration FC1 and SB BM per input frequency

It can be seen that for all input frequencies the phase shift increases for pipe locations further away from the TD point. It can also be seen that the phase shift is dependent on the input frequency and a clear trend can be recognized. Higher input frequencies result in a larger phase shift. The phase shift is dependent on frequency because the phase shift velocity increases for higher input frequencies. This phenomena is explained earlier in section 3.6.1.
The phase shift is also not constant per input frequency at the point of interest. Figures 3.38 and 3.39 demonstrates the phase shift at the sagbend minimum pipe radius per imposed axial frequency. The input frequencies are determined by steps of 0.1 rad/s.

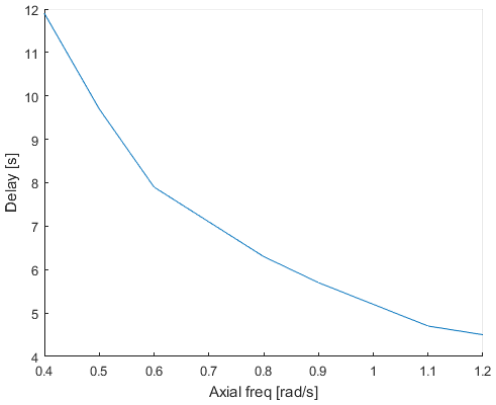

Figure 3.38: Delay between imposed motion and sagbend point of interest

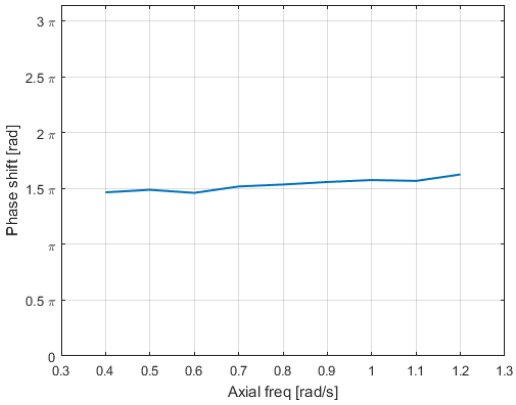

Figure 3.39: Phase shift between imposed motion and sagbend point of interest

3.6.3. Phase correction

The optimal vessel motions limits can be determined when a peak in axial acceleration at FC1 can be aligned with the according peak in sagbend bending moment at the point of interest. Now that the phase shift is known per axial input frequency it is possible to accurately predict when a peak in the sagbend pipe bending moment occurs. The relation between the phase shift and motion frequency can be used to align the sabend bending moment response to the imposed motion. The peaks of aligned signals occur at the same time and this increases the accuracy of the vessel motions limits.
Since the phase shift is dependent on the motion frequency, the sagbend bending moment response needs to be corrected in the phase in the frequency domain. The methodology to align the sagbend bending moment signal towards the axial motion is described in chapter 4.

3.7. Effect of irregular waves on the pipe integrity

So far only the pipe bending moments due to regular motions are investigated. During offshore activities the vessel motions are caused by the sea waves. These sea waves are almost always irregular and are modeled as a summation of multiple regular waves. In section 2.4 the vessel dynamics due to waves are further explained.

Due to irregular waves the vessels moves in all 6 degrees of freedom, therefore the pipe bending moment is no longer caused by only 1DOF motion. The behavior of the pipe bending moment due to multiple degree of freedom vessel motions are therefore investigated. Part of this investigation is to determine the governing motions for pipe bending moment at the points of interest. The governing motions regarding pipe bending moment can be calculated by using the Pearson Correlation Coefficient.

3.7.1. Pipe bending moment response due to irregular waves

In the previous sections a range of frequencies between 0.4-1.2 rad/s were investigated, this range covers a significant part of frequencies that are common at sea. To investigate how the system behaves for different wave frequencies, the transfer function in section 2.4 is applied to determine the vessel motion responses. This vessel motion response spectrum gives an idea of which wave frequencies result in large vessel motions.

Section 3.4.1 described that the axial accelerations at FC1 result in a significant pipe bending moment response at the sagbend. Therefore the response spectrum for displacement in the Z direction (global axis) is calculated. Due to a tower angle of 81.86 degrees the axial motions of the pipe are mainly dependent on the displacement in the Z direction.

The vessel's RAO for acceleration in the Z direction is shown in figure 3.40 for different frequencies. To gain insight in the systems behavior for irregular waves this RAO is multiplied by a wave spectrum. Heerema's in-house developed computer code LIFTDYN is used to generate multiple JONSWAP spectrum's with a peak range from 5 to 16 seconds and for multiple directions. All waves have a significant wave height of 1 meter, γ is set on 3.3 and no spreading is applied. Figure 3.41 presents the response spectrum for the z-displacement motion of the vessel at FC1. This figure suggests that large acceleration are expected for peak periods of around 10-14 seconds. This means that wave spectra's with peak periods around 10-14 seconds will probably result in large pipe bending moment in the sagbend.

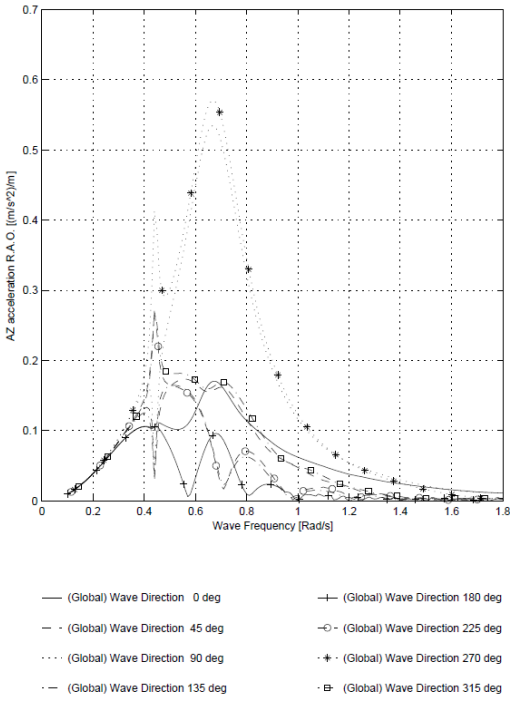

Figure 3.40: $Acceleration_Z$ RAO

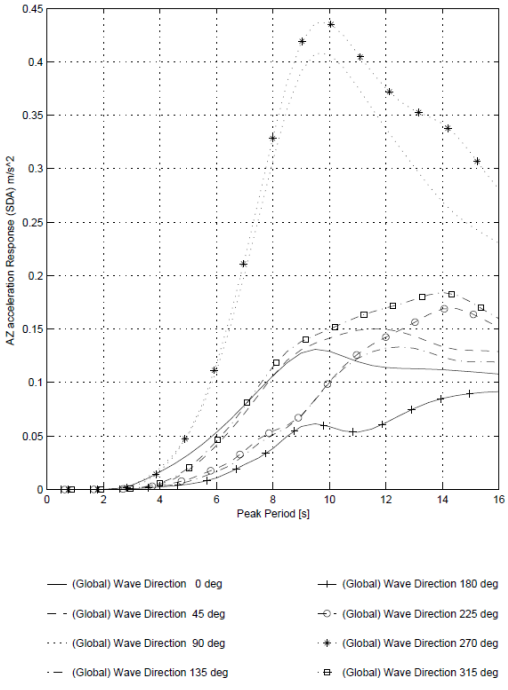

Figure 3.41: $Acceleration_Z$ Response for various JONSWAP spectra

3.7.2. Governing vessel motions for irregular waves

To determine the relation between vessel motions and pipe bending moment due to irregular waves a model based approach is performed. The vessel motions are located at FC1 and the pipe bending moment output at RB3 and where the pipe radius is minimum.

Two different methods are applied to gain insight in this relations. First the correlations between a single DOF vessel motion and pipe bending moment are determined to see which vessel motions are governing regarding the pipe bending moment. Secondly, the response amplitude operators are determined between both signals.

To achieve irregular vessel motions a large set of irregular waves are modeled. The pipe bending moment is dependent on the direction, amplitude and period of the input waves. Therefore multiple simulations are performed with different type of waves. In every simulation two wave spectra are applied. These JONSWAP spectra consists out of irregular head -and beam waves.

The Jonswap values that are applied are based on a targeted vessel motion. This means that the H_s -and T_p values are turned to a targeted vessel motion. Beam waves are used to achieve roll motions and head wave to achieve pitch motions.

Every simulation contains 1 targeted roll motions and 1 pitch motion, all possible combination parameters are shown in table 3.6. The total number of combinations that are used as an input is 108. Together these simulations cover a significant part of vessel motions that can occur at sea.

Table 3.6: Combinations of targeted vessel motions

Targeted Motion	Amplitude [deg]	Period [s]
Roll	2, 4, 6	12, 14, 16
Pitch	1, 2, 3	10, 12, 14, 16

Correlations in global and local axis

The first method to determine the relation between vessel motions and pipe bending moment is based on the Pearson correlation coefficient. The Pearson correlation coefficient is a measure of the linear correlation between two variables. The correlation equations can be found in Chapter 2.

To also have an idea what the effect of the tower angle is on the correlation coefficient, the vessel motions are presented in the local and global axis. The pipe bending moment at the overbend and sagbend will be discussed separately.

Every simulation results in different 6DOF vessel motions and a pipe bending moment signal. Therefore the correlation between 1DOF vessel motion and pipe bending moment differs per simulation. All the 108 correlations are transformed to a percentage. For example, if 11 out of the 108 correlations have a correlation of 0.8 or higher, the percentage is 10% for this correlation threshold. The correlations limits vary from 0 to 1 with a step size of 0.1.

Overbend

Figures 3.42 and 3.43 demonstrate the relation between the pipe bending moment at RB3 and the global and local vessel motions per single DOF. On the left axis the percentage of correlations that exceed a certain correlation threshold are presented. On the bottom axis the correlation threshold are given. It can be seen that for the global vessel motion higher correlations are shown for roll and pitch motions.

Figure 3.43 demonstrates the correlations to vessel motions in local axis. Lateral, transversal and axial rotation show the highest correlation to bending moment. Lateral and transversal rotation are understandable because these motions cause a direct bending the pipe. An axial rotation causes a bending moment due to a torsion reaction in the pipe. The tower angle has a significant impact on these figures. To have a generic methodology the vessel motions limits are given in local axis.

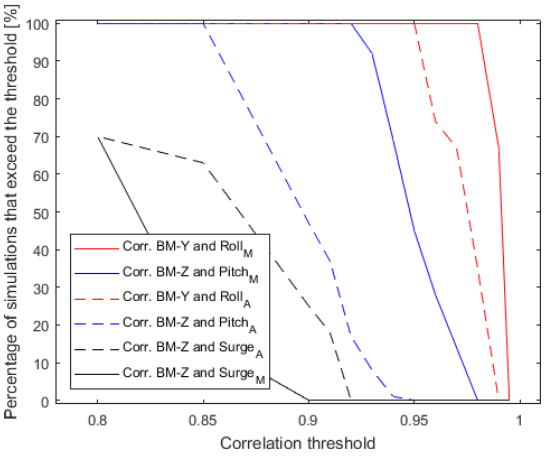

Figure 3.42: Correlation pipe bending moment at RB3 and global 1DOF vessel motion

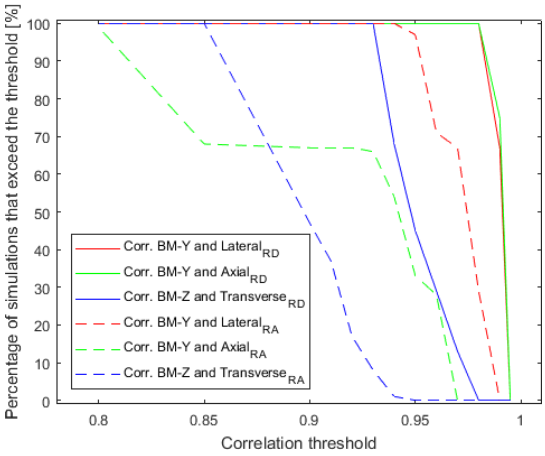

Figure 3.43: Correlation pipe bending moment at RB3 and local 1DOF vessel motion

Sagbend

The point of interest at the sagbend is at the min. radius of the pipe. In section 3.5.1 it was determined that a delay is present between vessel motions and pipe bending moment. This delay is dependent on the location of interest and input frequency. Without applying a phase shift correction, the correlation between the vessel motions and the sagbend pipe bending moment is affected by the delay. For example, in case that the displacement of an imposed motion is the governing driver of the sagbend pipe bending moment. If the delay for this point of interest is around 0.5 π, the velocity becomes the governing driver.

The same correlations are calculated as in the previous section despite the delay between the imposed motions and the uncorrected sagbend pipe bending moment. The correlations are presented in figures 3.44 and 3.45. It can be observed that the pipe bending moment is highly correlated to the axial velocity at FC1. That the velocity results in high acceleration is a coincidence of the sagbend location and input frequencies. However, the delay can only affect the correlation negatively for irregular motions. This means that that the axial motion is governing regarding the sagbend pipe bending moment. It can be observed that the effect of the tower angle is minimal at the sagbend. The difference in correlation between heave (global axis) and axial (local axis) acceleration and the sagbend pipe bending moment is relatively small due to the TA of 81 degrees.

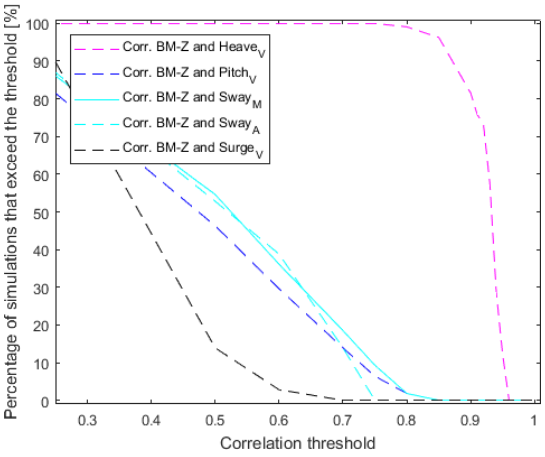

Figure 3.44: Correlation pipe bending moment at the sagbend and global 1DOF vessel motion

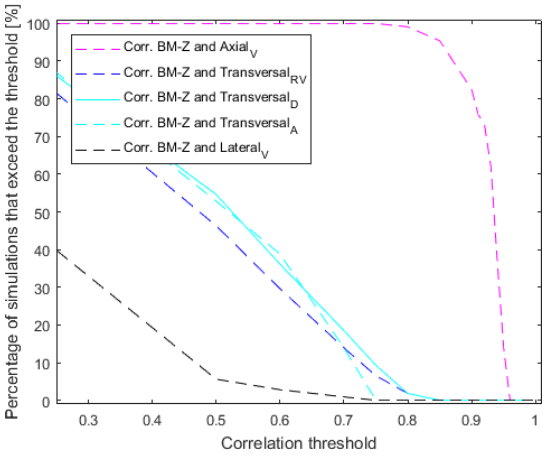

Figure 3.45: Correlation pipe bending moment at the sagbend and local 1DOF vessel motion

RAO between vessel motions and bending moment

The second method to determine the relation between motions and pipe bending moment is based on the Response Amplitude Operators between the two signals. The signals are converted to the

frequency domain to determine the RAO factor and the phase difference per frequency. The RAO factor is calculated by dividing the pipe bending moment spectrum by a 1DOF vessel motion.
For each simulation the RAO and phase is determined. In this section the 108 different RAOs and phases are plotted on top of each other in this section. The points of interest are again at RB3 and the where the pipe radius is minimum.

Overbend

In figure 3.46 RAO is shown between the lateral rotation at FC1 and the overbend BM-Y at RB3. The RAO difference shows no perfect straight line. In section 3.3 it was determined that the HOM settings result in a governing pipe bending moment for values higher than 1000 kNm. When low amplitude vessel motions are applied, RB3 three is not attached to the pipe and this results in a lot of non-linear behavior.
The lower figure concludes that the lateral rotation and bending moment have a phase around 180 degrees.The phase shift of 180 degrees is due to the signing coordination. It is expected to be constant due to the almost instantaneous reaction between vessel motions at FC1 and overbend BM at RB3.

Sagbend

In figure 3.47 the RAO is shown for axial acceleration and sagbend BM. As concluded before, the axial motion only changes the in plane shape of the catenary. Therefore the RAO's for vessel motions and BM-Y / BM-tot are similar. On the contrary of the overbend, the phase between axial acceleration and bending moment is around 270. This phase difference is dependent on the location of the pipe. In section 3.6.2 the delay between axial motions and sagbend pipe bending moment was determined around 1.5 π. Here the figures shows the phase shift around 270 degrees, which is equal to the phase shift in radians.

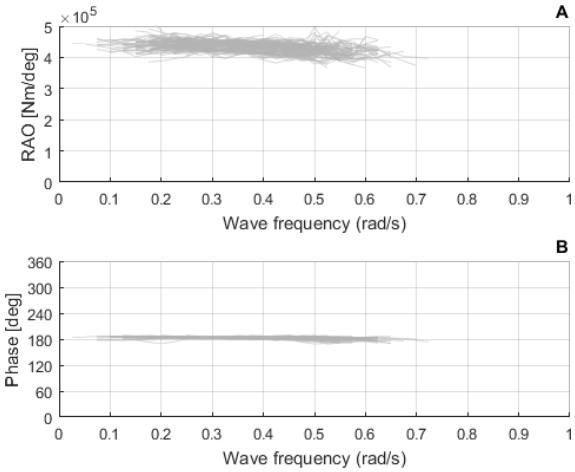

Figure 3.46: Frequency characteristics Lateral$_R$ at FC1 and overbend BM-Y at RB3 (A) in amplitude (B) in phase

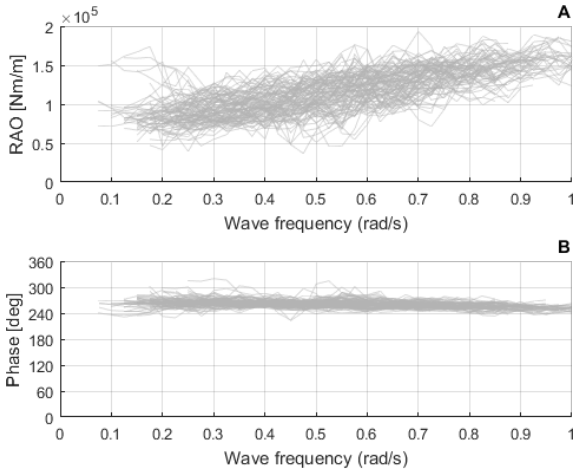

Figure 3.47: Frequency characteristics Axial$_A$ at FC1 and sagbend BM-tot (min. pipe radius) (A) in amplitude (B) in phase

3.8. Summary

The delay between vessel motions and sagbend bending moment need to be aligned to determine the optimal vessel motion limits. A methodology to align vessel motion and bending moment signals is given in Chapter 4. Hereby a summary of conclusions about the system behavior:

- Tensile wave propagates from the vessel to the seabed due to axial translations.
- BM-tot wave propagates from vessel towards the seabed due to rotational vessel motions.
- BM-tot wave propagates from seabed towards the vessel due to axial vessel motions.
- Overbend delay between vessel motions at FC1 and pipe BM at RB3 close to instantaneous.
- Sagbend delay is a summation of the tension wave and the reflection BM-tot wave.
- Sagbend delay is frequency dependent.

4

Align signals by shifting phase lag

The optimal vessel motions limits can be determined if the pipe bending moment response occurs instantaneous after the applied vessel motions. In this case the the governing vessel motions are aligned with the pipe bending moment response, which means that the peak of a vessel motions corresponds with the peak of the pipe bending moment.
Chapter 3 concluded that a delay is present between motions at FC1 and the sagbend bending moment where the pipe radius is minimum. The objective of this chapter is to align the delayed pipe bending moment response to the according motions at FC1. Section 3.6.2 determined that the phase lag is dependent on the applied motion frequency. This chapter describes the new methodology that aligns a pipe bending moment time signal to the according motion signal at FC1. The phase shift is applied in the frequency domain because the phase lag is frequency dependent.
Chapter 3 concluded that the sagbend bending moment is significantly affected by axial motions at FC1. To verify whether the correlation improves, an example is given that aligns the delay pipe bending moment towards the governing axial motion.

4.1. Methodology

Aligning an output signal in phase towards an input signal can be done by subtracting the phase difference of both signals of the phase of the output signal. This results in a output signal with an adjusted phase, in this thesis this is called the corrected signal. To explain the steps that are required to achieve a corrected signal an example given for a delay between vessel motions and a pipe bending moment response. The delay or phase lag between the initial vessel motions and the pipe bending moment is dependent on the frequency of the vessel motions. Aligning the response signal is therefore performed in the frequency domain. An overview of these steps are presented in figure 4.1.

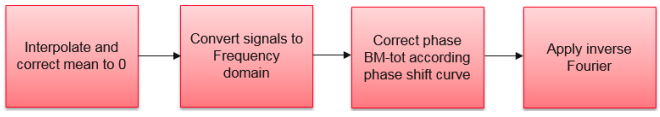

Figure 4.1: Overview methodology to apply phase shift

The first step is to interpolate both signals and to an equal time step. In this thesis cubic interpolation is applied, this is a spline where each piece is a third-degree polynomial. This fixed time step is required to convert a signal from the time domain to the frequency domain. If the mean of a signal is not equal to zero, subtract the static value of the signal. Reverse this amplitude shift on the output of this methodology to restore the signal to the original amplitude.
The output of this Fourier transform is a complex signal, to subtract the phase lag of the phase this complex number needs to be converted. The angle between the real and the imaginary part is the relative phase, the magnitude of these two parts is the amplitude of the signal.
Since the previous section calculated the phase lag between vessel motion and pipe bending moment in the sagbend per frequency, the phase of the sagbend bending moment signal can be shifted towards

the phase of the vessel motion. The phase lag between these signals is presented earlier in figure 3.39. This phase lag must be interpolated to the same frequency step size as the input -and output signals. The frequency domain of a signal exists out of frequencies that differ in the amount of energy. The more a frequency is present, the more energy this frequency contains. The power spectrum $S_{xx}(f)$ of a time series $x(t)$ describes the distribution of energy into frequency components composing that signal.
The frequency that have non or a relative low amount of energy result in inaccurate information. Therefore the phase shift need to be applied on frequencies that contain a minimum amount of energy. This threshold is called the cut-off frequency. The cut-off frequency is determined by the highest frequency peak present in the power spectrum with a maximum value of at least 0.1% of the most dominant peak. This cut-off frequency turned out of have a minimal loss of total energy. This selection criteria is also performed on the example pipe bending moment signal. The frequency characteristics of the bending moment signal are presented in figure 4.2. The red dots in the figure are the frequencies that contain more energy than the cut-off limit.
The interpolated phase shift (per frequency) from the previous chapter is applied on the phases that are selected. This is done by subtracting the phases that are selected by the according phase lag. The frequency domain of a real signal is "mirrored" in the real and negative halves of the Fourier transform because of the nature of the Fourier transform, this is called Hermitian symmetry [13]. The Fourier transform is defined as equation 4.1.

$$H(f) = \int h(t)e^{(-j2\pi ft)}dt \tag{4.1}$$

The mirrored side of the Fourier transform needs to be taken into account to be able to convert the signal from the frequency domain to the time domain. Due to the difference in signs of both sides, the phase lag is subtracted of the first part and summed on the second part. The phase characteristics of the bending moment signal are now 'corrected' towards the phase of the vessel motion. In figure 4.3 the frequency characteristics are presented for the original and corrected signal. The power spectrum is not adjusted because it represents the amplitude characteristics and the changes in phase can be observed in the bottom figure.
Now that the phase lag is subtracted from the phase, the next step is next step is to transform the magnitudes and 'corrected' phases back to a complex number. This can be done by using the complex conjugation, see equation 4.2. The magnitude and shifted phase are used to transform the signal to a complex number. Where i is a imaginary number and $i^2 = -1$.

$$a + i * b = magnitude * exp(i * phase) \tag{4.2}$$

Then the last step is to transform this complex number to the time domain. This is done with the inverse Fourier Transform. The output is a sagbend bending moment signal that is shifted in phase per frequency towards the phase of the vessel motion signal. This methodology can be applied for every type of vessel motions or responses for which the phase lag is known.

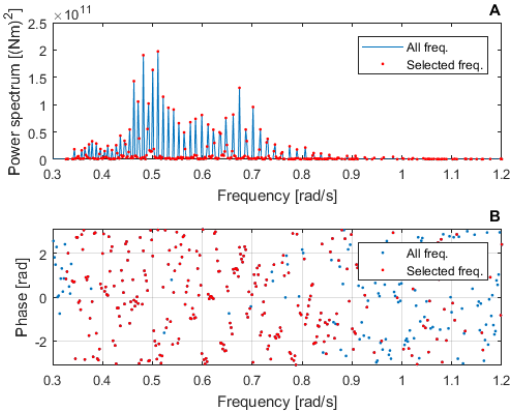

Figure 4.2: Selected sagbend BM-total frequencies (A) in the power spectrum and (B) in phase

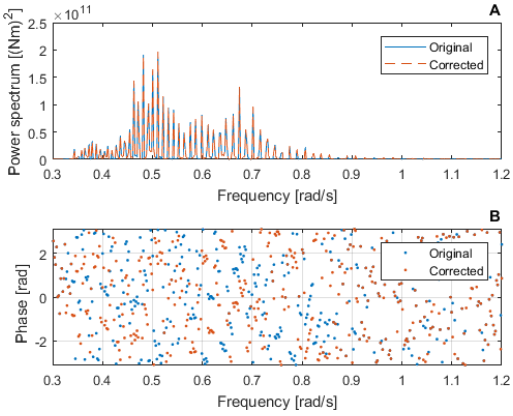

Figure 4.3: Original and corrected sagbend BM-tot (A) in the power spectrum and (B) in phase

4.2. Verification shifted pipe bending moment

The objective of aligning the pipe bending moment response to a single degree of freedom vessel motion is to improve the optimal correlation between both signals. This section verifies whether the correlation between the vessel motion and pipe bending moment signals improves. Based on the knowledge of Chapter three it is expected that axial motion at FC1 results in a significant response in pipe bending moment at the sagbend. Therefore the axial vessel motions are correlated to the sagbend pipe bending moment.

To verify this improvement a model based approach is applied. The model determines the pipe bending moment at the sagbend where the pipe radius is minimum and the vessel motion at FC1. To create different type of irregular vessel motions, this investigation consists out of types of input. A JONSWAP spectrum is applied for three types of waves: head waves, 45 degree waves and beam waves. It is expected that for these wave directions the behavior of the vessel will be significantly different. This is because of the shape of vessels hull. To compare the sagbend pipe bending moments are corrected towards the axial acceleration, the axial acceleration at FC1 should have more or less the significant axial acceleration value. This can be achieved by adjusting the significant wave height per wave direction. For example, beam waves will generally result in larger axial motions of the vessel than head waves. Figure 4.4 presents the significant wave height per wave direction and figure 4.5 presents the significant axial acceleration per direction. It can observed that the significant axial acceleration is around 0.45 $[m/s^2]$ for all directions.

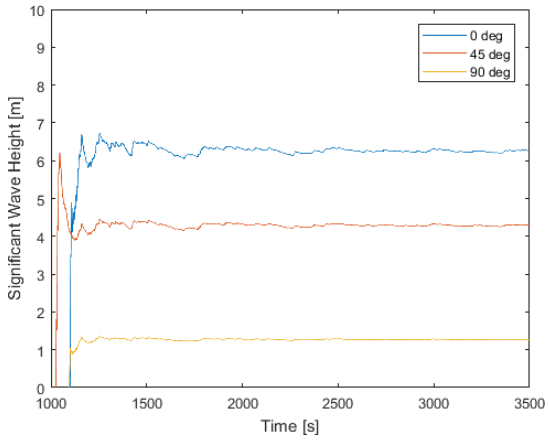

Figure 4.4: Significant Wave Height Input model

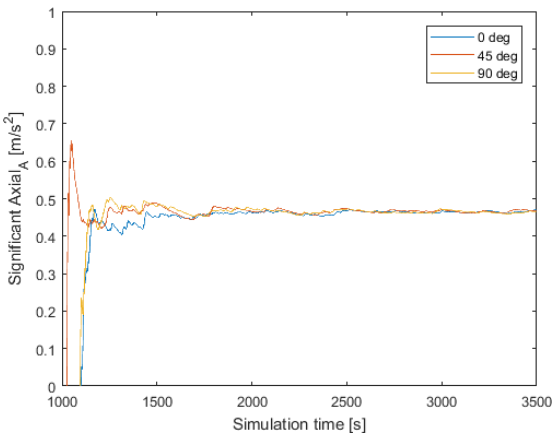

Figure 4.5: Significant Axial acceleration at FC1

As described in the previous section, the phase lag correction is performed in the frequency domain. Figures 4.6, 4.7 and 4.8 present the frequency domain in form of the power spectrum and phase of respectively the wave height, axial acceleration at FC1 and the sagbend pipe bending moment where the pipe radius is minimum. The presented figures are for the case where head waves are applied as input. Figure 4.6 shows to have a random phase, this logically due to random phase generator of Flexcom. The power spectrum should have the shape of a JONSWAP spectrum. The transformation from to power spectrum of the wave height towards the axial acceleration is affected by the RAO of the vessel.

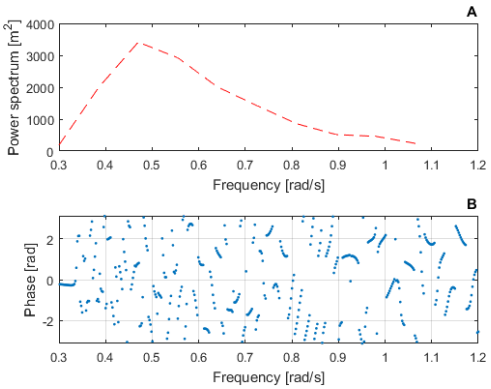

Figure 4.6: Frequency domain Wave height (A) in power spectrum (B) in phase

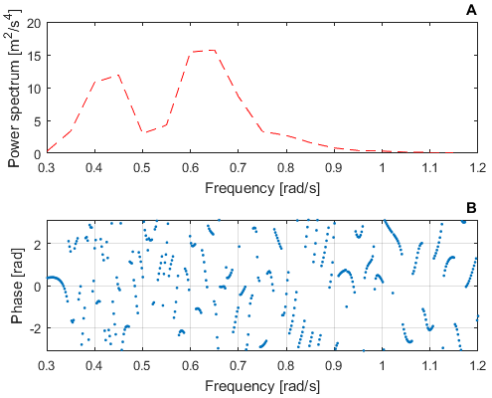

Figure 4.7: Frequency domain Axial Acceleration (A) in power spectrum (B) in phase

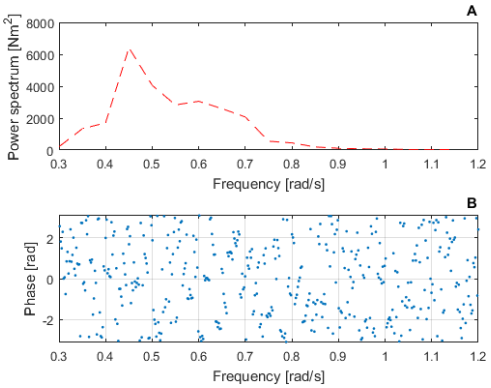

Figure 4.8: Frequency domain SB pipe bending moment (A) in power spectrum (B) in phase

The phase lag between the axial acceleration and the sagbend pipe bending moment is presented earlier in figure 3.39. This phase lag is subtracted of the phase of the pipe bending moment, presented in figure 4.8. This phase lag correction should only effect the phase of the pipe bending moment signal and therefore a built in check in performed. This 'QQ' plot, presented in figure 4.9, shows the relation between the original and shifted BM signal. The top figure shows a straight line, which means that both power spectrum's are equal. In the bottom figure, the straight line are the phases that do not exceed the cut-off frequency and the other values are the shifted phases.

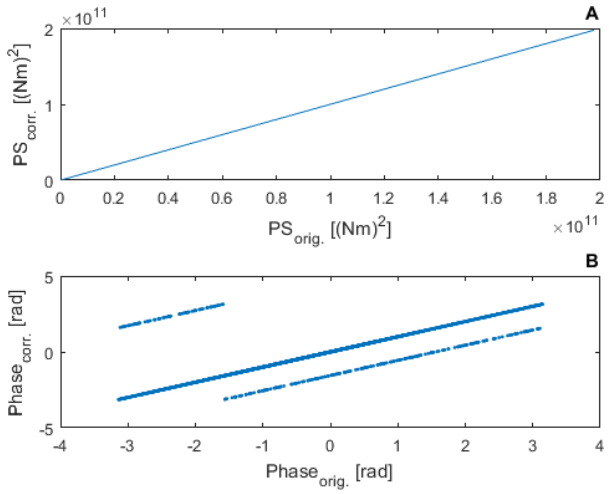

Figure 4.9: Built in check QQ plot (A) in power spectrum (B) in phase

Time domain signals

The objective of this methodology is to align the sagbend bending moment in the pipe with the axial vessel acceleration. The corrected pipe bending moment signal is converted back to the time domain. Figures 4.10 and 4.11 present the axial acceleration on the left axis and on the right axis the original and corrected pipe bending moment respectively. It can be observed that the peaks of the pipe bending moment are more aligned with the axial acceleration than for the original case. It should be noted that the result present in figure 4.11 is very accurate because the sagbend pipe bending moment is determined by the governing axial motions. It is expected that the peaks will be less accurate aligned if multiple vessel motions are governing for the sagbend pipe bending moment.

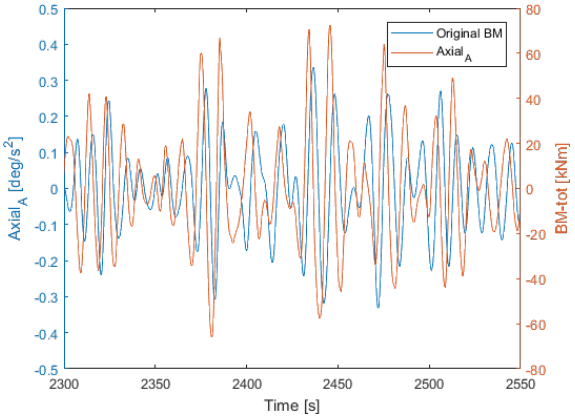

Figure 4.10: Axial acceleration at FC1 and original Sagbend BM-tot

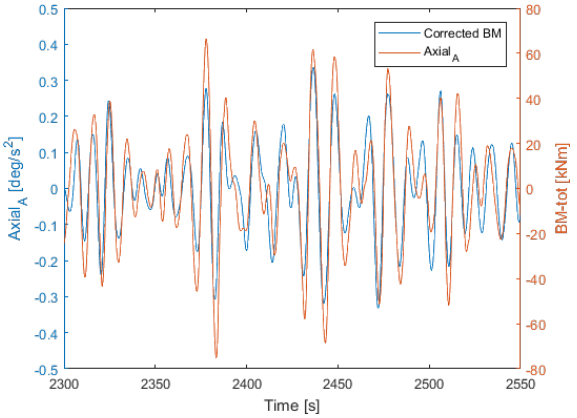

Figure 4.11: Axial acceleration at FC1 and corrected Sagbend BM-tot

RAO

The RAO between the vessel motion and pipe bending moment response give an overview of the frequency characteristics, presented in figure 4.12. This consist out of the amplitude -and phase characteristics. The amplitude characteristics is not affected, only a small change can be observed for frequencies around 1 to 1.2 rad/s. Since the wave peak period, presented in figure 4.6 is around 0.55 rad/s, it is expected the frequencies at 1-1.2 rad/s consist a low amount of energy but slightly higher than the applied threshold. After the transformation to the time domain it is expected that this effect will be negligible due to the low amount of energy.

The phase difference between both signals was initially around 270 degrees. After the applied phase correction this phase difference is now around zero degrees, which suggests that both signals are aligned. The phase is not perfectly zero degrees, this could be due to small effect of other degrees of freedom vessel motions that influence the sagbend pipe bending moment or the inaccuracy of the determination of the phase lag curve.

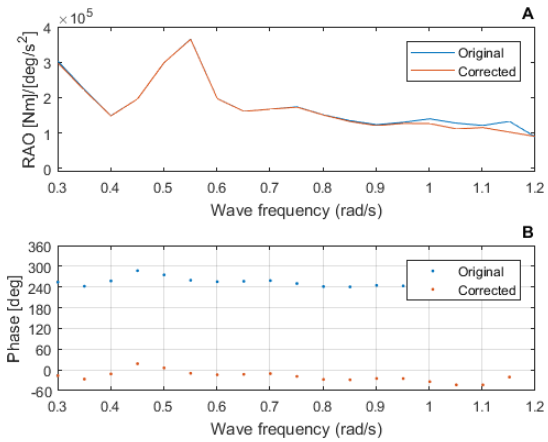

Figure 4.12: Frequency characteristics (A) in amplitude (B) in Phase

Density plot

To gain insight in the relation between the axial acceleration and the sagbend pipe bending moment density plots are created. A density plot is a variation of a Histogram. Histograms are constructed by binning the data and counting the number of observation in each bin. The more data in a certain bin, the darker the color in that specific bin. Figure 4.13 shows the density plot between axial acceleration and the original sagbend bending moment. It shows no clear trend, this is expected due to the low correlations between both signals. Figure 4.14 presents the improved relation between both sections, the density plot shows a much clearer (near linear) relation. It can also be observed that larger axial acceleration show a more linear relation than for low axial acceleration values. It is expected that for very low axial acceleration other degree of freedom vessel motions influence the pipe bending moment.

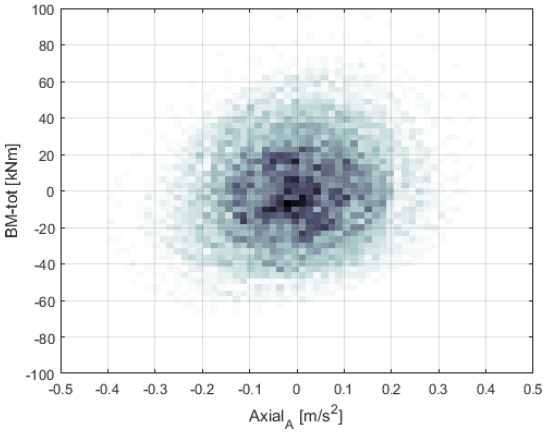

Figure 4.13: Density plot Axial acceleration FC1 and original Sagbend BM

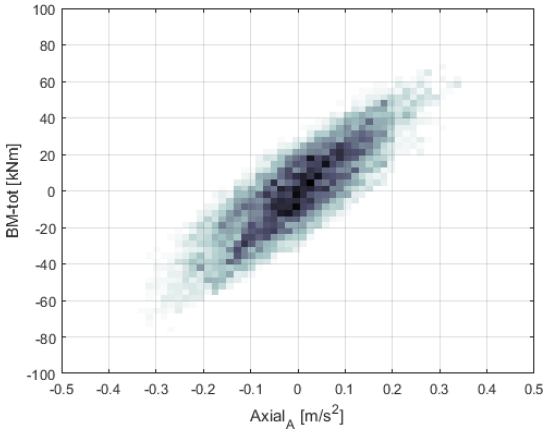

Figure 4.14: Density plot Axial acceleration FC1 and corrected Sagbend BM

Correlation

The objective of this investigation is to determine whether the correlation between the axial acceleration at FC1 and the pipe sagbend bending moment improves if the output signal is aligned to the axial motion. Figure 4.15 presents the correlation between the axial acceleration at FC! and the corrected sagbend bending moment. On the x-axis a threshold based on standard deviation is given. Instead of correlating all data values, a selection is made based on the amplitude of the acceleration signal. This increases the correlation because the larger axial acceleration will result in larger pipe bending moment response. The effect of other DOF vessel motions reduces and this results in a increase of correlation to the axial acceleration.

The correlation between axial acceleration and the original sagbend pipe bending moment was around 0.2, therefore it can be concluded that the correlation improves significantly for this type of input and location on the pipe.

Decreasing the amount of data that is used to determine the correlation also results in a decrease of confidence. A confidence of 95 % is taken to be acceptable and the according error bar is presented in figure 4.16. The error bars represent the uncertainty in the y-coordinates of the points due to approximate computation [14].

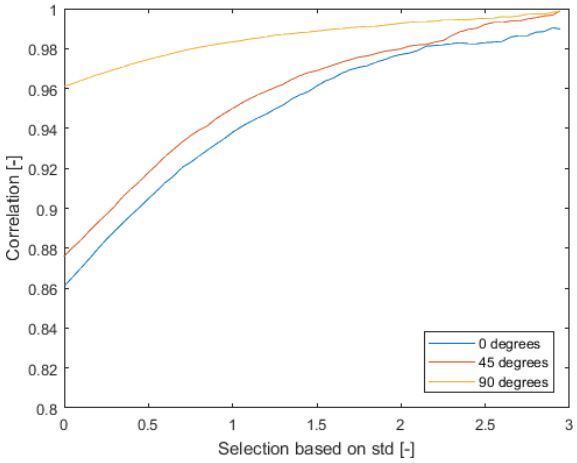

Figure 4.15: Correlation axial acceleration FC1 and corrected sagbend BM-tot

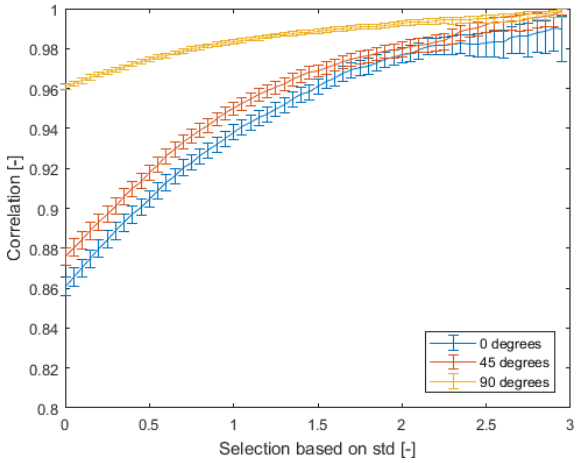

Figure 4.16: Correlation axial acceleration FC1 and corrected sagbend BM-tot with errorbar of 95% confidence

4.3. Discussion

As mentioned in Chapter 3, the phase lag is partly determined by the propagation velocity of the tensile -and pipe bending moment waves trough the pipe. In some cases it could be possible that for a type of input and location on the pipe the phase difference with axial acceleration is around 2π. In this case it is expected that the correlation between axial acceleration and sagbend pipe bending moment is significantly high without a correction in phase, but not optimal because the phase difference of 1 period.

An example is presented in figure 4.17 with in (A) the RAO and (B) the phase difference between the axial acceleration and the pipe bending moment. The phase is given in degrees and shown between zero and 360 degrees. The phase lag increases from the seabed towards the seabed. However, when the phase lag exceeds 360 degrees, it will start over at zero. This needs to be taken into account while interpreting the phase difference. A phase difference of zero would lead to a correlation of 1, 90 degrees to a correlation of zero and 180 degrees to a correlation of -1.

There are multiple options to achieve the objective of determining vessel motion limits regarding the delay/phase lag between the axial acceleration and the sagbend pipe bending moment. Know that it is known that the phase lag is present and dependent on frequency and the location of the pipe, the following options are possible:

- Do nothing. The correlation would be low in most cases, in the rare case that the position and input frequency result in a phase lag of 360 degrees, the correlation could be relatively high but not optimal.
- Align signals in time domain (constant value). The delay in time is not constant per motion frequency. In section 3.6.2 it was determined that the delay for an input frequency of 0.4 rad/s is around 8 seconds and for 1.2 rad/s around 2 seconds. Therefore it is expected that a shift in the time domain with an constant time shift will not result in an improvement of the correlation.
- Align signals in frequency domain (constant phase). The phase lag in radians is also not constant, however the difference between the phase lag for an input frequency of 0.4 rad/s and 1.2 rad/s is rather small and therefore it is expected that this will result in an improvement of the correlation but not in the optimal correlation.
- Align signals in frequency domain (phase per input frequency). This is the method that is presented in this chapter, it is taken the phase lag dependency of input frequency into account and therefore results in the optimal correlation for a single degree of freedom motion.

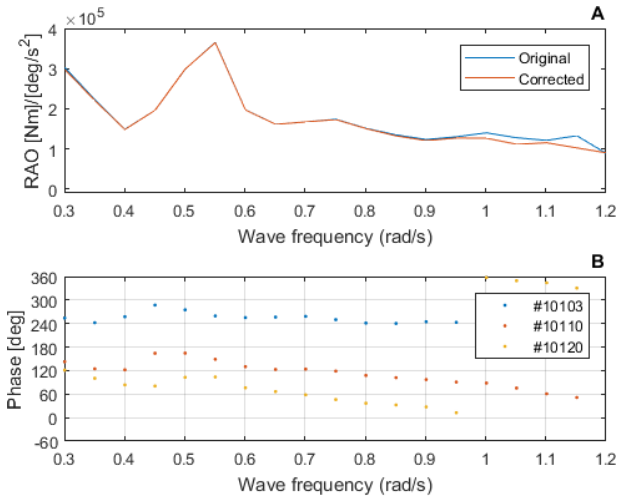

Figure 4.17: Frequency characteristics of multiple pipe sagbend BM-tot (A) in amplitude and (B) in phase

5

Methodology to determine vessel motion limits for pipe bending moment

The objective of this thesis is to determine the optimal vessel motion limit that describes the pipe bending moment at the point of interest(s). This chapter describes the methodology to determine vessel motion limit in section 5.1 and presents two examples of the obtained vessel motion limits in sections 5.2 and 5.3. The first example is to determine the vessel motion limit for the pipe bending moment at RB3 and the second example for the pipe bending moment at the sagbend where the pipe radius is minimum.

5.1. Methodology description

Part of this work is to developed a methodology that is able to determine the vessel motion limit at FC1 for the pipe bending moment responses at the point of interest. The vessel motion limit methodology is based on a model based approach. The methodology is separated in two phases and presented in figures 5.1 and 5.2. Phase 1 of the methodology determines whether it is possible to determine a relation between vessel motions and pipe bending moment and the second part of the methodology describes the required steps to determine the vessel motion limit.

The vessel motion limit consists only out of the relevant DOF vessel motion. In other words, if only two DOF vessel motion influence the pipe bending moment at the point of interest, the vessel motion limit describes a relation between the pipe bending moment and the two DOF vessel motions. This relation is presented in the form of an equation and will be discussed later on.

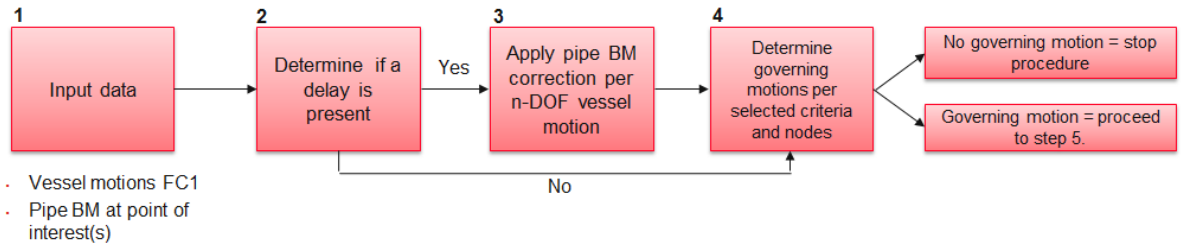

Figure 5.1: Part 1: Methodology to determine vessel motion limits

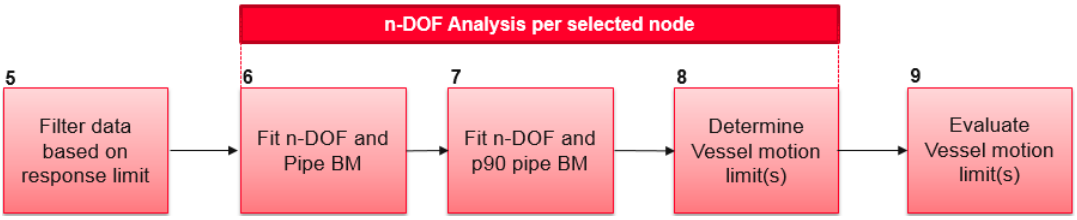

Figure 5.2: Part 2:Methodology to determine vessel motion limits

The first step is to obtain the required data from the model. The following data signals are processed: the vessel motions in each degree of freedom and the pipe bending moment responses at the points of interest(s). The second step is to determine whether a relevant delay is present between the vessel motion at FC1 and the pipe bending moment. If a delay is present, the pipe bending moment signal needs to corrected (see Chapter 4) to obtain the most accurate vessel motion limit. This can be achieved when the delayed pipe bending moment response is aligned towards the vessel motion.
Step 4 determines the governing vessel motions which are calculated in terms of correlation. An example is show in section 3.7.2. If none of the vessel motions are showing a good correlation the procedure is stopped. This means that it is not possible to determine an accurate vessel motion limit for the pipe bending moment. This could be the case if other phenomena result in large pipe bending moments instead of vessel motions.
The second part of the methodology describes how the vessel motions limit can be obtained using the governing vessel motions. Step 5 determines whether filtering of the data would improve the correlation between the vessel motions and pipe bending moment. If part of the data set decreases the overall correlation and it is not close to the point of interest, filtering is applied to improve the correlation. In step 6,7 and 8 the vessel motion limit is determined by a circulating loop. Within each loop another DOF vessel motion is added until the optimum vessel motion limit is obtained. The relation between the vessel motion(s) and pipe bending moment is found by applying a curve fit. This curve fit represents the best fit to a series of data points. This 'best fit' can be measured with the coefficient of determination. Curve fitting is based on a fitting function e.g. linear, polynomial, trigonometric (sine and cosine) or conic (circular, elliptical etc.) functions. Since the relation shows no linear behavior, this methodology applies curve fitting based on a polynomial function, other type of functions that are able to implement multiple degree of freedom vessel motions are recommended researches.
The degree of a polynomial is dependent on the number of variables of the function. The degree that results in the optimal coefficient of correlation is applied to curve fit the vessel motions and pipe bending moment. Equation 5.1 presents an example of the curve fit equation between a singular DOF vessel motion and the pipe bending moment for a second degree polynomial. The coefficients a,b,c are the polynomial coefficients that result in the optimal curve fit. Another example is given for the relation between 2DOF vessel motions and pipe bending moment in equation 5.2, which represents a polynomial surface of degree 2 in DOF1 and degree 3 in DOF2 direction. The degree that results in the highest correlation is applied.

$$BM(DOF_1) = a \cdot DOF_1^2 + b \cdot DOF_1 + c \tag{5.1}$$

$$\begin{aligned} BM(DOF_1, DOF_2) = a + b \cdot DOF_1 + c \cdot DOF_2 + \\ d \cdot DOF_1^2 + e \cdot DOF_1 \cdot DOF_2 + f \cdot DOF_2^2 + \\ g \cdot DOF_1^2 \cdot DOF_2 + h \cdot DOF_1 \cdot DOF_2^2 + i \cdot DOF_2^3 \end{aligned} \tag{5.2}$$

The curve fit equation describes the best fit value for all combinations of DOF vessel motions. It is expected that a combinations of vessel motions results in a range of pipe bending moments because the pipe bending moment is not only influenced by the vessel motions. The vessel motions that are lower than the vessel motion limit should result in pipe bending moments lower than the pipe bending moment limit. The curve fit describes the relations between the vessel motion(s) and the pipe bending moment. For any given BM limit the according motion limit can be determined. An overview of how to obtain the vessel motion limit out of a curve fit equation can be seen in figures 5.3 and 5.4.

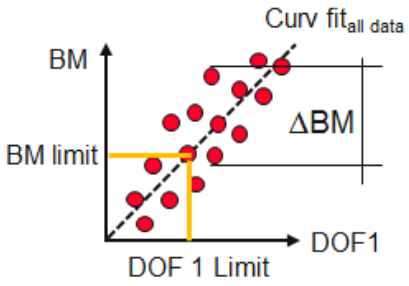

Figure 5.3: Curve $fitting_{alldata}$ to determine vessel motion limits

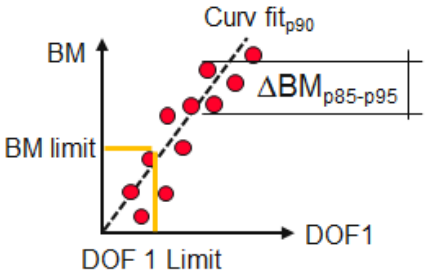

Figure 5.4: Curve $fitting_{p90}$ to determine vessel motion limits

Figure 5.3 represents step 6 in figure 5.2, where all the filtered data are curve fitted by a polynomial function. This 'best' curve fit function determines the DOF1 limit for a chosen BM limit. Since the fit is applied on all data assuming normal distributed data it is expected that around 50% of the data exceeds the BM limit. It is possible to fit all the extreme values and to determine the curve fit equation that result in a DOF1 limit for which the BM limit is not exceeded but this is a very conservative approach. The DNV GL [15] introduces the p90 value that allows around 10% of the data to exceed the determined limit and is applied in this thesis.
To determine the p90 curve fit a small selection of data must be selected. This is based on the ΔBM presented in equation 5.3 and in figures 5.3 and 5.4. This ΔBM describes the difference in bending moment between the measured pipe bending moment and the curve fit of the selected data. Positive ΔBM values means that the measured BM is higher than the fitted BM and visa versa. Important note, the p90 values of the DNV indicated that 10 % of pipe bending moment exceeds the BM limit. The p90 curve fit is based on the p90 BM values that occur per measured motion value.
To fit the p90 curve fit it requires a range of pipe bending moments around the ΔBM_{p90} values. This range is between the 85% and 95% of the pipe bending moment values and described in equation 5.4. All the values between these threshold are used to determine the p90 curve fit. A test is performed to check whether 10% of the values exceed the p90 curve fit. The p90 curve fit has 90.3% of the values lower than the curve fit and 9.7% higher than the curve fit. This shows that this methodology results in an accurate p90 curve fit.
This p90 curve fit describes the relation between vessel motions and pipe bending moments for which only 10% of the pipe bending moments exceed the curve fit. At step 8 a BM limit is chosen and applied e.g. in equation 5.1 or 5.2. Depending of the number of DOF vessel motions that are applied. For example, when two DOF are applied, the final vessel motion limit can be described as $DOF1(DOF2) = a \cdot DOF2^2 + bDOF2 + BM_{limit}$. This loop is repeated until the the optimal vessel motion limit is obtained. This can be measured with the correlation coefficient, when the correlation is not improved by adding a DOF vessel motion the loop is stopped. The final curve fit is used to determine the vessel motion limit. An example of the evaluation of the obtained vessel motion limit is given later on in this chapter.

$$\Delta BM = BM_{measured} - BM_{fitted} \tag{5.3}$$

$$\Delta BM_{p90} = \Delta BM_{p85} \leq \Delta BM < \Delta BM_{p95} \tag{5.4}$$

5.2. Vessel motion limit for the overbend

The methodology described in section 5.1 is performed in this section for the same set of data presented earlier in section 3.7. The relevant data of these 108 simulations are the vessel motions at FC1 and the pipe bending moment at RB3. For this case study it was already concluded in Chapter 3 that the delay at RB3 is close to zero and no phase correction need to applied. Chapter 3 also stated that the overbend pipe bending moment is significantly dependent on the transversal and lateral rotations at FC1. These two DOF vessel motions are the starting point to determine the vessel motion limit for the pipe bending moment. Step 5-8 is presented in section 5.2.1 and the evaluation of the vessel motion limit (step 9) is presented in section 5.2.2.

5.2.1. Analysis vessel motion limit

Section 3.3 described that the pipe bending moment at the overbend is a complex system and that relatively low vessel motions can result in a maximum pipe bending moment located elsewhere than RB3. These relatively low pipe bending moment will negatively influence the relation between the vessel motions at FC1 and the pipe bending at the overbend. This is because other phenomena than the vessel motions influence the pipe bending moment. For example, wave loading on the pipe or non linear effects in the HOM. Step 5 therefore filters the data and this filtering is based on a range around the chosen pipe bending moment limit. The optimal selection is a balance between the amount of data points and points located close to the chosen limit. In this thesis the range that is applied is 50 %, this means that all pipe bending moment values between $0.5 * limit_{BM}$ and $1.5 * limit_{BM}$ with the according vessel motions are applied for the vessel motion limit at the overbend. The sensitivity study about the filtering of data is described in Chapter 6.

Step 6,7 & 8 are performed for the lateral and transversal rotations at FC1 and the pipe bending moment at RB3. Step 6 performs a curve fit on all filtered data which is presented in figure 5.5. The optimal polynomial curve fit function that gives the highest correlation has degree 2 in lateral rotation and degree 3 in transversal rotation. This 'best' fit is used to determine the p90 curve fit in step 7. From the p90 curve fit the vessel motion limit can be calculated for any chosen BM limit.

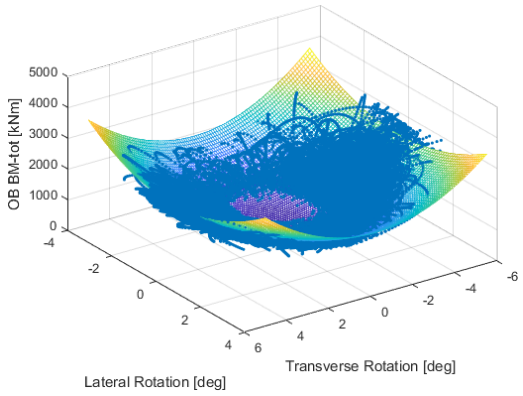

Figure 5.5: Curve fit of filtered data

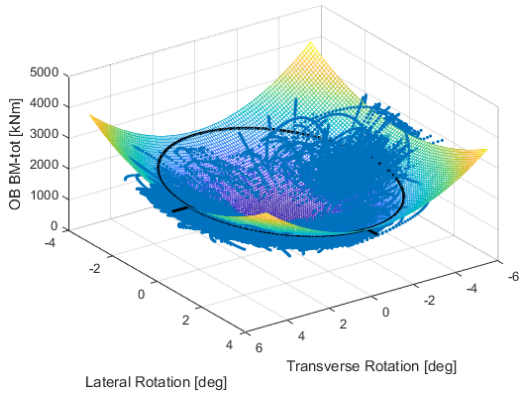

Figure 5.6: p85p95 Curve fit with vessel motion limits

The p90 curve fit is determined on the selection of data between the p85 and p95 thresholds. The ΔBM is calculated with equation 5.3 and represents the distance between the measured data and the 'best' curve fit. The cumulative ΔBM is presented in figure 5.7 and the according histogram is presented in figure 5.8. The p85 and p95 ΔBM values are obtained of these figures and used to filter the data. The p85p95 curve fit is determined based on this selection of data. The correlation coefficient between the p85p95 curve fit and the selected data is 0.9918. This shows that the curve fit is a good representative of the selected data.

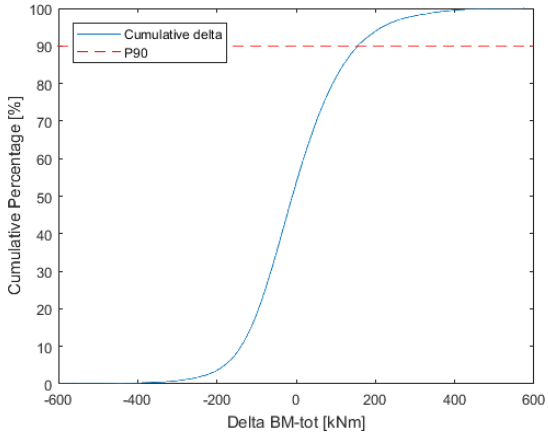

Figure 5.7: Cumulative ΔBM

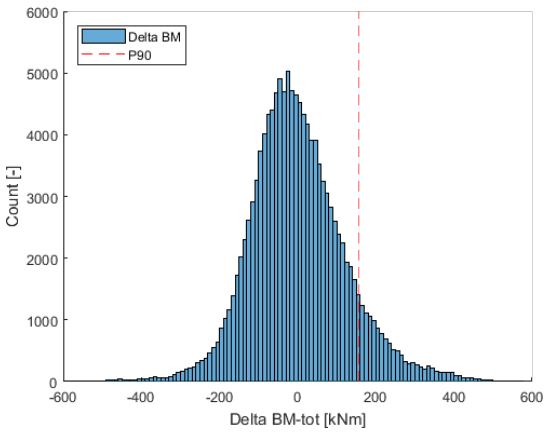

Figure 5.8: Histogram ΔBM

For the chosen BM limit of 2000 kNm at RB3 the p85p95 curve fit equation can be solved for the bending moment parameters in the curve fit equation. This gives an equation where lateral rotation is dependent on transversal rotations and visa versa. The obtained vessel motion limit is the black line presented earlier in figure 5.6 and in figure 1. In figure 5.9 the pipe bending moment at RB3 is plotted in colors, red represents a pipe BM of >3500 kNm and blue represents the pipe BM of <1000 kNm. It can be observed that the black vessel motion limit is around the chosen BM limit of 2000 kNm.

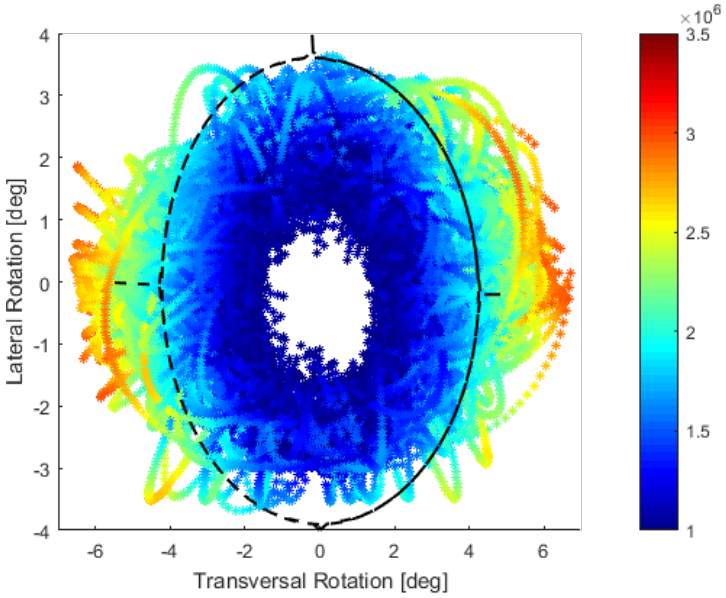

Figure 5.9: 2DOF Vessel motion limit with BM at RB3 in the color axis

Since the vessel motion limit is obtained by the data between p85 and p95 also larger pipe BM values than 2000 kNm occur inside the motion limit. The larger the area inside the vessel motion limit the higher the workability will be. However increasing this area will lead to higher bending moment values that can occur. Adding a third degree of freedom vessel motion and the determination of 3DOF vessel motion limit is a recommended research. It is suggested to apply axial rotation as a 3th DOF vessel motion based on 3th highest correction shown in section 3.7.2. However, due to the high correlation of the 2DOF vessel motion limit and the modeled data it is expected that the added value of another DOF is rather small.

5.2.2. Evaluation vessel motion limit

The last step of the methodology is to evaluate the obtained vessel motion limit. This evaluation can be divided in two parts. Firstly, the case where the pipe bending moment exceeds the BM limit and where the vessel motion are not exceeding the vessel motion limit. The exceedance of the BM limit can cause can cause damage on the pipe. The occurring pipe bending moments that exceed the chosen BM limit of 2000 kNm are presented in figure 5.10. To gain insight in the relevance of this exceedance the duration of the event where the pipe bending moment is exceeded is compared with the total simulation time. This Histogram shows the percentage of the simulation time that the BM limit is exceeded. It can be observed that most of the bending moments that exceed the limit are close to the BM limit. The highest BM value that occurs is around 2350 kNm.

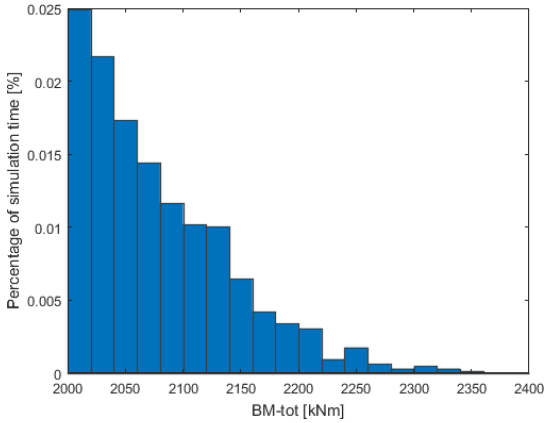

Figure 5.10: Histogram of pipe bending moment that are lower than the vessel motion limit

Secondly the obtained vessel motion limit is evaluated by comparing it with the chosen BM limit in terms of the number simulations that would be pass the limit. This gives insight in the workability of the obtained vessel motion limit. 59 out of 108 simulations have no pipe bending moment values that exceed the BM limit. Regarding the vessel motion limit, 55 out of 108 simulations have no combination of lateral and transversal rotation that exceed the vessel motion limit. This comparison is not fully justified because the vessel motion limit allows bending moment values that exceed the BM limit, however it gives an insight of the workability.

The transformation from the BM limit to a vessel motion limit leads a lower number of simulations that pass the limit and are therefore are further investigated. Figure 5.11 presents a cumulative maximum pipe bending moment that occurs per simulation. The black dash line represents the chosen BM limit of 2000 kNm. It can be observed that the simulations that have a maximum bending moment close to the chosen BM lead to a loss of workability. Because the vessel motion limit allows a small percentage of BM values above the BM limit some vessel motion simulations are lower than the vessel motion limit but larger than the BM limit. The smallest maximum BM that is outside the motion limit is 1900 kNm and the highest BM limit that is inside the motion limit is 2350 kNm.

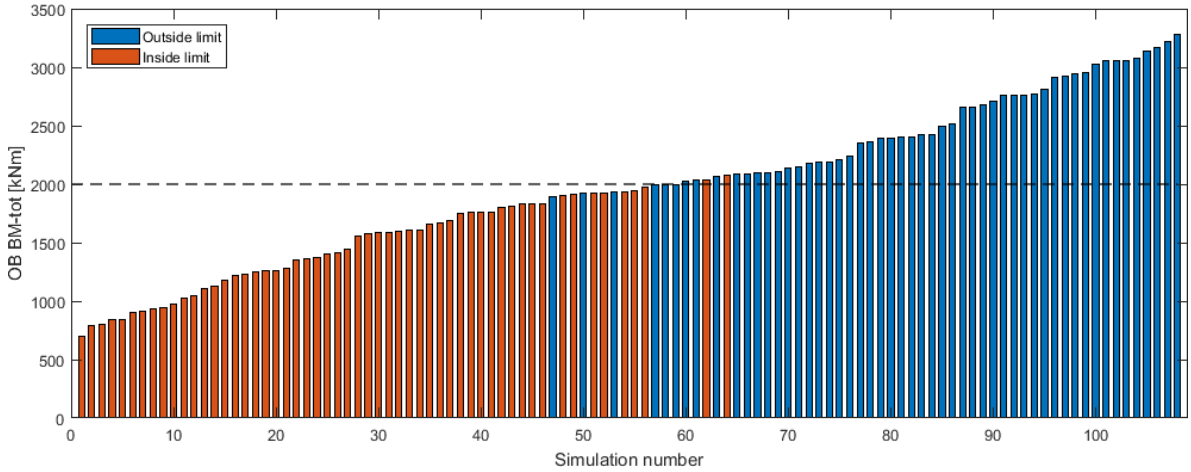

Figure 5.11: Vessel motion limit compared to BM limit

The simulations that have a maximum pipe bending moment close to but lower than the BM limit are further investigated. Figures 5.12 and 5.13 presents two examples of simulations where the vessel motion limit is exceeded but the maximum pipe bending moment is lower than the BM limit. It can be observed that the error of the vessel motion limit that represents the BM limit is very small because the yellow dots are not far outside the blue vessel motion limit.

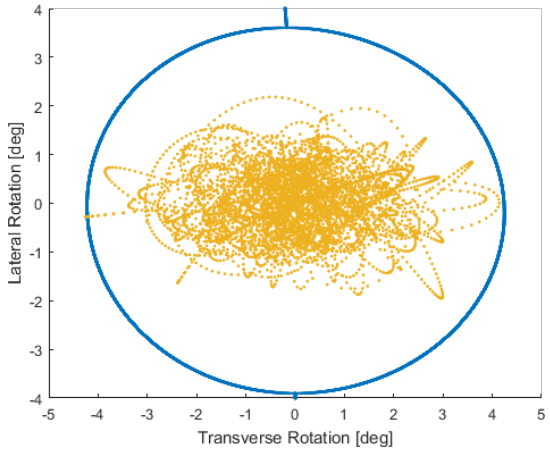

Figure 5.12: Simulation A vessel motions with max. BM of 1992 kNm

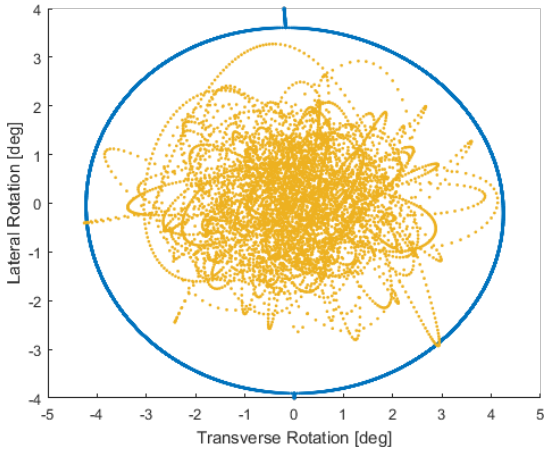

Figure 5.13: Simulation B vessel motions with max. BM of 1929 kNm

5.3. Vessel motion limit for the sagbend

The pipe bending moment can also be governing at the sagbend where the pipe radius is minimum. Therefore this section determines the vessel motion limit for the sagbend pipe bending moment. In Chapter 3 it was concluded that a delay is present between the vessel motion at FC1 and the sagbend BM.

In difference with the previous section, this section applies the phase lag that is determined in section 4.2. This is because the sagbend BM was corrected towards the axial acceleration in Chapter 4 and high correlations between these signals were determined. The corrected sagbend BM and the axial acceleration are used as input to determine the vessel motion limit. Step 5-8 are presented in section 5.3.1 and the evaluation (step 9) is discussed in section 5.3.2.

5.3.1. Analysis vessel motion limit

In section 4.2 it was observed that larger axial acceleration give higher correlations between the corrected sagbend bending moment and the axial acceleration. However, due to the linear behavior between both signals no filtering is applied. It is also expected that the p90 curve fit will already be based on the higher bending moment values which will probably result in a good correlation.

First the 'best' fit is determined between the sagbend bending moment. The same as in the previous section, the cumulative ΔBM is calculated and the p85and p95 threshold are calculated. These thresholds select only a part of the data and the p90 curve fit in the form of a second degree polynomial is performed. The 'Best' fit and the p90 curve fit are presented in figure 5.14 and figure 5.15 presents the p90 fit on the data that is between the p85-p95 selection.

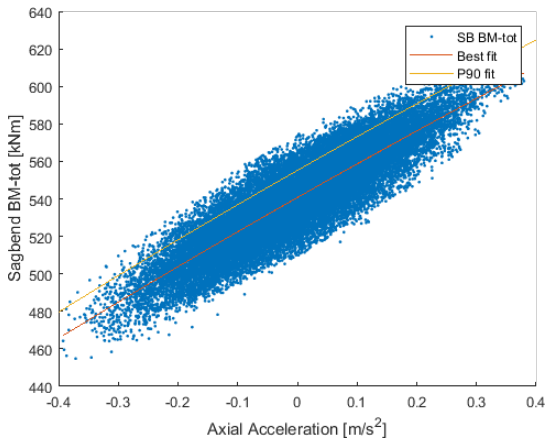

Figure 5.14: Curve fitting the corrected sagbend BM and axial acceleration

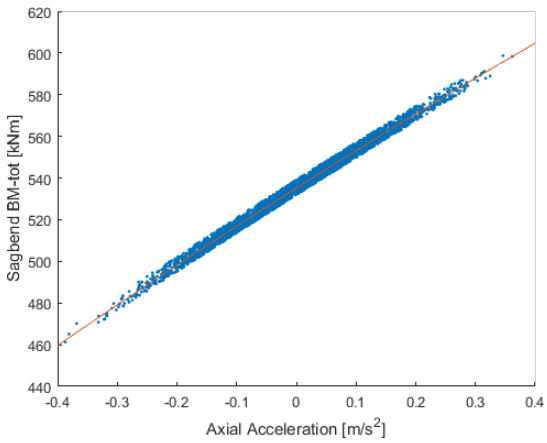

Figure 5.15: Curve fitting the selected p85-p95 data

Each degree of freedom vessel motion has a different delay with the sagbend pipe bending moment. This work is not able to combine multiple degree of freedom vessel motions with different delays. The water depth of this project is 1400m and therefore relatively deep water. It was concluded that the 1DOF vessel motion (axial acceleration) has a high correlation with the bending moment, which also result in accurate vessel motion limits. When more vessel motions become governing e.g. shallow waters, the methodology needs to be further developed.
Step 8 in figure 5.2 applied to determine the vessel motion limit. The sagbend bending moment limit is varying significant per project type. To have an idea about the vessel motion limit an example sagbend limit is set on 590 kNm. This limit is rather low compared to typical values but the data set that is used contains relatively low bending moment values.

5.3.2. Evaluation vessel motion limit

The last step of the methodology is to evaluate the obtained vessel motion limit. This evaluation is presented in figure 5.16. It can be observed that the chosen sagbend BM limit results in an axial acceleration limit of around 0.2 m/s^2. The values that presented in red are the sagbend bending moment at exceed the SB limit but are lower than the motion limit. These values are further investigated and presented in a Histrogram in figure 5.17. It can be observed that the maximum sagbend BM that occurs falls with 2.5% of the SB limit.

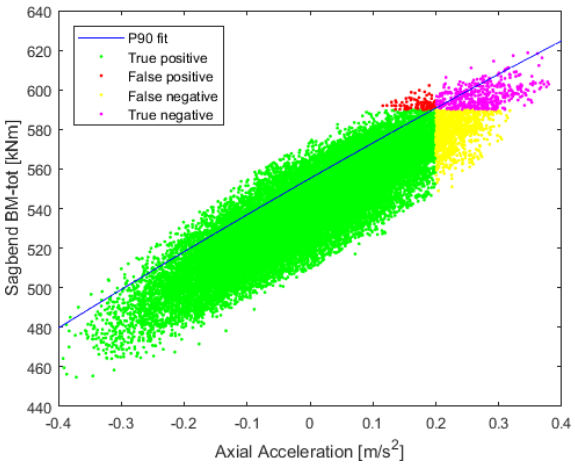

Figure 5.16: Evaluation 1DOF vessel motion limit sagbend

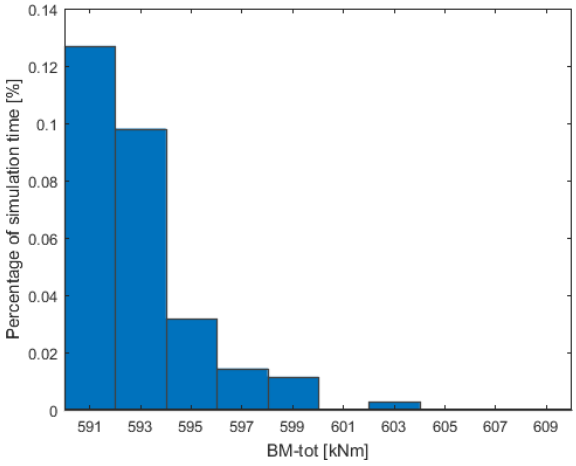

Figure 5.17: BM values that are lower than the vessel motion limit

5.4. Implementation

In Chapter 1 is was explained that vessel motion limit can be applied to calculate the workability of a project. Section 5.4.1 describes how the vessel motion limit can be implemented in the calculations of workability. Sectoin 5.4.2 describes how the vessel motion limit can be implemented at the deck of the pipe lay vessel.

5.4.1. Workability based on vessel motions limits

Currently the workability is calculated based on sea states. The determined critical sea states are simulated for a given project location and this results in a workability. These calculation are performed by a marine engineer and are also able to calculate the workability for vessel motion limits. The n-DOF vessel motion limit is determined in the form of an equation. The project model is simulated for the same project environments as for the case with critical sea states and it can be calculated how many times the vessel motion limit is exceeded. The determination of a project workability based on vessel motions is outside the scope of this thesis.

5.4.2. Vessel motion limits during offshore execution

Another advantage of vessel motion limits is on deck of the vessel. As explained in Chapter 1, the crew has to assess the actual sea state and compare it to prescribed limiting sea states. The human

assessment of the actual sea state lead to inaccuracies which can lead to a loss of workability. To method to implement the vessel motion limit during offshore execution is presented in figure 5.18. The forecasted data consists out of wave energy, frequency and direction. This data is currently converted to critical sea sates, with an H_s and T_p and direction. The critical sea states are a simplification of the forecasted data. This step leads to inaccuracies, which lead to uncertainties and this leads to a loss of workability. The vessel motions that occur due to sea waves can be calculated using a 6DOF RAO. This RAO is based on a specific load case. The loads on deck vary as well as the position of the crane. These effects introduces also inaccuracies. The RAO determines the motions of each DOF and is presented in a spectrum. This spectrum shows the energy per frequency per DOF vessel motion. The last step is applies a new RAO that is calculated using the obtained relation between the vessel motion and the sagbend bending moment. This can be used to convert the single DOF motion spectrum to a bending moment spectrum per degree of freedom. Combining can only be performed if the spectra show linear behavior. This implementation is outside the scope of work and is a recommended research.

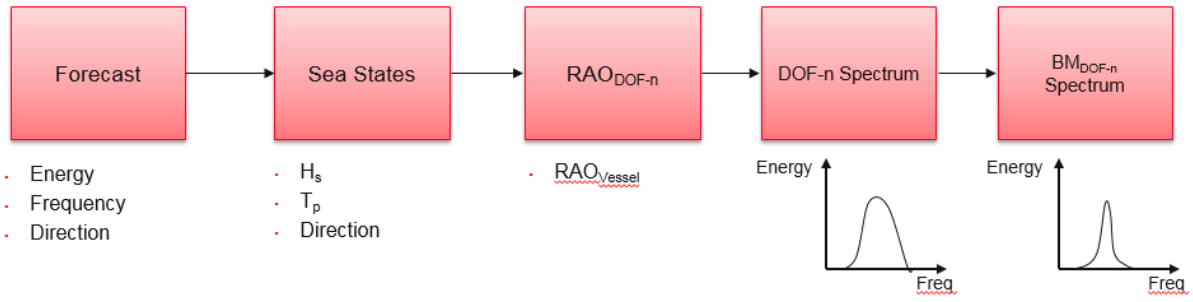

Figure 5.18: Implementation of vessel motion limits

6

Verification and sensitivity analysis

In chapter three the pipe responses due to 1DOF vessel motions are shown. This chapter gives insight about the relative impact per 1DOF of freedom. In other words, is it necessary for this type of project to take all the effects 6DOF into account to determine the sagbend bending moment limit. The phase lag between vessel motions and sagbend bending moment in the pipe is determined in chapter 3, the methodology to solve this phase lag is given in chapter 4. The section 6.2 gives insight on the influence of pipe integrity parameters on the behavior of this phase lag. The last part of this chapter are sensitivity studies of the methodology. Assumptions are made in the development of this thesis and the effect of these assumptions are investigated.

6.1. Governing vessel motions on pipe bending moment

Chapter three gives insight about the pipe response due to 1DOF vessel motion. The conclusions were that rotational vessel motions results in a pipe bending moment wave propagating from the vessel towards the seabed. Axial vessel motions result in a bending moment wave that propagates from the seabed to the vessel. This section is determining the effect of these bending moment waves on the area of interest.

In figure 6.1 a lateral rotation is applied and the bending moments are shown for at the red location (450m under the vessel) and the green location (min. radius pipe). The lower figure shows that the rotations (2 degrees) at FC1 have a negligible effect at the sagbend. The static BM in the sagbend is relatively high compared to the static BM at the overbend. A significant bending moment response at the top is required to see this response at the sagbend. This concludes that for reasonable values of rotations, the effect of these rotational motions on sagbend bending moment is very small.

In figure 6.2 an axial displacement is applied. For this DOF the situation is different compared to pipe rotations. The top figures shows that the total bending moment is dependent on both BM-Y and BM-Z. The lower figures concludes that the the bending moment total is exactly the same as BM-Z direction. This is because axial displacement causes no effect in the out of plane section. The axial displacement causes a significant bending moment response at the sagbend. As concluded in Chapter 3, a bending moment wave propagates towards the vessel, this results in a delay at node 10440 (see figure 3.9) which is located 450m under the vessel. The bending moment wave that propagates towards the vessel will have influence on the pipe bending moment at RB3, however, the amplitude of bending moment due to rotations is much higher than due to propagating BM wave towards the vessel.

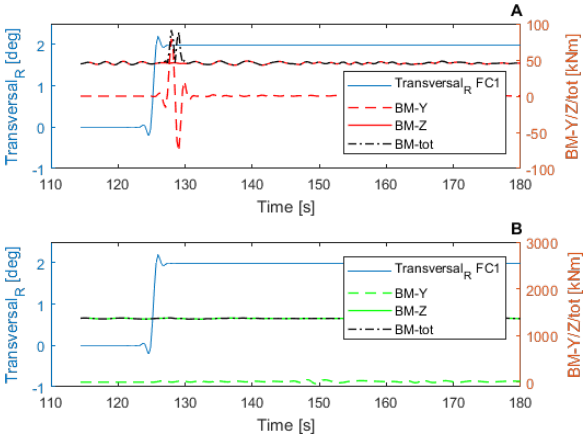

Figure 6.1: Impact of rotational motions 450m under the vessel and at the SB

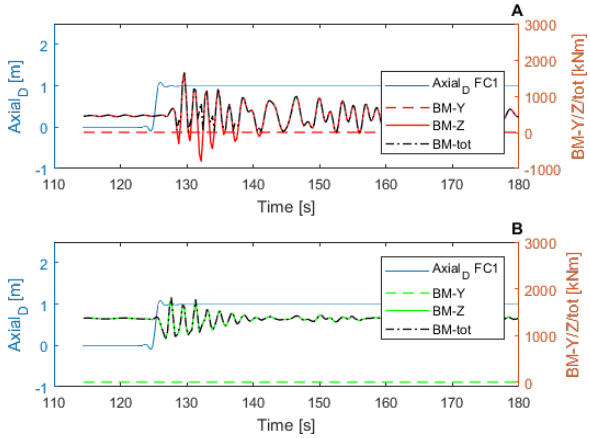

Figure 6.2: Impact of axial displacement 450m under the vessel and at the SB

6.2. Effect of pipe integrity on phase lag

Project characteristics

The phase lag between vessel motions and sagbend bending moment is determined in chapter three. To gain insight on the parameters that influences this phase lag a case study is performed. This case study contains 9 projects, differentiating in pipe diameter, water depth and centenary shape. To have equal sagbend strain for different outer diameters of pipe, the static offset is adjusted, away from the nominal position. Due to this offset, the overbend bending moment at RB3 is not close to zero, as it normally is in nominal position. A positive offset is towards the touchdown point, a negative offset is in the length op the pipe. Figure 6.3 shows a visualization of the static models that are used in this case study. Details about these projects can be found in the appendix.

Table 6.1: Project characteristics case study

Property	**Unit**	**8.25”, 16” & 22” Flowline**
Method of installation	[-]	Light J-lay
Condition	[-]	Empty at nominal position
Water depth	[m]	500 - 1400 - 2200
TA	[deg]	81.86
Draft	[m]	10.5
Pipe OD	[inch]	8.25 - 16 -22
Pipe WT	[inch]	3.76

The hydrostatic properties that are used for this entire case study can be found in table 6.2.

Table 6.2: Hydrodynamic properties case study

Hydrodynamic properties	**Unit**	**Value**
Normal drag coefficient	[-]	0.8
Tangential drag coefficient	[-]	0
Normal inertia coefficient	[-]	2
Tangential added mass coefficient	[-]	1

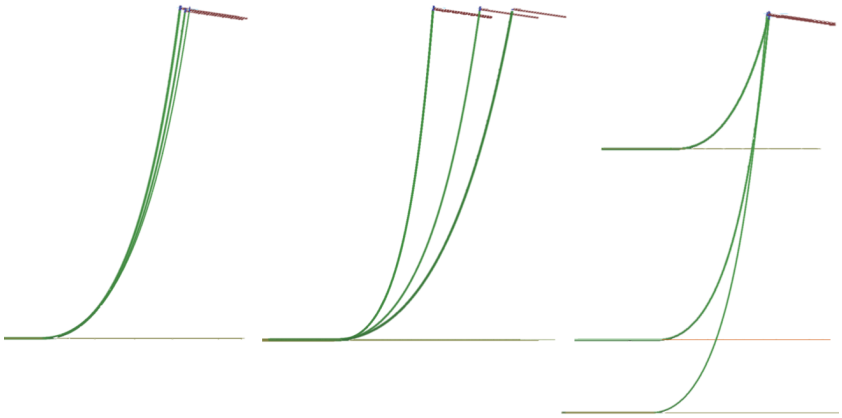

Figure 6.3: Overview 9 projects case study (Influence SB strain, SB radius and water depth)

For this case study a sinusoidal motion is applied in the axial direction of the pipe. This motion is applied at FC1 and is in line with the tower angle. The amplitude of this sinusoidal function is 1 meter. A ramp up function is used to slowly build up the ship motion in the Flexcom model, otherwise the model will not converge.

Impact sagbend strain and radius and WD

To quantify the phase lag, the delay is the time between a peak of the input (axial acceleration) and the output bending moment. The top figure, see figure 6.4 shows the static bending moment per project case. TD means the static touchdown point, this is where the pipe is on the seabed and the blue rounds are at the pipe min radius. These figures concludes the following about these set of projects:

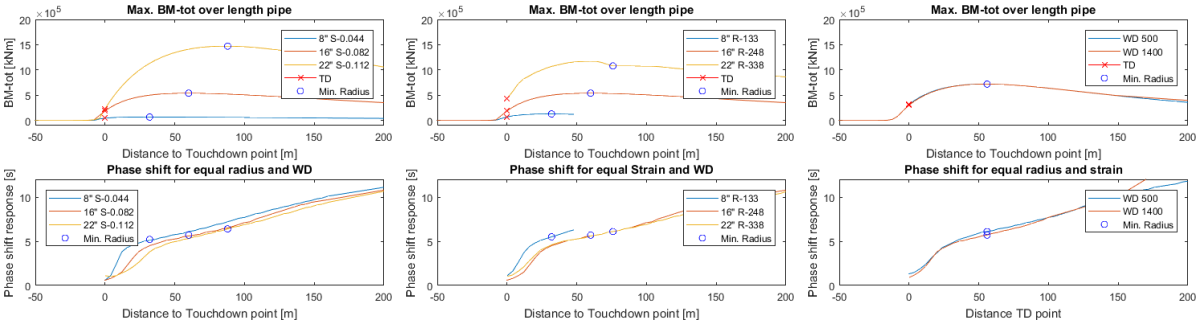

Figure 6.4: Static bending moment and phase shift for all 9 case projects

- The phase shift between vessel motions (axial acceleration) and sagbend bending moment-total develops from the touchdown point to the vessel.
- The phase shift is mainly dependent on pipe properties pipe radius and pipe strain. Water depth has a less significant impact on phase shift. This is due to the fast propagation of tensile waves trough the pipe.
- The phase shift is increasing rapidly between TD point and the min. pipe radius. This could be due to the change in pipe radius over the length of the pipe. This is not proven and is a recommended research.

6.3. Sensitivities methodology

6.3.1. Sinusoidal fit of output data

In order to determine the phase shift accurate, a small time step and low tolerance setting is needed. If these settings are set to low or small, the model will not converge and it can result in numerical errors. The time step is variable to prevent aliasing and the tolerance is set on 0.0002%. These settings give the smoothest and most accurate results. However, the output is not perfectly smooth, therefore it is

numerically difficult to calculate the delay between the vessel motion and bending moment. To solve this problem, all the output data is fitted to a sinusoidal function. The error of fitting is larger for bending moment outputs near the touchdown point, because the output is no sinus function. At the point of interested, min. radius of the pipe, there is an error around .5 seconds, equal to 0.31 rad for an input frequency of 0.62 rad/s. This methodology can be approved and is an recommendation in this thesis. An example of the original data is presented in figure 6.5 and an example of the sinusoidal fit is presented in figure 6.6.

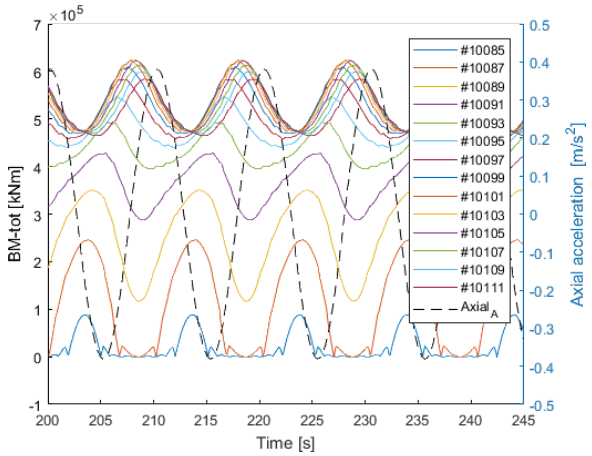

Figure 6.5: Output Flexcom model

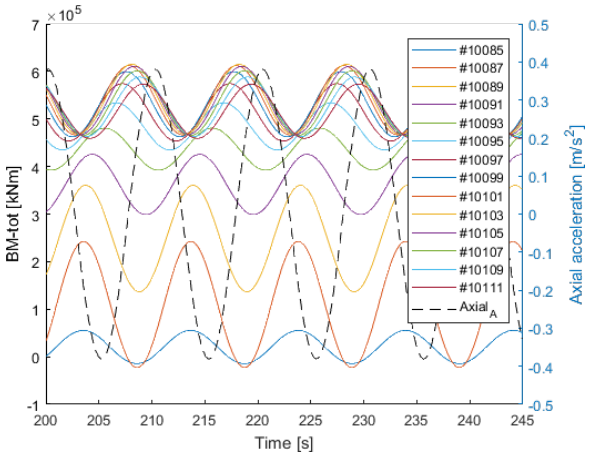

Figure 6.6: Sinusoidal fit

6.3.2. Location of the pipe boundary condition at seabed

Chapter 3 concluded that axial displacement causes a tension wave towards the seabed, which results in a pipe bending moment wave towards the vessel. The time that it requires the tension wave to convert to a bending moment wave is influenced by pipe properties, vessel motion frequency and water depth. The distance between the touchdown point and the Flexcom boundary condition is set at 350m. To check whether this distance is large enough to have no influence on the transformation from a tension wave to a bending moment wave another model is simulated with a boundary set on 1350m of the touchdown point. Figures 6.7 and 6.8 show the the results for a boundary conditions at 350m and 1350m respectively. It can be observed that that the difference in time of peak occurrences is very small. The difference in BM is 0.02 seconds and for tension 0.15 seconds. This small difference is not effecting the methodology as explained in the earlier chapters. The difference could also be a result of numerical inaccuracy and tolerance settings of the Flexcom model, but are not significant enough to investigate further.

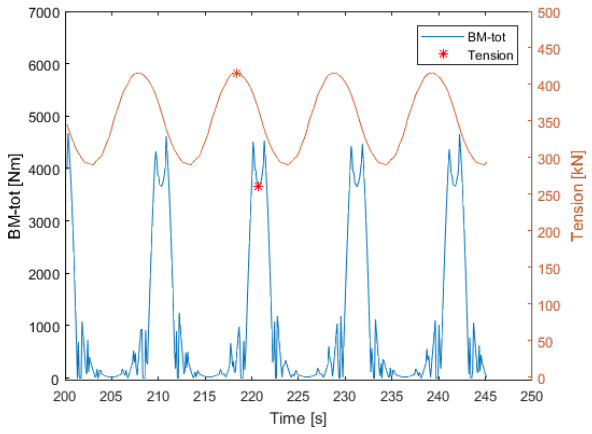

Figure 6.7: Impact BC at 350m on pipe tension/BM-tot

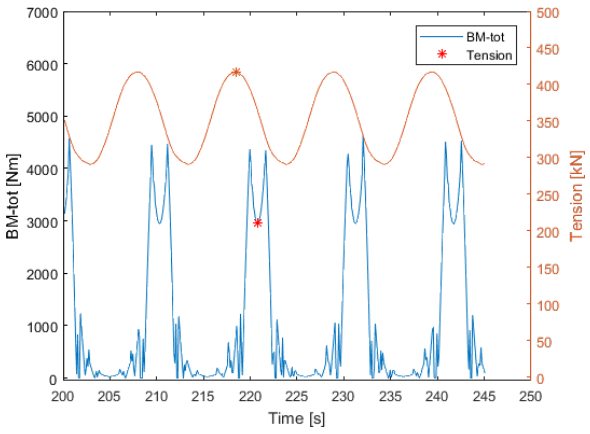

Figure 6.8: Impact BC at 350m on pipe tension/BM-tot

6.3.3. Filtering data to obtain vessel motion limit

In step 5 of the methodology, filtering is performed to select the data that is close to the chosen BM limit. This is done to neglect the low bending moment values that contain non-linear behavior which would negatively influence the curve fit. This section investigates the vessel motion limit that would be obtained for different ranges of filtering. The previous chapter used 50% as a range and in figure 6.9 it can be observed that the highest percentage of simulation that are lower than the vessel motion limit are at a range of 50%. To determine whether this is the optimal range different ranges are compared with respect to the maximum bending moment, the correlation coefficient of the p85p95 curve and the number of data points. The results are shown in table 6.3. It can be seen that less data results in a lower correlation and less simulations that are lower than the vessel motion limit. Based on figure 6.9 and table 6.3 it is concluded that this range is the optimal range to selected for this BM limit.

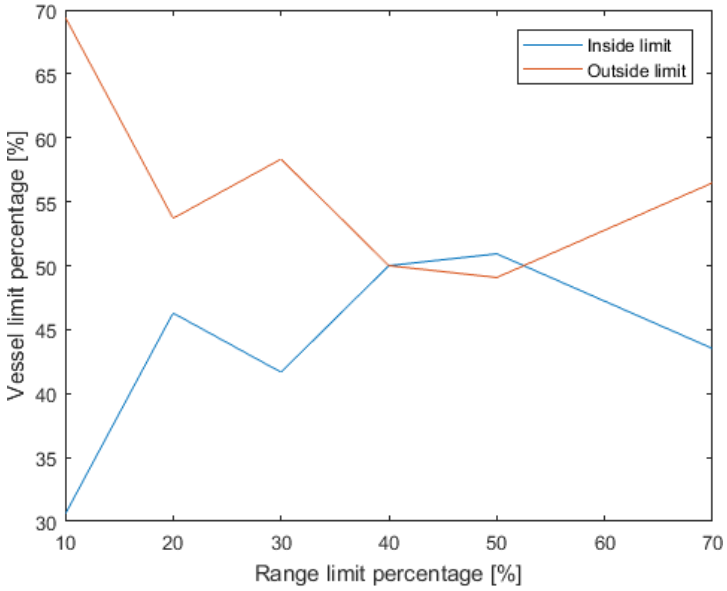

Figure 6.9: Percentage of simulations that are lower than the vessel motion limit

Table 6.3: Sensitivity study data selection based on ranges around the BM limit

Range of limit	[%]	10	20	30	40	50	70
Max. BM	[kNm]	2120	2300	2230	2336	2350	2310
Correlation p85p95	[-]	0.930	0.980	0.989	0.992	0.992	0.992
Datapoints	[-]	12000	27000	47000	81000	128000	291000

7

Conclusions and recommendations

In section 1.4 the objective of this thesis is formulated: "To develop a methodology that determines the operability conditions based on vessel motion limits for pipe bending moment during normal lay. " In this chapter conclusions and recommendations regarding the objective are formulated. To accomplish this objective, it is required to understand the characteristic pipe responses for normal-lay operations, to align bending moment signals to vessel motions if a delay is present and to develop a methodology to determine vessel motions limits. Therefore the conclusions are split up in three sections.
The first section is about the pipe bending moment characteristics due to vessel motions 7.1.1, the second section is about the new methodology to align signals with a phase difference 7.1.2, the third section is about the methodology to determine vessel motions limits 7.1.3. The recommendations are given in section 7.2.

7.1. Conclusions

7.1.1. Characteristic pipe responses for normal-lay operations

Pipe bending moments occur along the pipe catenary. The typical hotspots are the overbend and the sagbend. Each hotspot is excitated by specific vessel induced motions at the top of the catenary.
To determine accurate vessel motions limits for these hotspots high correlations are required between the governing vessel motions and the pipe bending moment. The optimal correlation can be achieved if no delay is present and when the pipe bending moment is significantly dependent on the magnitude of the motion.
The overbend pipe bending moments originate primarily from rotations around two radial local axes. The delay between the rotational motions and the overbend bending moment is close to zero. The maximum pipe bending moment is significantly dependent on the magnitude of the rotations and not to the motion frequency. Therefore these vessel motions can be used to accurately determine the vessel motion limits for the overbend.
The vessel motions that are governing for the sagbend pipe bending moment depend on the shape of the catenary. For the deep water project that is described in this thesis, the sagbend bending moment is driven by the axial acceleration of the vessel. For more shallow waters the dependency on lateral translations increases and transverse translations have a insignificant influence on the sagbend BM for these conditions.
The axial acceleration at the top of the catenary is governing because for deep water projects the axial pipe stiffness is significantly larger than the transverse and torsional pipe stiffnesses. A low stiffness result in a relatively low effect in pipe bending moment at the sagbend. The acceleration is governing because the model is inertia dominated for typical wave frequencies that occur at sea.
This research showed that the delay between the imposed motion at the top of the catenary resulted in a delay of the pipe bending moment response at the sagbend. This delay is dependent on the location of the hotspot and the frequency of the imposed motion. The delay is frequency dependent because the phase velocity is dependent on the vessel motion frequency. The delay is a summation of the duration that a tensile wave propagates from the vessel towards the seabed and the duration that a bending moment reflection wave propagates from the seabed to the location of the hotspot. Due to

the delay phenomena it is required to correct the pipe bending moment signal in phase towards the axial acceleration of the vessel to achieve accurate vessel motion limits.

7.1.2. Align signals by shifting phase lag

To determine an accurate vessel motion limit for the sagbend bending moment a methodology is presented that aligns the pipe bending moment response towards a single DOF motion at the top of the catenary. This is performed in the frequency domain since the delay is frequency dependent.
This research determined the phase lag by imposing regular axial motions at the top of the catenary. The calculated phase difference between the imposed motions and the sagbend bending moment is applied to corrected irregular sagbend bending moments. This phase lag is applied on a deep water case study and resulted in a correlation improvement from 0.2 towards 0.9-0.95.

7.1.3. Vessel motions limit Methodology

The relation between vessel motions and pipe bending moment can be fitted. The fitted equation can be used to predict the maximum pipe bending moment that occurs at the point of interest. This work presented a curve fitting methodology that obtains a relation based on the highest 85% - 95% bending moments that occur within small ranges of motions. A polynomial curve fit equation is applied on this selection of data and resulted in a p90 curve fit. This p90 curve fit is therefore not the same as the p90 value in the DNV-GL code, which represents a p90 value for the highest 10% pipe bending moments that occur. The p90 curve fit doesn't result in an exceedance of 10% of the BM values.
The vessel motions limits are determined for two case studies. The obtained overbend vessel motion limit resulted in an error range of 5% on the conservative side (max. BM doesn't exceed the BM limit) and around 15% on the side where the maximum bending moment exceeds the BM limit. However, the vessel motion limits are compared with the maximum BM value that occurs of a 20-min simulation for a generally three hour event. Therefore the determined maximum BM value is not very reliable. The obtained sagbend vessel motion limit has an error range of 10% on the conservative side and 2.5% on the side where it exceeds the BM limit. It is expected that the overbend inaccuracy is mainly caused by the effects of other DOF vessel motions. The sagbend inaccuracy is expected due to the dependency of the axial acceleration frequency.

7.2. Recommendations

This work presents a methodology that achieves vessel motion limits for the overbend and sagbend pipe bending moment locations of interest. However, the development of the vessel motions limits is not fully finished. Therefore the 4 most important recommended researches are presented.
The first recommendation is an improvement of the methodology to determine the phase lag between a vessel motion and a pipe bending moment signal. The phase lag is of great importance to determine accurate vessel motion limits for the sagbend. The current methodology applies a sinusoidal fit and introduces an error in the phase lag calculation. It is recommended to study the options to improve this method. Part of this study is to investigate different fitting algorithms and whether is it possible to determine the phase lag without the use of fitting.
The second recommendation is to determine the vessel motion limit for the sagbend for multiple degree of freedom vessel motions. It is expected that shallow water projects have multiple governing vessel motions regarding the sagbend pipe bending moment. Each governing vessel motion has a different phase lag and need to be corrected differently. The methodology presented in this work is not able to determine the vessel motion limit for multiple and differently corrected sagbend pipe bending moments.
The third recommendation is to determine the vessel motion limits based on the unity check. The unity check represented the pipe integrity criteria based on combinations of (dynamic) loads. The combination of these loads can result in failure of the pipe. Therefore is it recommended to determine the vessel motion limit for the unity check instead of only the pipe bending moment.
The fourth recommendation is to determine the vessel motion limits for structure installation project. The focus of this work is on the J-lay installation method and normal-lay. The knowledge and methodology of this thesis is a step forward in the direction to determine vessel motion limits for structure installation. Since the operability limits are lower than for normal-lay installation, a more accurate method to determine the operablity limits can have a significant impact.

Artificial Intelligence

The most common engineering method of the last 1/2 century in the offshore industry are model based approaches. Developed software is able to determine the pipe responses to vessel motions among other variables, but it is difficult to comprehending the behavior of the system. With results in too little insight in which parameters are the drivers of a specific outcome.
One of the most fruitful avenues of Artificial Intelligence research is machine learning. This refers to algorithms that, through a set of training data, allow computer programs to learn to do something for which they were not explicitly programmed. For example, one might expose an algorithm to images of both dogs and cats, with the hope that the program would learn to differentiate the two. Some of the most effective methods of machine learning are based on the concept of artificial neural networks (ANNs), which have been studied on-and-off since the beginning of AI research. ANNs are modelled after the neurons in the human brain, and consist of a network of nodes (analogous to neurons) connected with varying degrees of correlation (analogous to synapses). See reference [16].
The benefit trained network could be that it predicts the pipe response for a set of vessel motions in a very short time. To train such a network efficiently, correlations between parameters can be implemented in a hidden layer between inputs and outputs. Instead of modeling software that calculates responses numerically, this approach would be trained to predict and it is therefore able to do this faster in most cases. The downside of AI is that it difficult to comprehending the behavior.

- This thesis gives insight the the behavior of pipe response due to vessel motions. It is now possible to predict when the response occurs based on a certain vessel motion. This knowledge can be applied in the selection of ranges between correlated signals and results in a reduction of involved parameters in artificial structure. This also reduces the required amount of data to have a properly trained artificial model. It is recommended to study the possibilities to combine the gained knowledge of this thesis with artificial intelligence.

8

Discussion

In this chapter multiple subjects are discussed, knowing the results of this thesis. The first section is about the alternations in results for different project characteristics. The seconds section is about vessel motion limits for the unity check. The thirds section discusses the validation of the achieved limits. The last section is the potential of future applications of this methodology.

8.1. Project characteristics

8.1.1. Shallow water

For a water depth of 1400m the governing vessel motions for overbend bending moment are the rotational motions, the sagbend bending moment is driven by the axial motions of the vessel. For shallow water it is expected that the lateral and transversal displacement motions (especially in-plane) will be more governing with respect to bending moment in the sagbend. For shallow waters the total system is more stiff than for deep waters. The impact of a 1m displacement in plane will have a larger impact on change in the catenary shape. In this case it is required to correct the sagbend bending moment to multiple DOF vessel motions to have accurate vessel motion limits. It is expected that for shallow water projects other DOF vessel motions, such as surge, become more governing regarding the sagbend bending moment. The phase lag between a vessel motion and sagbend pipe bending moment is different for each single DOF vessel motion. This would give multiple corrected sagbend bending moment signals per governing DOF vessel motion. The current methodology should be enhanced to determine the vessel motion limit that is dependent on 2 or more DOF vessel motions.

8.1.2. Combination of phase lags per DOF

To determine accurate vessel motion limits for a pipe bending moments response that is delayed, the phase lag is of great importance. The delay depends on the DOF vessel motions because the axial, torsional and bending stiffness of the pipe are not equal. The delay for each DOF vessel motion is different and dependent on the frequency of the according vessel motion. The phase lag need to be determined for each DOF vessel motion for multiple motion frequencies. This phase lag can be applied to correct the sagbend bending moment for each of the governing vessel motions. The delay for each DOF vessel motion is different because the propagation of the tension and bending moment waves are dependent on the pipe stiffness and motion frequency. The resulting BM from different vessel motions that occur simultaneous, arrive at different times at the location of interest in the catenary. This shows the problem of the current methodology, the next step is to extend the methodology for multiple governing DOF vessel motions with their according bending moment correction. In this thesis the correlation with respect to sagbend bending moment is very high for vessels axial acceleration and the sagbend bending moment is corrected to the vessels axial acceleration. However, it doesn't always have to be that the axial acceleration (inertia dominated system) is the motion to correct to. For every DOF it should be investigated to which type of motion (displacement, velocity and acceleration) the sagbend bending moment in the pipe should be corrected.

8.1.3. Structure installation

The next step in the development of vessel motions limit would be to extent the scope of work to structure installations. During the installation of structure the workability limits are relatively low and therefore accurate vessel motions limits can have significant impact. For structure installation the total system is more complex because it is a multi body system, with 6 DOF for the vessel and 6 DOF for the structure. The body of the vessel will probably still governing for the bending moment in the pipe but the structure will also have significant impact. It should also be investigated whether the phase lag between governing vessel motions and responses in the structure are constant during lowering of this structure. It could be an outcome that multiple DOF need be corrected for different stages of the installation. During structure installation also other type of loading become more governing. The wave loads on the structure are more governing compared to normal-lay installation. This work correlates the vessel motions to the pipe bending moment. Large wave loads can affect this correlation negatively.

8.2. Unity check

The unity check is a combination of bending moment, tension and hydrostatic pressure in the pipe. Therefore the final vessel motion limits should be based on the combinations of these loads. Due to to dynamic behavior of the vessel the limit per load is not fixed. The dynamic part of pipe bending moment is relatively large compared to the dynamic part of the tension and hydrostatic pressure. For the overbend is it therefore expected that this also leads to high correlation for the unity. The sagbend unity checks encounters different types of the delay. The delay for a tension wave and a pipe bending moment wave vary significantly. To determine the relation between the vessel motions and the unity check at the sagbend further research is required.
Two methods are suggested to determine the vessel motion limit for the unity check and the location(s) of interest. Firstly, the unity check is separated for each relevant type of loading. The outcome of the unity check should be lower than 1. An option could be that the unity check is divided for pipe bending moment, pipe tension and hydrostatic pressure in 0.6/0.3/0.1. For each part of the unity check vessel motion limits can be determined. By applying the methodology presented in this work it is expected that this results in accurate vessel motion limit. The downside of this method is that the unity check parts have to be separated. An outcome can be that the total unity check is not exceeded but one of that the UC of the pipe bending moment is exceeded. This inaccuracy leads to a loss of workability. Secondly, all the relevant loads are integrated in the unity check. This increases the complexity of the problem. The relation between the different loads are non linear in the UC equation. It is expected that this non linear relation negatively affects the vessel motion limit. Further research is required to determine which of the two methods results in the most accurate vessel motion limits.

8.3. Validation of the predicted phenomena using measurements

This work verifies the obtained vessel motion limit with modeled data using Flexcom. It would be interesting to validate the vessel motions limits with measured pipe integrity. It is possible to determine the pipe bending moment and pipe tension during offshore installations. The vessel motions are measured with the MRU system on board. The relation between the vessel motions and the pipe bending moment that is presented in this work can be used to compare the different between the measured and predicted pipe bending moment.

8.4. The potential of future applications of this methodology

To determine the workability based on vessel motions limit instead of critical sea states is relatively new in the industry. So far only 1DOF vessel motions limits have been applied. The correlations that have been achieved for the sagbend (>.95) and overbend (>.99) are high. This leads to an accurate fitting equation that describes the vessel motions limit. These results show the potential of vessel motions limits to describe an accurate relation between the vessel motions and the pipe bending moment responses during normal-lay installation. The research journey towards vessel motions also brings up valuable understanding of the behavior of the system. I see a significant potential for vessel motion limits if the proposed problems regarding the unity check and multiple delayed pipe bending moments can be solved. The solutions of these problems can also be applied to extend the methodology for structure installations. These projects can have a large benefit of accurate vessel motion limits.

Bibliography

[1] M. Kooy, *Improved Calculation Method for the Workability during Pipe Laying,* Repository TU DELFT (2004).

[2] State of NSW, *Human Factors Integration - General Requirements,* State of NSW through Transport for NSW 2017 (2017).

[3] J.-L. Legras and S. . Jue Wang, *Criteria for the Operation of Lowering a Structure to the Seabed Based on the Installation Vessel Motion,* OTC (2011).

[4] D. Norske Veritas, *Modelling and analysis of marine operations,* (2011).

[5] Stefan Meeuwissen, *Memo Motion_limits,* Heerema Marine Contractors (2017).

[6] Oliver Knill, *Correlation in statistics,* Harvard Mathematics Department (2011).

[7] D. G. As, *DNVGL-ST-F101 Submarine pipeline systems,* (2017).

[8] J. M. J. Journée and W. W. Massie, *OFFSHORE HYDROMECHANICS,* (2001).

[9] C. N. Westland, *Motion behaviour analysis of 18" ILT-structures An installation procedure enhancement study,* .

[10] N. Denton, *Guidelines for submarine pipelines installation,* .

[11] *ISO-19901-1 - Metocean design and operating considerations_2005,* .

[12] G. Takacs, *Basics of Vibration Dynamics,* Springer (2012).

[13] Forrest M. Hoffman, *Fourier Introduction,* University of Warwick .

[14] S. Papers, E. Bertini, J. Kennedy, E. Puppo, A. Sarkar, A. F. Blackwell, M. Jamnik, and M. Spott, *Interaction with uncertainty in visualisations,* Eurographics Conference on Visualization (EuroVis) (2015).

[15] D. Norske Veritas, *Offshore standard Det Norske Veritas AS Submarine Pipeline Systems,* (2013).

[16] Michael Alba, *Artificial Intelligence and Engineering _ ENGINEERING,* (2017).

A

Project Characteristics

A.1. Impact of waves on overbend bending moment

The water (included waves) causes slamming and hydrostatic pressure on a pipe and , where the vessel motions have an effect on the pipe as well. In this thesis motion limits are determined based on summation of all three types of loading (wave slamming, pressure, vessel motions). No distinction is made between the different types of loading and bending moment. In order to derive the vessel motions for the bending moment, the other two types of loading should be relatively small.

To determine whether the vessel motions are the governing input load for this project a check needs to be done. Four types of loading, which are shown in table A.1 are modeled for this case study.

The first output is based on all three types of loading. The second output is only based on vessel motions and hydrostatic pressure. This is done by extracting the vessel motions of the first run and apply them in the second run. The vessel motions are the only loading applied in the second run, no waves are used as an input. The output, bending moment, is located at rollerbox three in the HOM of the Aegir. Rollerbox three is located above the sea level, therefore the hydrostatic pressure is negligible.

Table A.1: Targeted wave input

Target 1	Direction 1	Target 2	Direction 2
1 degree Pitch	0 degrees	1 degree Roll	90 degrees
1 degree Pitch	0 degrees	6 degree Roll	90 degrees
3 degree Pitch	0 degrees	1 degree Roll	90 degrees
3 degree Pitch	0 degrees	6 degree Roll	90 degrees

In figures A.1 and A.2 the results of four case study are shown. It can be concluded that the difference between both cases, in bending moment, is maximum 15% of the case where all three loadings are applied, with an average around 5%. An higher wave amplitude results in a higher percentage of the total bending moment at roller box 3 due to wave loading. From this point on, vessel motions will be determined for all three types of loading included.

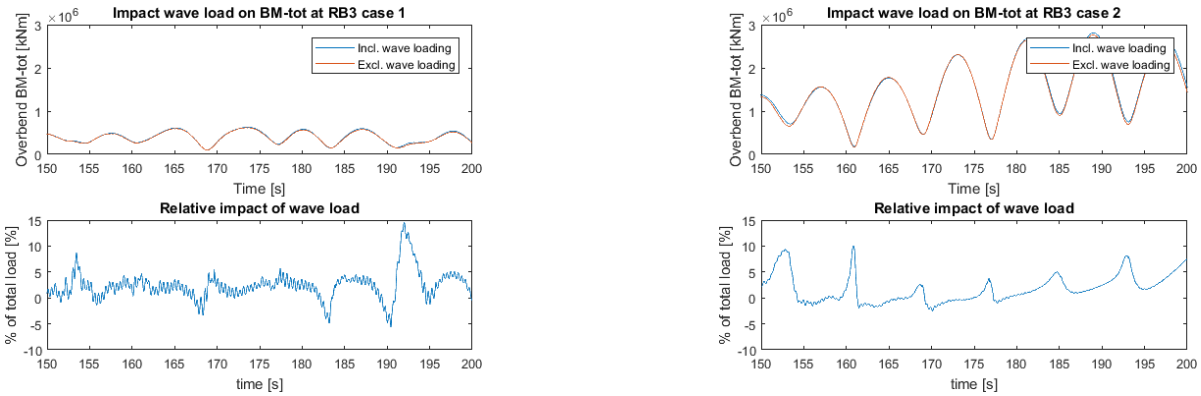

Figure A.1: Impact of waves on overbend BM 1

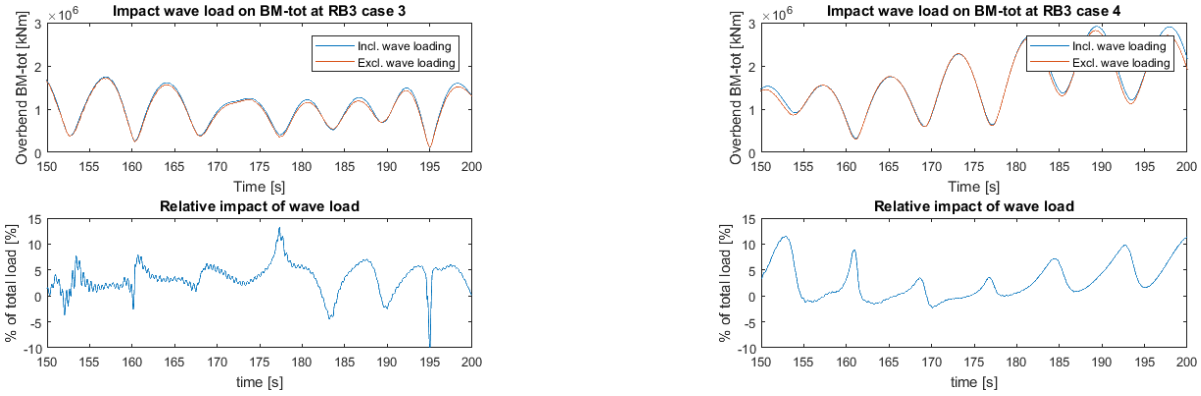

Figure A.2: Impact of waves on overbend BM 2

A.2. Model characteristics

Table A.2 shows the project characteristics for the models that are used for this research.

Table A.2: Static project characteristics

Project #	WD [m]	OD [”]	Offset [m]	Sagbend Radius [m]	Sagbend Strain [%]
1	1400	8.625	-12	248	0.044
2	1400	16	NP	248	0.082
3	1400	22	17	248	0.112
4	1400	8.625	119	133	0.082
5	1400	16	NP	248	0.082
6	1400	22	-68	338	0.082
7	500	16	-55	186	0.11
8	1400	16	70	186	0.11
9	2200	16	183	186	0.11

Table A.3 shows the settings of the HOM for the model that is used.

Table A.3: Rollerbox and friction clamp settings case study 2

Equipment	Node	Type	Displ. [m]	Stiffn. [N/m]	Displ. [m]	Stiffn. [N/m]	Displ. [m]	Stiffn. [N/m]
Friction Clamp 2	6518	Linear	-	62e+06	-	-	-	-
Friction Clamp 3	6514	Linear	-	40e+06	-	-	-	-
Rollerbox 1	6524	Non linear	0	0	0.001	10	100	846e+06
Rollerbox 2	6510	Non linear	0	0	0.001	10	100	683e+06
Rollerbox 3	6506	Non linear	0	0	0.001	10	100	610e+06

A.3. Distribution of pipe bending moment over the roller boxes

This section verifies whether roller box three is the governing location at the overbend during offshore execution. The input of the 6 DOF investigation are used as an example. The bending moment in the overbend is divided in three sections of 0-500 [knm], 500-1000 [kNm] and 1000 > [kNm]. Figure A.3 shows that for bending moments > 1000 [kNm], rollerbox three is alway governing.

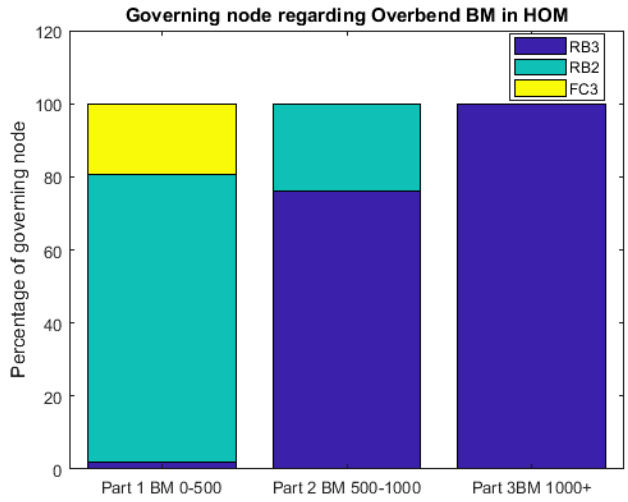

Figure A.3: Distribution pipe bending moment at HOM

A.4. Eigenmodes model

In table A.4 the eigenpairs are shows for the system. This eigenvalues contains the eigenmodes for axial and bending direction of the pipe. The bold selection shows the range of periods that are within the range of input frequency in chapter 3.

Table A.4: First 31 eigenpairs of the system

Eigenpair no.	Eigenvalue	Period (s)	Period [rad/s]
1	0.0038	101.5471	0.061875
2	0.0138	53.4431	0.117568
3	0.0142	52.7551	0.119101
4	0.0305	35.9743	0.174658
5	0.0442	29.8992	0.210146
6	0.0546	26.884	0.233715
7	0.086	21.4287	0.293214
8	0.0901	20.9282	0.300226
9	0.125	17.7702	0.35358
10	0.1491	16.2701	**0.38618**
11	0.1718	15.1592	**0.41448**
12	0.2244	13.2641	**0.473699**
13	0.2272	13.1831	**0.476609**
14	0.2922	11.6239	**0.54054**
15	0.3136	11.2193	**0.560034**
16	0.3665	10.3791	**0.605369**
17	0.4205	9.6889	**0.648493**
18	0.4499	9.3672	**0.670765**
19	0.543	8.5266	**0.736892**
20	0.5444	8.516	**0.737809**
21	0.6511	7.7868	**0.806902**
22	0.685	7.5918	**0.827628**
23	0.7694	7.1631	**0.87716**
24	0.8443	6.8379	**0.918876**
25	0.8989	6.6271	**0.948105**
26	1.0252	6.2054	**1.012535**
27	1.0414	6.1569	**1.020511**
28	1.1991	5.738	**1.095013**
29	1.2256	5.6755	**1.107072**
30	1.3717	5.3647	**1.171209**
31	1.4498	5.2182	**1.204091**

B

Equation of motions for SDOF system

B.1. SDOF mass dashpot system

To understand the physics and behavior of a vessel in seawater a comparison is made with a Single Degree of Freedom system with harmonic forcing, see figure B.1. The Equation of Motion of this system is shown in equation B.1. In this case the harmonic forcing is representing the waves and the equation of motion represents the behavior of the vessel. The first term of the EoM $(m\ddot{x})$ represents the inertia force and consist of mass and acceleration. The second term ($c\dot{x}$) represents the damping force and consist of damping and velocity. The last term (kx) represents the spring force and consists of stiffness and displacement. The harmonic forcing function is described by $F(t) = F_0 cos(\omega t)$.

$$m\ddot{x} + c\dot{x} + kx = F_0 cos(\omega t) \tag{B.1}$$

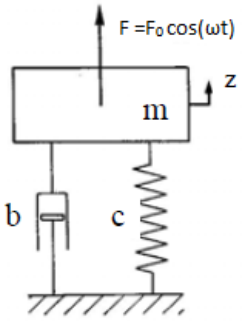

Figure B.1: Single Degree of Freedom system

The particular solution is also expected to harmonic. The assumed solving form becomes:

$$x_p(t) = Xcos(\omega t - \phi) \tag{B.2}$$

The derivations of this particular solution are the velocity and acceleration respectively.

$$\begin{aligned} x_p(t) &= Xcos(\omega t - \phi) = displacement \\ \dot{x}_p(t) &= -X\omega sin(\omega t - \phi) = velocity \\ \ddot{x}_p(t) &= -X\omega^2 cos(\omega t - \phi) = acceleration \end{aligned} \tag{B.3}$$

where X and ϕ are constants to be determined that denote the amplitude and phase angle of the response, respectively. By substituting equation B.2 into equation B.1, equation B.4 is obtained:

$$X[(k - mw^2)cos(wt - \phi) - cwsin(wt - \phi)] = F_0 cos(wt) \tag{B.4}$$

Using the following trigonometric relations:

$$\begin{aligned} cos(\omega t - phi) &= cos(\omega t)cos(\phi) + sin(\omega t)sin(\phi) \\ sin(\omega t - phi) &= sin(\omega t)cos(\phi) - cos(\omega t)sin(\phi) \end{aligned} \tag{B.5}$$

Equations B.1 are obtained:

$$\begin{aligned} [(k - m\omega^2)cos(\omega t - \phi) + c\omega sin(\omega t - \phi)]X &= F_0 cos(\omega t) \\ [(k - m\omega^2)sin(\omega t - \phi) - c\omega cos(\omega t - \phi)]X &= 0 \end{aligned} \tag{B.6}$$

Solve equation :

$$\begin{aligned} X &= \frac{F_0}{\sqrt{[k - m\omega^2)^2 + (c\omega)^2)]}} \\ \phi &= \tan^{-1}(\frac{c\omega}{k - m\omega^2}) \end{aligned} \tag{B.7}$$

Insert X into $x_p(t) = Xcos(\omega t - \phi)$ and the particular solutions is obtained. Using the parameters in equation B.8, X can be simplified.

$$\begin{aligned} w_n &= \sqrt{\frac{k}{m}} = undamped \quad natural \quad frequency \\ C_c &= 2m\omega_n = critical \quad damping \\ \zeta &= \frac{c}{c_c} = \frac{c}{2m\omega_n} = \frac{c}{2\sqrt{mk}} = damping \quad factor \\ r &= \frac{\omega}{\omega_n} \\ \delta_{st} &= \frac{F_0}{k} = deflection \quad under \quad static \quad ForceF_0 \end{aligned} \tag{B.8}$$

$$\begin{aligned} \frac{xk}{F_0} &= \frac{1}{\sqrt{[1 - (\frac{\omega}{\omega_n})^2]^2 + [2\zeta\frac{\omega}{\omega_n}]^2}} = \frac{1}{\sqrt{(1 - r^2)^2 + (2\zeta r)^2}} = \frac{X}{\delta_{st}} \\ \phi &= \tan^{-1}(\frac{c\omega}{k - m\omega^2}) = \tan^{-1}(\frac{2\zeta r}{1 - r^2}) \end{aligned} \tag{B.9}$$

The quantity $M = \frac{X}{\delta_{st}}$ is known as the magnification factor, amplification factor or the amplitude ratio. The amplitude of the forced vibration becomes smaller with increasing values of the forcing frequency. The phase angle is dependent of the damping factor ζ. For an undamped system (ζ = 0), the phase angle is zero for 0<r<1 and 180 degrees for r>1. This implies that the excitation and response are in phase for 0<r<1 and out of phase for r>1 when ζ = 0.
For ζ >0 and 0<r<1, the phase angle is given by 0<ϕ<90, implying that the response lags the excitation. For ζ>0 and r>1, the phase angle is given by 90<ϕ<180, implying that the response leads the excitation.

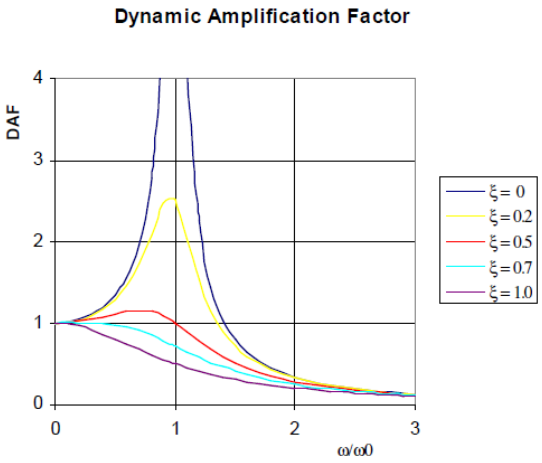

Figure B.2: Dynamic Amplication Factor

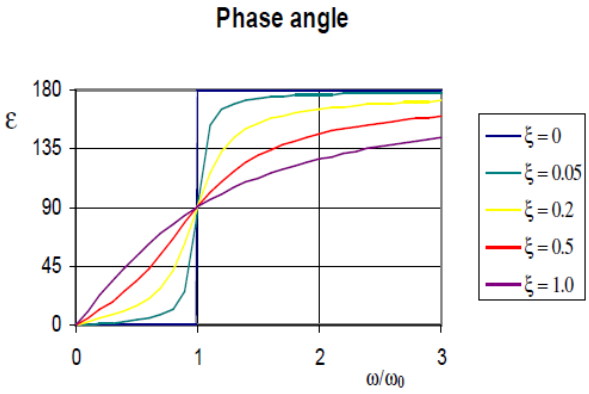

Figure B.3: Phase angle

The DAF (Dynamic Amplification Factor) can be categorized in three different phases. The first phase, first figure in figure B.5, is where the response is stiffness dominated. The load frequency is lower than the natural frequency. This means that the wave period is higher than the natural period of the vessel. The second phase (second figure in figure B.5) is were resonance occurs. The response can become large when r is close to 1 or when ω is close to ω_n. The reduction in M in the presence of damping is very significant at or near resonance.This is where the load frequency is close to the eigenfrequency of the vessel.
The third phase (third figure in figure B.5) is an inertia dominated response. This occurs for the situation where the load frequency is higher than the eigenfrequency of the vessel. In other words, the wave period is lower than the natural period.
Frequency of input (wave) and output (motion) are always the same. The ratio between the motion amplitude and the wave amplitude is called the RAO (Response Amplitude Operator). RAO's and phase angles are dependent of wave frequency and wave direction.

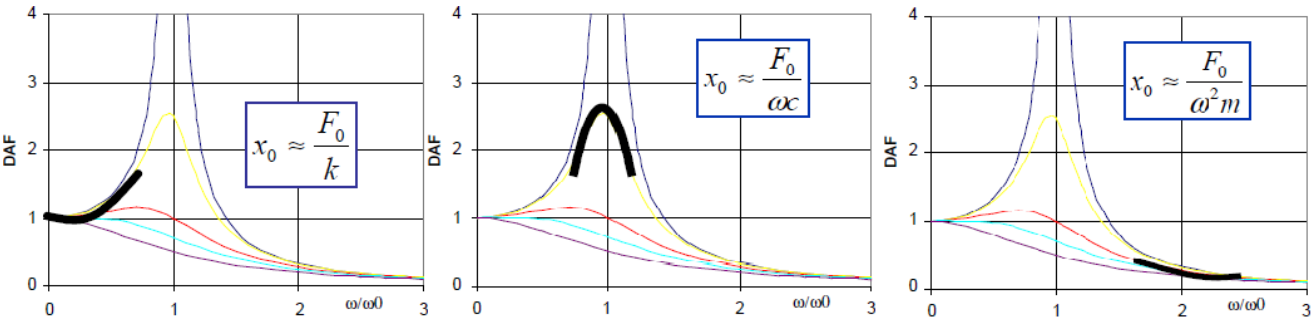

Figure B.4: Stiffness dominated response, Resonant response, Inertia dominated response

The nature of resonance and the phase angles can be seen in the force polygon of figure B.5. This figure shows three different force polygons, for at resonance, far before resonance and far after resonance, respectively. The polygon contains the spring force (kx), damping force (cωx), inertia force (mω^2x) and the external force F. The angle between the external force and the displacement vector is ϕ.As mentioned before, the damping factor ζ influences the resonance condition. The displacement term is always in anti-phase with the acceleration. This can also be concluded from the equation $m\ddot{x} + kx = 0$ for example.

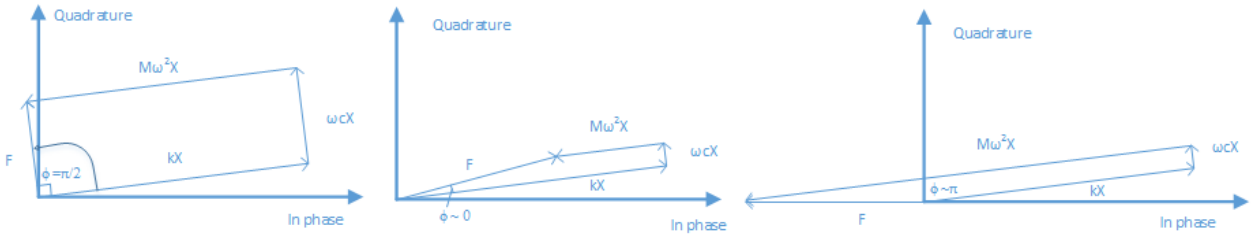

Figure B.5: Polygon at resonance, far before resonance, far after resonance.

During resonance the following statements are true:

- ϕ is close to $\pi/2$ and r is equal or close to 1
- The inertia term ($m\omega^2x$) and stiffness term are equal and opposite
- The damping term ($c\omega x$) and input Force are equal and opposite
- Damping affects the response only for excitation frequency close to resonance
- Damping causes lag between input and output
- The lag between wave and displacement is maximum during resonance, see figure B.6
- The smallest value of the driving force occurs during resonance because the driving force is only acting against damping.

Before resonance the following statements are true:

- ϕ is close to 0.
- The system is stiffness dominated. The stiffness term is larger than the inertia term.
- The displacement is almost in phase with the force. Their is a small lag.

After resonance the following statements are true:

- ϕ is close to π.
- The system is inertia dominated. The inertia term is larger than the stiffness term.
- The displacement is out of phase with the force.
- The response leads the excitation.

Figure B.6 shows the force and excitation (displacement) at resonance, far before resonance and far after resonance. The wave period/frequency are equal to the period/frequency of the displacement. It is easy to concluded that the displacement is shifting over the horizontal axis for different input frequencies.

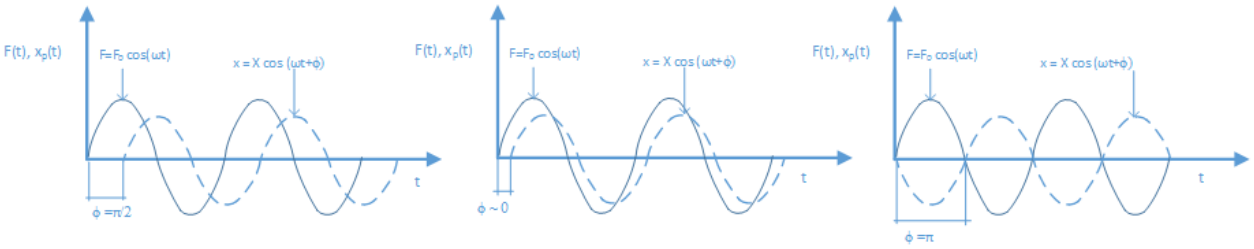

Figure B.6: Force and excitation (displacement) at resonance, far before resonance, far after resonance.

In figure B.7 the velocity and acceleration are added to figure B.6. The green plot represents the intertia term and the red plot represents the damping term. As mentioned before the displacement and acceleration are in anti-phase. The first figure shows that the displacement term and inertia term are equal, the damping term is contributing as well. The second figure shows that that the system is stiffness dominated with a low contribution of the damping term. The third figure shows a inertia dominated system with a low contribution of the damping term as well.

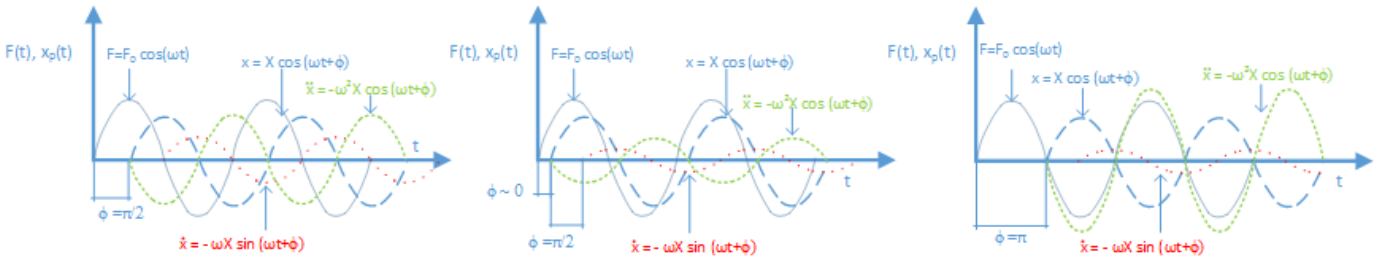

Figure B.7: Force, displacement, velocity and acceleration at resonance, far before resonance, far after resonance.

B.2. Stiffness modes cantilever beam

To give an example of the effect of the mode of vibrations on a pipe, a simplification is made in fthe form of a cantilever beam. Figure B.8 demonstrates three modes of vibrations. The stiffness of the system is different per type of mode. This explains why a tensile wave propagates faster than a bending moment wave trough a pipe.

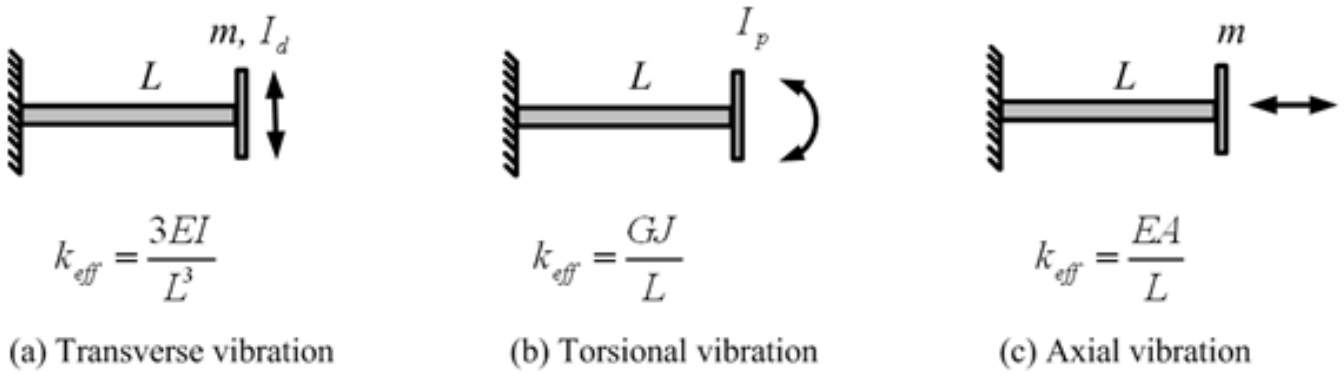

Figure B.8: A cantilever beam with different mode of vibrations

Each mode of vibration has a different eigenfrequency. The first eigenfrequencies can be calculated as follows:

$$\omega_{n,Transverse} = a_n^2 \sqrt{\frac{EI}{m * L^4}} \tag{B.10}$$

where:

m = mass per unit length
$a_1 = 1.875^2$ (first eigenfrequency)

$$\omega_{n,Torsional} = b_n * L \sqrt{\frac{GJ}{m * L}} \tag{B.11}$$

where:

m = mass polar moment of inertia per unit length
$b_1 * L$ = 0.8605 (first eigenfrequency)

$$\omega_{n,Axial} = b_n \sqrt{\frac{EA}{m}} \tag{B.12}$$

where:

m = mass polar moment of inertia per unit length
$b_1 = \frac{1}{2} * \pi$ (first eigenfrequency)

For the pipe characteristics that are applied in chapter 3, the first eigenfrequencies are: $w_{1,Transverse} = 0.47 rad/s$, $w_{1,Torsional} = 60.8 rad/s$ and $w_{1,Axial} = 3.52 rad/s$.

The dispersion relation describes the effect of dispersion in a medium on the properties of a wave traveling within that medium.

$$v = \frac{\omega}{k} \tag{B.13}$$

ω = frequency [rad/s]
k = wave number

C

Delay sagbend bending moment by imposed motions at friction clamp 1

C.1. Effect of model boundary settings on the delay

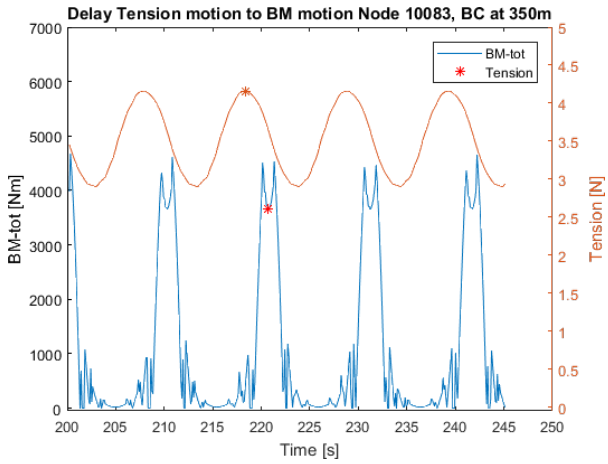

Figure C.1: Transformation of motion with boundary condition at 350m of touchdown point

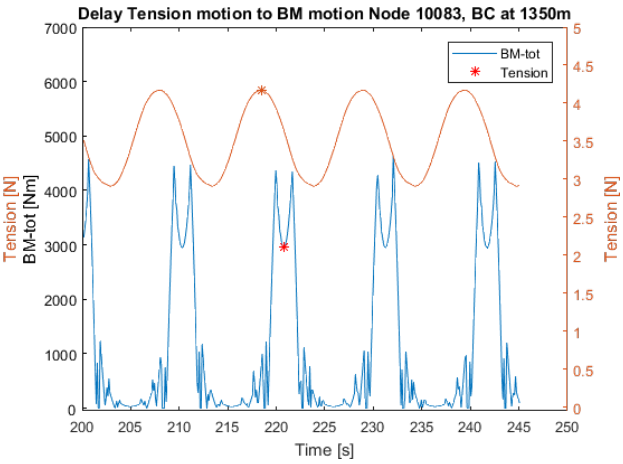

Figure C.2: Transformation of motion with boundary condition at 1350m of touchdown point

C.2. Effect motion frequency on delay

In this section a small study is performed to calculate the correlation between the vessels axial acceleration and the sagbend bending moment at the pipe min. radius. Two harmonic axial displacements with a period of 0.6 rad/s and 1.2 rad/s are used as inputs for the model.

Table C.1: Pipe integrity responses for multiple axial input frequencies

Location / Value	Parameter	Peak (s) for 0.6 rad/s	Peak(s) for 1.2 rad/s
FC1	Acceleration vessel	217.3	223.8
TD	Tension pipe	+1.1	+0.5
TD	Heave pipe	+3.5	+1.9
TD	BM-tot	+3.9	+2.7
Sagbend min. radius	BM-tot	**+8.1**	**+4.6**
FC1	Velocity vessel	**+7.8**	+3.9 & +6.6
FC1	Acceleration vessel	+5.2 & +10.4	+2.6 & **+5.2**

- Correlation vessel acceleration and sagbend bending moment (min. radius) for 0.6 rad/s: 0.22
- Correlation vessel acceleration and sagbend bending moment (min. radius) for 1.2 rad/s: 0.82
- Correlation vessel velocity and sagbend bending moment (min. radius) for 0.6 rad/s: 0.97
- Correlation vessel velocity and sagbend bending moment (min. radius) for 1.2 rad/s: 0.22

This concludes that the correlation for an uncorrected sagbend bending moment is dependent of the input frequency and of the location of the point of interest.

C.3. Effect of fitting sagbend bending moment output

In order to determine the phase shift accurate, a small time step and low tolerance setting is needed. If these settings are set to low or small, the model will not converge and it can result in numerical errors. The settings that are applied for this case study can be found in table C.2. Multiple settings are modeled and these settings give the smoothest and most accurate results. However, the output is not perfectly smooth, therefore it is numerically difficult to calculate the delay between the vessel motion and bending moment. To solve this problem, all the output data is fitted to a sinusoidal function. The error of fitting is larger for bending moment outputs near the touchdown point, because the output is no sinus function. At the point of interested, min. radius of the pipe, there is an error around .5 seconds, equal to 0.31 rad for an input frequency of 0.62 rad/s. This methodology can be approved and is an recommendation in this thesis. An example of this fitting is shown in figure C.3.

Table C.2: Time step and tolerance settings model

Settings	**Type**	**Value**
Time step	Variable	min. 0.05, [s] suggested 0.1 [s]
Tolerance	Constant	0.0002

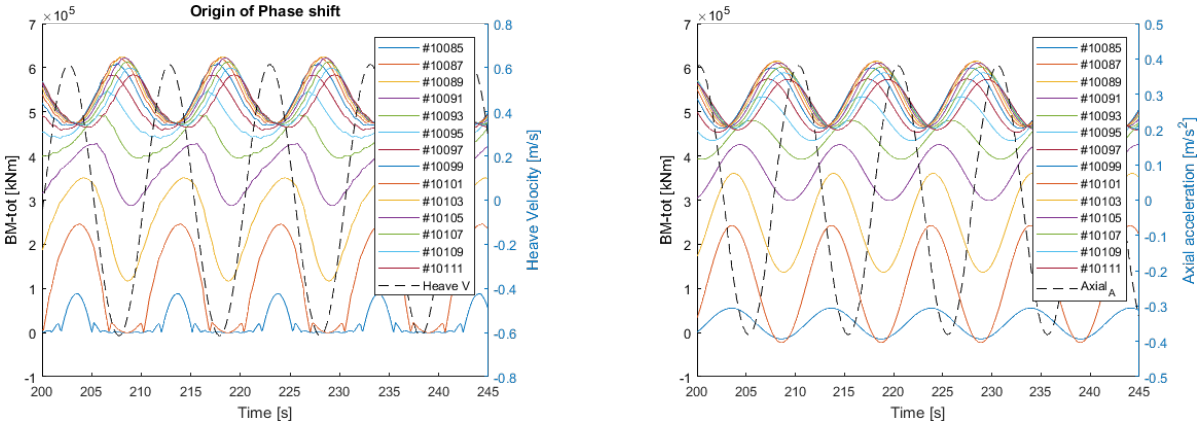

Figure C.3: Output Flexcom model, Sinusoidal fit output

C.4. Acceleration pipe at the Touchdown point

The displacement at the static touchdown point causes a change in the catenary shape. Therefore the pipe bending moments peaks occur shortly after this displacement. Figure C.4 demonstrates that the pipe bending moment and the vertical acceleration of the pipe.

This suggest that the an imposed axial motion at friction clamp 1 result in a tensile wave towards the seabed, lifts the pipe upwards and results in a reflecting pipe bending moment wave towards the vessel. Further investigation is required to confirm the propagating pipe bending moment wave.

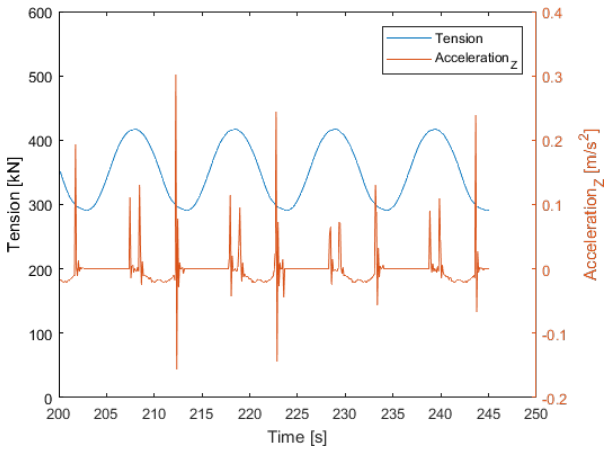

Figure C.4: Output Flexcom model, Sinusoidal fit output

C.5. 3DOF Vessel motion limits at the overbend at RB3

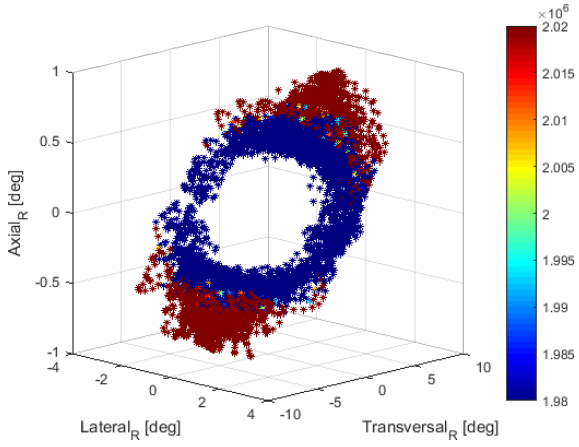

Figure C.5: Dataset for 3DOF

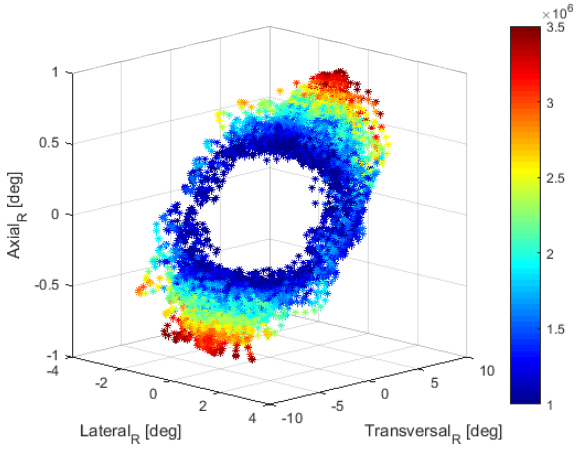

Figure C.6: Dataset for 3DOF

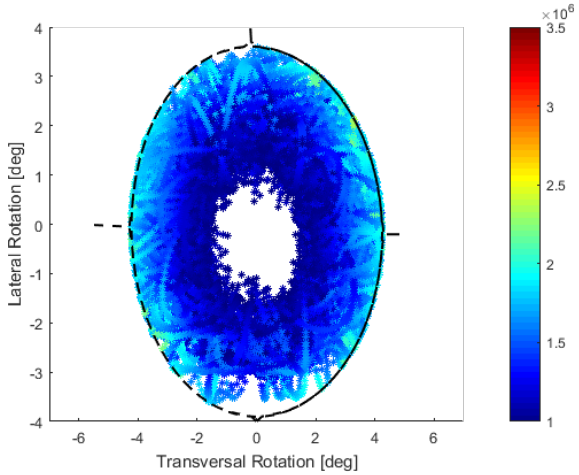

Figure C.7: Pipe bending moments inside vessel motion limits

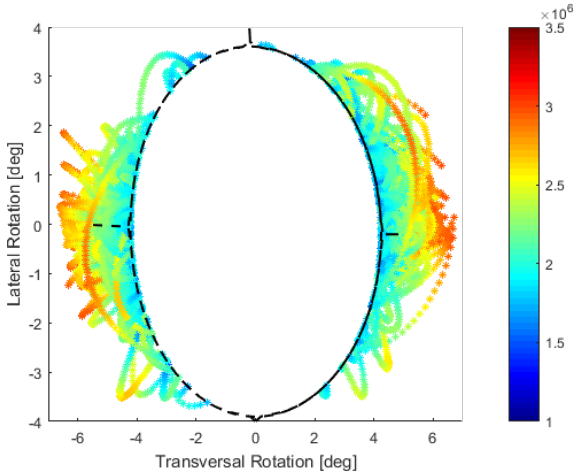

Figure C.8: Pipe bending moments outside vessel motion limits

List of Figures

List of Tables